ALMA MATER STUDIORUM – UNIVERSITÀ DI BOLOGNA
CAMPUS DI CESENA
SCUOLA DI INGEGNERIA E ARCHITETTURA

CORSO DI LAUREA MAGISTRALE IN INGEGNERIA BIOMEDICA

Cartilage contact pressure in the knee during walking in healthy and degenerated conditions: a subject-specific Finite Element modeling analysis

Tesi in
BIOMECCANICA COMPUTAZIONALE

Relatore
Prof. Giordano Valente

Presentata da
Stefano Di Paolo

Correlatori
Prof.ssa Ilse Jonkers
Ing. Mariska Wesseling
Ing. Maria-Ioana Pastrama
Ing. Enrico Schileo

III sessione

Anno Accademico 2016/2017

“A long way to go,

and a long memory”

L.P.

Contents

ABSTRACT

Osteoarthritis highly affects knee biomechanics through the degeneration of articular cartilage. Early osteoarthritis detection is crucial to limit cartilage damage and delay its progression. Computational modeling plays a relevant role in osteoarthritis research, as it can contribute quantitative analyses of *in-vivo* loading distribution in bone and soft tissues. The overall aim of this study was to analyze knee contact pressure in the cartilage during walking in healthy and degenerated conditions using a subject-specific finite element model developed to the purpose. The healthy model was created from MRI of an adult and included five bodies (femur, femoral cartilage, tibia, tibial cartilage, pelvis), the tibiofemoral joint, cruciate and collateral ligaments, eleven muscles and the hip joint. Cartilage was modeled as hyper-elastic nearly-incompressible material, cartilage-to-cartilage contact was frictionless, boundary conditions were adapted from a previous multibody analysis. A finite element analysis of the stance phase of the gait cycle was performed. Two degenerated models were created: one including a medial cartilage defect (i.e. change in geometry) and one including softening of material properties around the defect rim (i.e. change in material properties), and the same simulation was performed. The contact pressure and areas of the healthy model were first compared to those obtained through a previously-developed multibody model, and then the differences between healthy and degenerated models were analyzed. A general agreement in cartilage contact pressures was found between the outcomes from our finite element model and the multibody model (R^2 = 0.9), with no significant differences (Mann-Whitney U test, p=0.06) which indirectly validates the latter model. We found that a medial cartilage defect led to a significant increase in contact pressure and strain compared to healthy conditions, particularly on the medial compartment at the first peak of knee contact force (up to 75% increase in the medial contact pressure), as a major consequence of reduced contact surface. Adding softening material properties led to a different pressure distribution following a larger contact area and lower, although not significant (Mann-Whitney U test, p=0.4), contact pressure values. Although with some limitations, this study represents an important step to understand load-related mechanisms of cartilage degeneration. The modeling strengths resides in the MRI-based and open-source approach, and the ease in implementing different contact, material properties, boundary conditions to improve the model and study a wide variety of tissue-interaction mechanisms and motor tasks.

KEY WORDS

Knee, Osteoarthritis, Finite Element, Cartilage, Contact pressure

ABSTRACT

L'osteoartrosi inficia gravemente la biomeccanica di ginocchio. L'individuazione precoce è cruciale per limitare danni alla cartilagine e il suo processo degenerativo. Nella ricerca sull'osteoartrosi, i modelli computazionali hanno un ruolo importante nell'analisi quantitativa della distribuzione *in-vivo* dei carichi nei tessuti.

Lo scopo di questo studio è analizzare le pressioni di contatto sulla cartilagine di ginocchio nel cammino in condizioni sane e patologiche, utilizzando un modello agli elementi finiti personalizzato da MRI.

Il modello con cartilagine sana include: articolazione tibiofemorale con relative ossa, cartilagini, legamenti e muscoli, e articolazione d'anca. La cartilagine è modellata come iperelastica, e il contatto tra cartilagini senza attrito.

Sono stati sviluppati due modelli con cartilagine degenerata: con difetto cartilagineo, e con materiale più cedevole intorno al difetto. L'analisi è stata condotta per la fase di appoggio del ciclo del passo. Sono state confrontate le pressioni di contatto del modello sano con quelle ottenute da un modello multi-corpo precedentemente sviluppato, e sono state analizzate le differenze tra modelli con cartilagine sana e degenerata.

Abbiamo ottenuto pressioni di contatto simili tra il nostro modello sano e quello multicorpo (R^2=0.9), e ciò valida indirettamente quest'ultimo.

Abbiamo riscontrato che un difetto cartilagineo induce un significativo aumento di pressione fino al 75% in confronto a condizioni sane, in particolare intorno al difetto. L'indebolimento nelle proprietà materiali induce poi una diversa distribuzione di pressione a seguito di una maggiore area di contatto.

Nonostante i limiti, questo studio risulta rilevante nella comprensione dei meccanismi di degenerazione cartilaginea. La forza del modello risiede nell'approccio MRI-based ed open-source e nella parametrizzazione del modello per studiare molteplici attività motorie ed interazioni tra i tessuti.

PAROLE CHIAVE

Ginocchio, Osteoartrosi, Elementi Finiti, Cartilagine, Pressioni di contatto

INTRODUCTION

The knee can be considered one of the most important synovial joints of the human body, and the one on which the research in the biomechanics field is mostly focused. Due to locomotion and daily activities, the joint continuously undergoes very large stresses which affect, in different ways, all the tissues it is composed of. Different pathologies can be related to these stresses, especially the ones that include the degeneration of the tissues, such as osteoarthritis (OA).

OA is one of the most common musculoskeletal pathologies among men and women over 60 years old [1], [2], although it can harm young athletes as well. In late stages of the disease, people affected tend to adopt an altered gait pattern, that can cause further joint instabilities [3]–[6]. Consequently, the risk of comorbidity increases, in tandem with the rehabilitation failures.

Several studies tried to analyze knee mechanics in altered conditions [5]–[8], while other studies concentrated on gait retraining strategies to reduce pain and disease progression [9]–[11]. Multiple techniques have been adopted along the years to treat and prevent the escalation of this pathology, with a significant improvement of patients' quality of life [4].

Nonetheless, early detection is still a debated point, and approaches to the issue are heterogeneous and barely reliable. In this clinical scenario, computational models and simulations can play an important role. Multiscale analyses can help researchers (and clinicians) to deeply understand the mechanisms and the warning signs of the first appearances of OA, and consequently set the bases for prevention steps. To do that, detailed and realistic computational models of the knee joint are strictly required. Finite Element (FE) models are commonly used to this purpose, because of their value in focusing on the internal biomechanics of the knee and calculating contact forces and pressures. Recently, detailed Musculoskeletal (MS) models have also been developed for the same scope.

We developed a FE model of the knee joint with the aim of calculating contact pressures caused during daily life motor tasks in healthy and pathological subjects. We used detailed boundary conditions and tissue geometries from a previous MS analysis. In this Master Thesis, we aim to describe the development process, the modelling choices and the first results obtained with the present FE model. The newly developed model allows the quantification of contact loading effects in knee cartilage in a variety of boundary conditions and material properties, thus, could be valuable in terms of simulation early OA stages.

Chapter 1 – BACKGROUND

1.1 *Knee anatomy and motion*

The knee joint is a complex structure which provides stability and control while guiding the motion between the lower and the upper leg. It must allow locomotion and absorb, redistribute and transmit loads caused by daily life activities, with the minimum energy requirements from the muscles [12]–[14]. The knee is a weight-bearing joint that can be described through 6 Degrees of Freedom (DoFs) (3 rotations and 3 translations), although it's commonly defined as an "unresisted one DoF" joint [15], [16].

Three bones are part of these joint: the femur, the tibia and the patella. The anatomy of the entire knee, including the bones and the soft tissues, is shown in Figure 1.

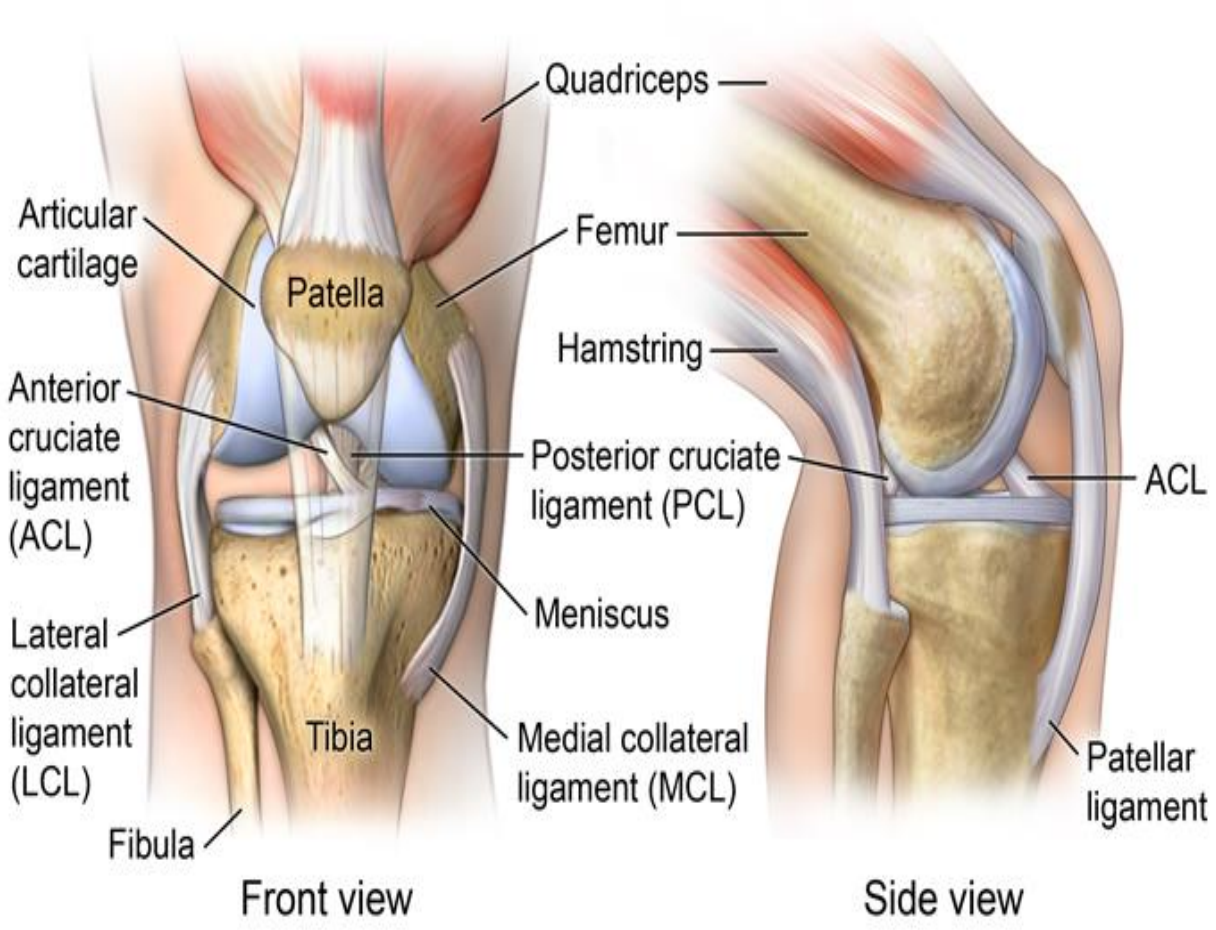

Figure 1 *- Knee anatomy*

As Wu et al. [17] report, a precise coordinate system is desirable to express the knee motion: Medio/lateral translation (ML) and Flexion/Extension (FL/EXT) must occur along and about an epicondylar femoral axis; distraction and Internal/External rotation (IE) must occur along and about a tibial long axis; Anterior/Posterior translation (AP) and Adduction/Abduction (ADD/ABD) rotation must occur along and about a floating axis, which is perpendicular to both femoral epicondylar and tibial long axes (Fig. 2). In normal conditions, along the unresisted DoF there is a coupling of rotation and translation, i.e. flexion and posterior translation. Compared to the single movements, this configuration allows a larger range of motion, in agreement with the anatomy of the bones [18].

More specifically, the knee consists of 2 joints: the Tibiofemoral (TF) and the Patellofemoral (PF) joint. The TF joint allows a wide range of rotation along the sagittal plane (FL/EXT up to 160°) and a moderate range along the coronal and transverse plane (ADD/ABD up to 15°, IE up to 35°). The principal role of the PF joint is to contribute to a minimal quadriceps contraction during the TF joint flexion, transmitting the extensor force across the knee at a greater distance from the axis of rotation. Therefore, its action varies a lot over the range of motion [14].

The complexity of the knee joint reflects an intrinsic instability of the bone structures, which means that the presence of soft tissues is required to obtain a suitable and fluid motion. Soft tissues can act in several ways: they can either passively limit the relative movement between the bones (i.e. ligaments), or actively contribute to pull them during the motion (i.e. muscles) or reduce the large contact forces acting in the joint, allowing the slide of the bones (i.e. menisci and cartilages).

Ligaments act as connectors between the bones of the joint: distal femur and proximal tibia are connected by collateral (medial – MCL and lateral – LCL) and cruciate (anterior – ACL and posterior – PCL) ligaments; the patellar ligament connects the patella to the tibial tuberosity. Essentially, they contribute to the stability of the joint limiting translations and rotations within certain ranges, behaving passively until those limits are reached. The ACL is the primary restraint to anterior tibial translation and a secondary restraint to the rotations when the knee is in full extension. The PCL acts in the same way but in the posterior translation and in deep flexion. Overall, they stabilize the knee along the unresisted DoF, being the most solicitated during daily life activities [12], [14], [18]. Unfortunately, their injuries are common, and are one of the principal cause of knee instability [19]. The MCL and LCL are the primary restraints to respectively valgus and varus angulation, and they contribute to the restraint of the posterior translation in knee flexion.

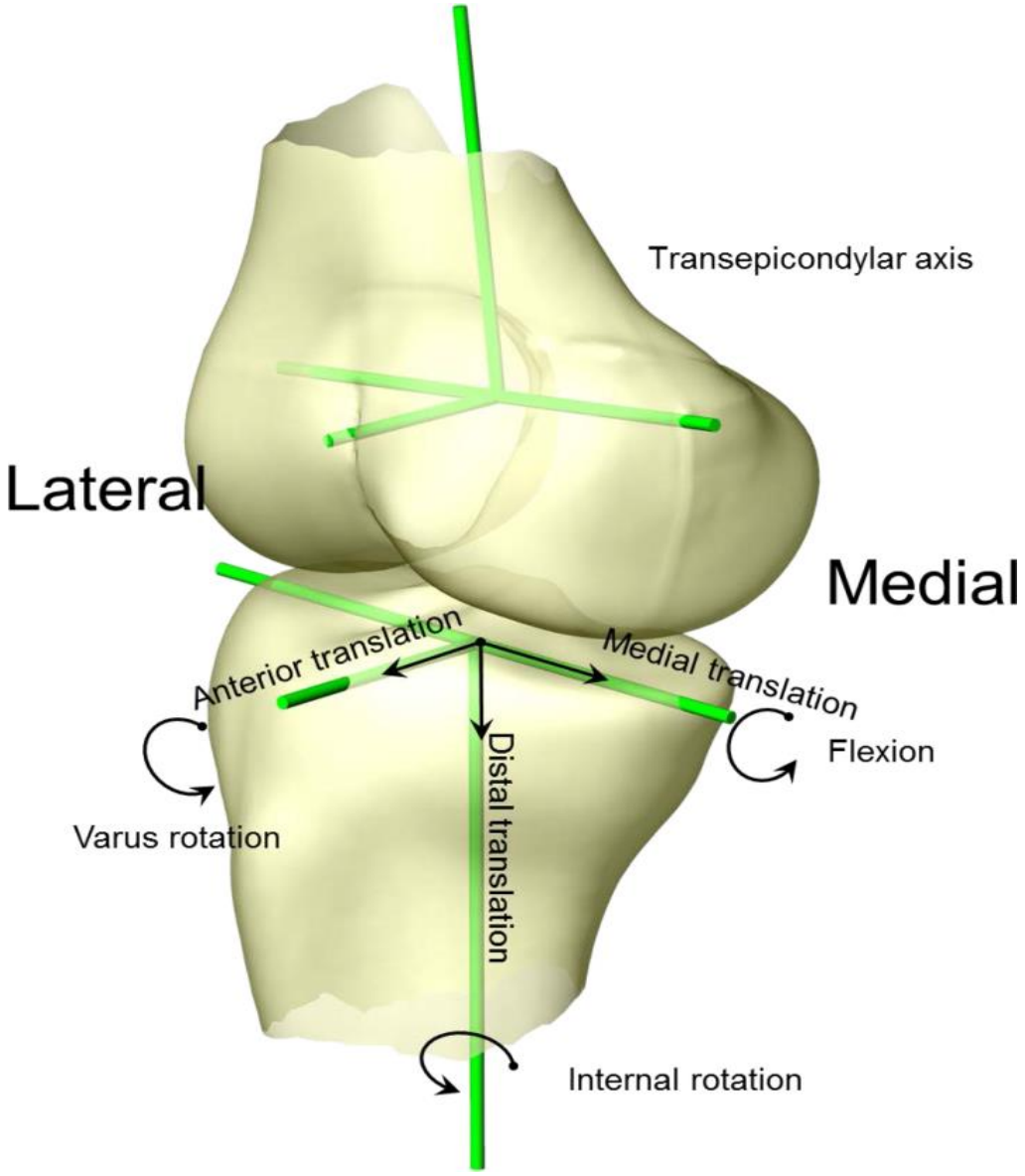

Figure 2 - *Knee axis, following the ISB rules for standardization in reporting kinematics data. Epicondylar femoral axis: ML and FL/EXT; tibial long axis: distraction and IE; third axis perpendicular to both the other two: AP and ADD/ABD. Figure adapted from* [20]

Muscles acting on the knee joint can be efficiently divided according to the role they play:

- *Flexors*: gastrocnemii (medial – MEDGAS and lateral – LATGAS), semimembranosus (SMEM), semitendinosus (STEN), biceps femoris short head (BFSH), biceps femoris long head (BFLH), gracilis (GRAC) and sartorius (SART);
- *Extensors*: vasti (medial – VASMED, internal – VASINT and lateral - VASLAT) and the rectus femoris (RECFEM);
- *Abductors*: iliotibial band (ITB) (tendon) and tensor fascia latae (TFL) [21].

Menisci are semilunar pads located between the femoral condyles and the tibial plateaus. Their shape allows them to maximize the conformity of the articulation, especially during the flexion, distributing the contact forces in order to reduce stresses on the structures [12].

Finally, each bone of the knee is covered by a layer of hyaline cartilage on the contact surface of the joint. Articular cartilage is the highly specialized connective tissue of diarthodial joints. It is 2 to 4 mm thick, devoid of blood vessels, lymphatics and nerves [22]. The function of articular cartilage is to provide a smooth, lubricated surface for near-frictionless bearing surface, and distribute loads to the underlying subchondral bone [23], [24]. This is possible thanks to its complex structure: depth-dependent collagen fibril networks regulate the tensile properties of the tissue; proteoglycans, saturated with an interstitial fluid phase, regulate its compressive behavior. The combination of these two actions provides the load support mechanism and yield the necessary lubrification of the joint. Cartilage is highly stressed during every kind of motor activity and undergoes large deformations: compressive strain can reach up to 30% in healthy conditions [24].

Injury to articular cartilage is recognized as a cause of significant musculoskeletal morbidity. OA degeneration alters the cartilage internal structure, leading to changes in its mechanical properties and affecting the stability of the knee joint and of the entire locomotion. Therefore, accurate knowledge of structural and mechanical changes could facilitate a better understanding of the initiation and progression of OA, leading to an improvement in treatment therapies.

1.2 *Knee Osteoarthritis*

OA is very common joint diseases, which affects millions of people all over the world, and is predicted to become the 4th cause of disability worldwide by 2020 [25]. It is a complex, chronic, degenerative and multifactorial disorder that especially harms weight-bearing joints, with higher rate for the knee than the hip [1], [2], [26], [27]. So far, no unique and perfectly effective treatment has been developed for this pathology. Patients with OA face a loss of articular cartilage that starts from the contact surface and penetrates along the depth of the tissue to reach the subchondral bone (Fig. 3). In the last stage of the disease, since their “cushions” wear away, bones can rub one against the other, causing pain, stiffness and motor instability (Fig. 4). This degeneration ultimately ends in an irreversible structural and functional failure of the joint. Often, the result is a restricted physical capacity in daily life activities, from sport, to stairs ascending/descending, until simple walking. These aspects contribute to reducing personal independence and, lastly, the quality of the life.

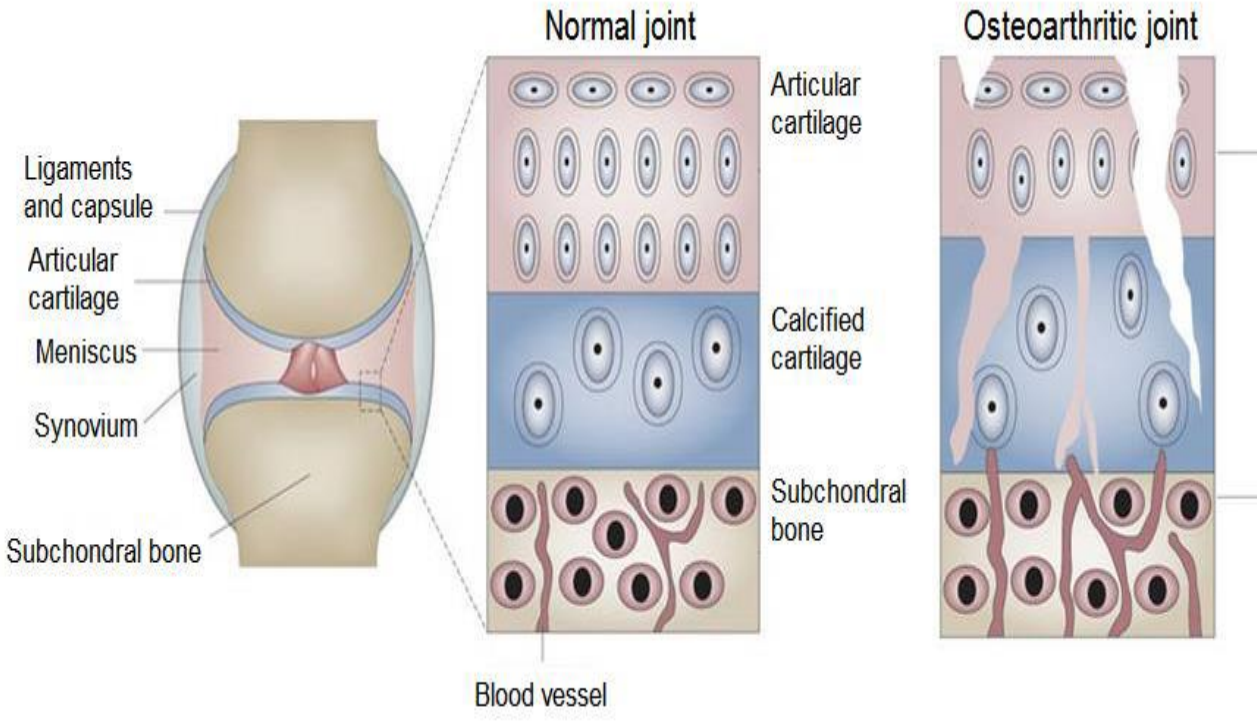

Figure 3 *- Bone-cartilage unit in normal and osteoarthritic joint. Cartilage in OA knees degenerates along the depth from the contact surface to the calcified cartilage until the subchondral bone (figure adapted from* [28]*)*

According to the World Health Organization, about 2.5% of the world population is affected by OA. Among them, the majority is made up of people aged 60 years or older [1], [2], [4], [27], so the number of people suffering from this disease is going to increase as life expectancy increases. Furthermore, another important risk factor, particularly for knee joint OA, is obesity [29]–[31]. Epidemiologic studies also observed a genetic contribution to the disease [30], [32]. Despite the wide knowledge of the major risk factors, a deep understanding of the pathology is still lacking. Nevertheless, a more detailed explanation of the causes that lead to the initiation and the progression of the disease can be obtained studying the biomechanics of the joint.

Overall, changes in normal load bearing contact and excessive loading lead to the degeneration of the cartilage [3]–[6], [28], [30], [33]–[35]. Since chondrocytes, which are responsible for the homeostasis of the cartilage extracellular matrix, are mechanosensitive, they directly feel load changes. Abnormal loading patterns can disturb the physiological balance of matrix internal processes: this imbalance can induce inflammation and eventually degeneration of the tissue. Moreover, cartilage is devoid of blood vessels and nerves, so any internal damage cannot easy be self-repaired. Evidence in literature

proves that abnormalities in the surrounding tissue, such as bone deformities or malalignment, muscle weakness, previous ligament and menisci injuries, also have an influence on OA initiation [26].

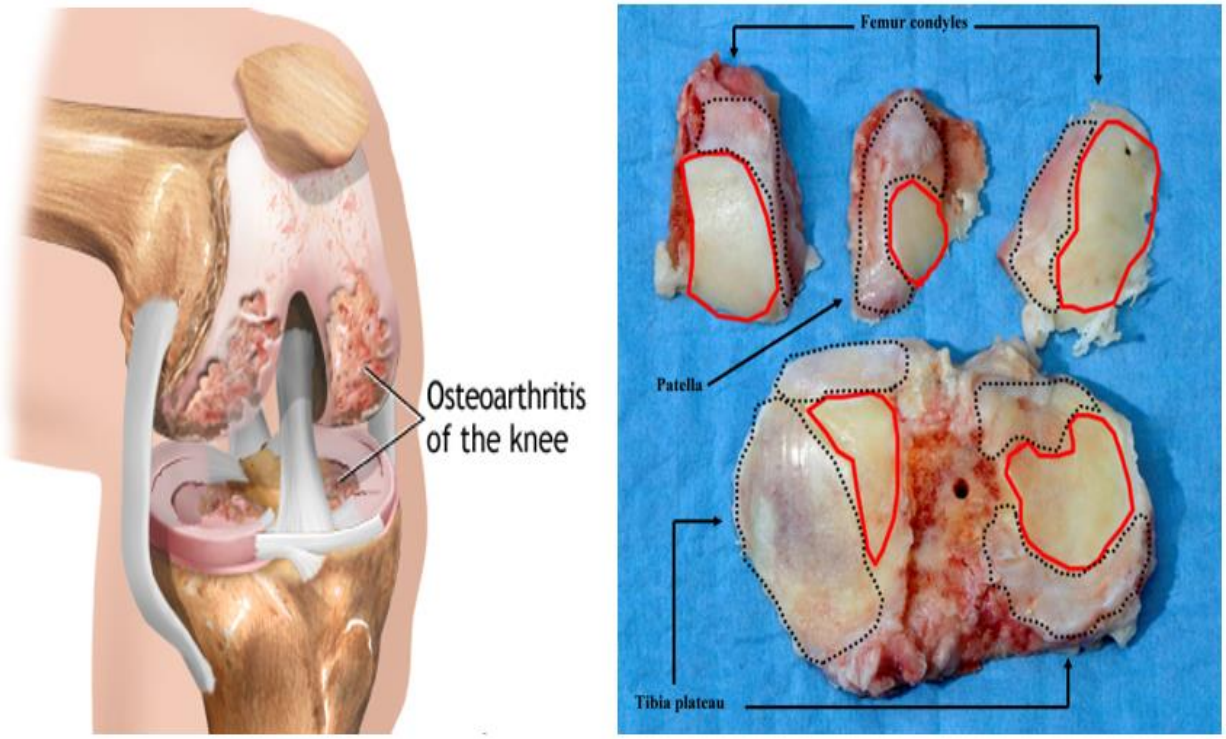

Figure 4 *- Effect of OA on articular cartilage in knee joint. (*left*) Graphic simulation of the damage in the joint; (*right*) effect of late stage OA on portions of rest joint (figure adapted from* [36]*)*

Rehabilitation procedures and surgical treatments are very delicate, since many concurrent issues can happen, e.g. formation of fibrocartilaginous tissue, limited ingrowth or integration, weakening of the surrounding tissues [25], [37]. Furthermore, these procedures are expensive and maybe even dangerous for elderly people. Thus, it is clear that early detection of OA is important to limit its damages and therefore delay its progression. Studies in literature, focused on joint mechanical overloading, put accent on detecting both the magnitude of the contact pressure on the cartilage surface and the location of the loaded region, as these factors could influence OA initiation and progression [7], [28], [33], [34], [37], [38]. These factors are the most studied during human walking. In a neutrally aligned joint, physiological values of contact stress during walking are in the range of 2-12 MPa [23], [33], and the medial condyle is predominantly loaded [8], [39]–[42]. In accordance with this knowledge, many articles show how cartilage on the medial compartment is often more worn out than the lateral at all stages of the pathology. Therefore, abnormal loading on the medial side of the knee has been associated with OA occurrence [37]. Moreover, some studies underline that

focal defects are commonly found in OA subjects who do not report pain yet, especially on the medial cartilage [8], [40]–[42]. The mechanical response of the tissue in presence of a defect can be significantly altered, and so lead to a further progression of the pathology. Obeid et al. [42] studied the articular cartilage with a unicompartmental defect under physiological loading, and found changes in tissue composition and material properties, compared to control subjects. They described it, especially on the rim of the defect, as "thinner and softer than control cartilage, and slightly weaker". Since thinning and softening impairs the ability of cartilage to equalize stresses in the joint, a tissue which is damaged in this way is mechanically inferior than normal one. This statement is in agreement with other studies (e.g. [41]) that also underline how these early signs of OA are not easily shown through clinical analyses but are instead well predicted by animal and human models.

As highlighted, it is essential to analyze and comprehend in detail the biomechanics of the knee relating to all the tissues it is composed of. Quantification of internal loads, kinematics and contact pressures is necessary to make predictions about the actual condition of a subject and to define a line of action, when required. Experimental measures *in vivo* cannot easily be conducted for practical and ethical reasons, while *ex vivo* studies often cannot represent correctly the pattern and the composition of the live tissues, and donor conditions must be appropriate for the investigations. In this complex scenario, computational models and simulations are playing an increasingly important role in OA research, thanks to the possibility to deeply analyze the internal loading conditions of subjects without invasive techniques.

1.3 *Computational models for knee contact loading prediction*

Computational models and simulations are commonly used in scientific research. For the specific biomedical field these techniques are relatively new, but always more frequently used to achieve a deeper comprehension of human-related biological phenomena. Models have proven useful in the context of parametric, phenomenological, or population-based investigations. They can contribute significantly to many clinical scenarios, e.g. in surgical planning or rehabilitation procedures, thanks to the possibility of general understanding, quantification and prediction that they offer beside a noninvasive kind of analysis [43].

More specifically, computational models can actively contribute to biomechanical analysis of the body during both daily and unconventional activities. Movement can be precisely simulated and the related parameters, such as kinematics, dynamics and loads, can be estimated. This statement is particularly true for the biomechanics of the joints, especially the most studied, the knee.

As already mentioned in the previous section, the anatomical and structural complexity of the knee make challenging to accurately measure the forces within its different tissues during movement. On the one hand, *in vivo* measurement of ground-reaction forces, joint motion and muscle EMGs do not provide direct information about the interaction between the knee components such as bones, cartilage, ligaments and muscles; on the other hand, *ex vivo* measurements have severe limitations in reproducing the loading patterns during every kind of activity [44]. Conversely, detailed models of the joint with multiple segments and multiple DoFs have been used as an alternative to experimental testing to determinate ligament, muscle and joint-contact loading in a wide range of different activities [21], under various boundary conditions.

The so-called "multiscale approach" allows researchers to go deep into the biomechanical parameters of the subjects in different tasks and tissue conditions [45]. A novel practice is to follow a precise workflow: motion analysis is the first step of the study, then data are used as input for MS models, and finally MS outputs are used in FE models (Fig. 5). MS models are more and more frequently used to evaluate kinematics, dynamics, joint forces and muscle forces of the human body in motion. FE models allow to calculate parameters such as stresses, strains, pressures and contact areas in joint tissues for different geometries and boundary conditions. The combination of the two techniques is powerful to quantify the mechanical response of an individual during various motor activities, particularly the gait [46]. Computer modeling and simulation can also be viewed as an extension of the motion analysis experiment, for two reasons: firstly, they provide information not accessible by empirical experiments; secondly, they can be helpful in explaining the results of the same motion analysis.

A MS model is an idealized mathematical representation of the body, comprising the bones, muscle-tendon units, joints, and passive structures in varying degrees of complexity. MS models can calculate forces in tissues and the corresponding movement of the joints during motor exercises like flexion/extension, stair ascent and descent, or gait. They allow a subject-specific multi-body simulation of the movement: patterns are taken directly from motion analysis, ground-reaction forces are given as an input and body segments are scaled to the anthropometry of the studied subject [47]. In general, input data are processed along a framework of inverse analysis, which first provide the kinematics related to the motion. Starting from the kinematics and the input files, it is possible to estimate the muscles excitation that produced that specific pattern, and consequently the joint contact loads. These results give information on how different motor tasks challenge muscles and joints and allow to speculate on how abnormal activation and magnitude can be related to one or more different musculoskeletal pathologies. In fact, if studies on a wide sample of individuals are conducted, it could be possible to determinate general principles and causes of movement deviations and disorders.

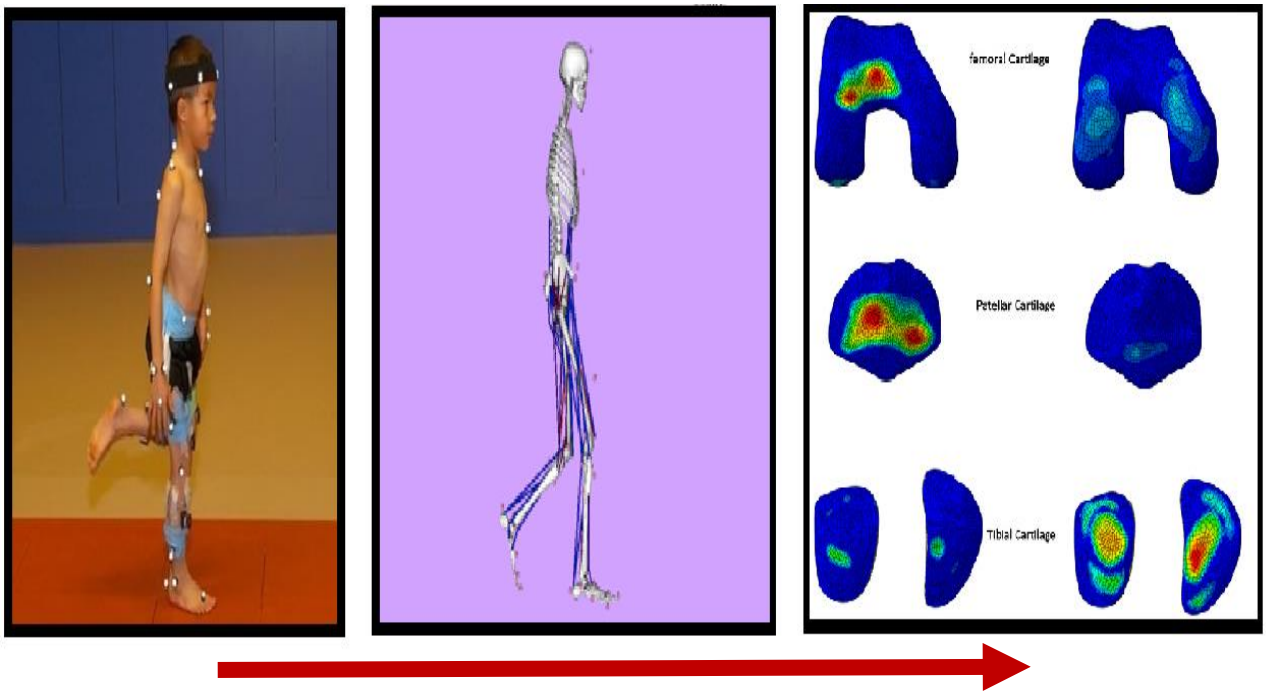

***Figure 5** – A common Multiscale body-organ approach workflow. (left) first step, motion analysis; (middle) second step, MS model; (right) third step, FE model results*

MS models output data are commonly used as boundary conditions for FE simulations. Typically, in FE models the focus of the study changes in scale, from a whole-body simulation to a single joint or segment. This is useful to characterize joint and tissue behavior in specific conditions, and allows for understanding the individual role of the components with a high level of detail that would be impossible to obtain experimentally [48]. In brief, FE analysis consists in the discretization of the entire volume of a body in a limited number of small elements (finite elements), connected to each other by nodes, in which displacement, stress, strain and contact pressure are estimated solving partial differential equations. FE software calculate these results starting from the relative displacement of the single nodes of every small element. In order to do so, it is mandatory to impose boundary conditions as either muscle and joint reaction forces obtained from a MS simulation, or data obtained from *in vitro* or *in vivo* experiments (e.g. joint loading measured *in vivo* with instrumented prostheses [21], [49]). Appropriate constraints are also requested by the software as boundary conditions. Furthermore, material properties must be assigned to all materials together with the corresponding constitutive models. Normally, detailed imaging data (e.g. from MRI or CT scans) are required to build an accurate model, and procedures like segmentation and meshing [50] need to be performed. Actually, accuracy of FE models strongly relies on the level of detail used in the appropriate reconstruction of all geometries and boundary conditions [48]. The power of FE analysis is in the

prediction of the mechanical response of a body (or of an entire joint) under all the imposed loads and boundary conditions. Quantification of the mechanical response allows to deeply evaluate what happens with the studied components during a motor task and to comprehend possible alterations of the internal structure, also drawing on the comparison with experimental data in literature [51]. More specifically, when studying the knee joint, FE modelling can be used to determinate cartilage pressure in the TF and PF joints under the effect of muscle and joint contact forces obtained by a MS model [52].

Nonetheless, the ability to predict patient-specific contact mechanics is questionable due to accuracy of joint mechanics representation and the lack of model validation. Furthermore, there is still extensive room for improvement, especially concerning simulations that involve injuries and pathologies.

1.3.1 *MS elastic foundation model*

Recently, a very interesting multi-body dynamic model of the knee joint was developed. This subject-specific model, developed by Thelen et al. [53], can simulate full 6 DoFs of TF and PF joint load-dependent behavior during locomotor activities. The model was used in the context of full body movement to simulate secondary knee kinematics in walking and was validated through the comparison with load-dependent kinematics measured *in vivo* in a motion analysis. This innovative approach allows to overcome some limitations of common multi-body models. Common gait models lack in that they are based on a highly simplified representation of the knee, which is often represented as a 1 DoF joint in which all PF kinematics and secondary TF kinematics are calculated as a function of knee flexion [54]. This representation does not allow to estimate the loading patterns of soft tissues, like cartilage and ligaments, and does not take into account the relevant variation of the kinematics caused by these patterns over the gait cycle. Conversely, a key feature of this model is the capacity to simultaneously predict the TF and PF mechanics that arise from the interaction of muscle, ligament, and contact forces, instead of relying on pre-assumed behavior based on cadaveric studies. Thus, it is possible to include articular cartilage in the model, and accurately understand the variation in magnitude and location of contact pressures relying on the impact that secondary kinematics has on the motion pattern.

In Thelen's study, geometries of bones, ligaments and cartilage surfaces were reproduced by the segmentation of MR images. Three bones, three articular cartilage surfaces and 14 ligament bundles were segmented [53]. The knee components were incorporated into a generic lower extremity MS

model with pelvis, hip, ankle and 44 musculotendon units acting on them. For femur and tibia, only the distal and the proximal part were respectively considered (Fig. 6). The model was then scaled to the segment lengths of the studied subject [47], [53].

TF and PF cartilage contact pressure was computed using an elastic foundation model [55]. This approach has been recently used to study contact mechanics in synovial joints such as hip, knee and ankle. In this kind of models, pressure is assumed to be a function of the depth of penetration between overlapping cartilage surface meshes during contact. In elastic foundation theory, cartilage is considered as an elastic tissue bonded to a rigid bone substrate. According to this, cartilage surface meshes are free to interpenetrate, and pressure on each element in contact is computed independently of adjacent elements. The contact pressure (p) is calculated according to the following law:

- $$p = -\frac{(1-v)E}{(1+v)(1-2v)} ln\left(1-\frac{d}{h}\right)$$

p: contact pressure on each triangle of the mesh; E: elastic modulus of the cartilage; v: Poisson ratio of the cartilage; d: local overlap depth; h: local cartilage thickness

Estimates of the cartilage contact pressure, provided by elastic foundation models, are shown to be comparable with prediction of FE models [56].

To sum up, a dynamic multi-body knee model, like the "MS elastic foundation model" shortly described here, may be extremely relevant in simulating movement, leading to a deep understanding of the mechanics of the knee joint. Particularly, it can be powerful to simulate the alterations in knee mechanics in the presence of injuries or tissue-related diseases, and it can provide a basis for surgical treatments on functional knee mechanics.

The MS elastic foundation model has been recently used in a study with the aim to evaluate the relationship between movement, knee loading and structural properties of the cartilage in both healthy and OA patients [34]. In the study, the model was scaled to participants' anthropometry and mass, and then rotations and translations were calculated through an inverse analysis [47], [57]. Muscle forces were calculated using a particular algorithm, the "Concurrent Optimization of Muscle Activation and Kinematics algorithm" (COMAK), that simultaneously solves for the first and the second knee kinematics, allowing the last one to evolve as a function of muscle, ligament and contact forces. Contact pressure was then calculated using the elastic foundation algorithm, with parameters: E=10 MPa, v=0.45, cartilage thickness 4mm (tibial) and 7mm (patellar).

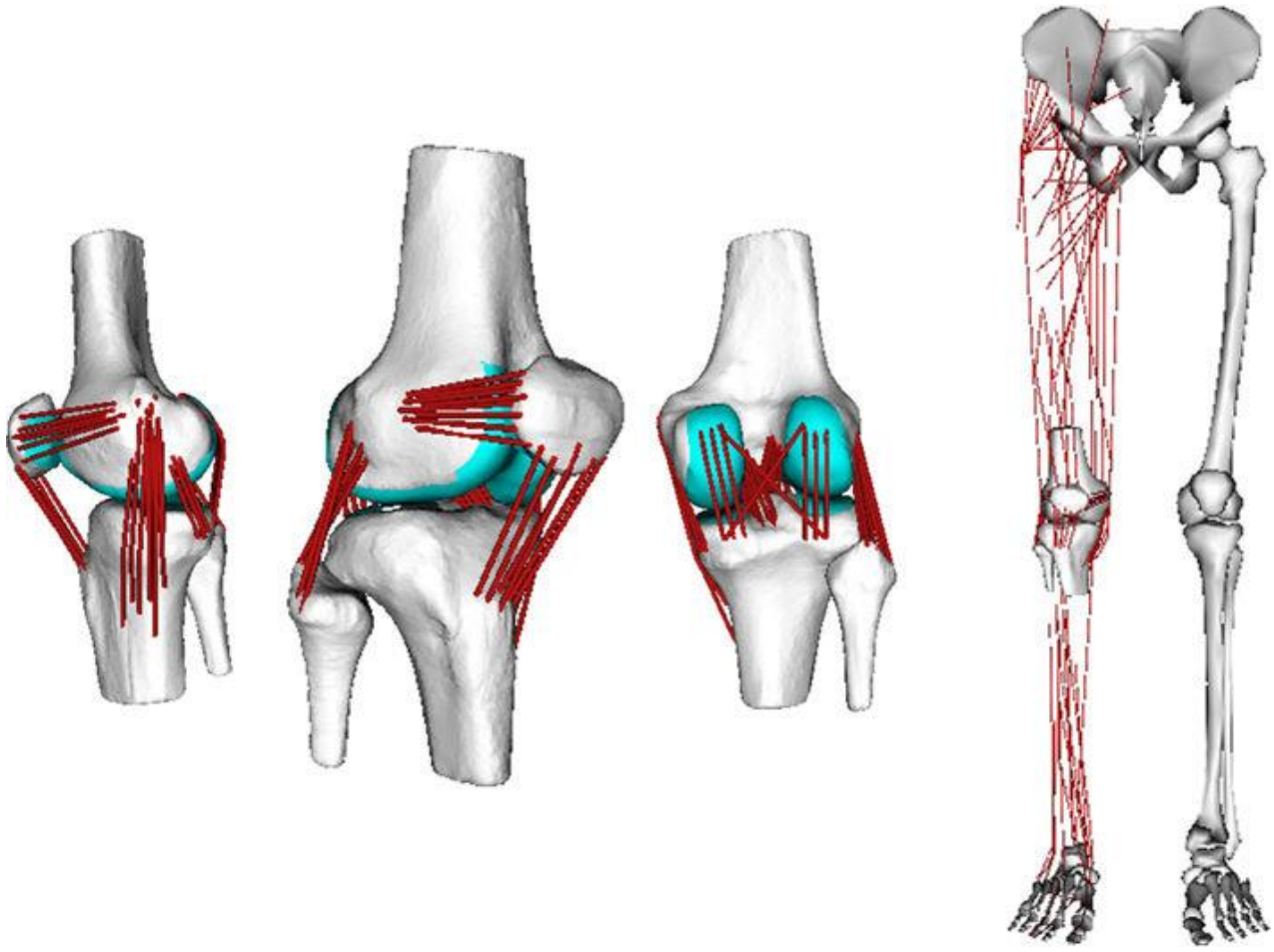

Figure 6 *- MS elastic foundation model (model and figure adapted from* [53]*). (left) view of the segmented components: bones, cartilages and ligaments; (right) view of the entire MS lower limb model*

The study of Van Rossom et al. [34] provided detailed data on contact pressures and contact areas in the knee joint during common daily life activities, such as gait. Additionally, it proved the quality of the MS elastic foundation model on many subjects, both healthy and OA affected. Nevertheless, the results obtained in this study should be critically discussed and compared with other models, to strongly confirm the quality of the analysis performed and its value in the clinical panorama. For example, the outputs can be compared with those of a conventional FE model, in which kinematics, muscle and contact forces are used as boundary conditions. For a complex constitutive representation of the cartilage, FE models are attractive, as they provide estimates of internal tissues mechanical parameters and can be developed in an ascending level of detail according to the specific purpose they are developed for. Thus, a literature study of the knee joint FE models is necessary for a better comprehension of the level of detail needed for a comparison with the MS elastic foundation model.

1.3.2 *Review of literature on FE models of knee joint*

In the last years, many FE models representing the knee joint have been developed. Overall, they are built for specific research purposes, so they differ a lot in terms of complexity and final usage and are seldom comparable. The aim of this section is to underline the differences among the main models found in literature, especially the ones including knee soft tissues, and to define the global choices to develop an FE model of the knee joint.

Firstly, a huge distinction in model complexity is evident in terms of boundary conditions: in ascending complexity in some studies, the choice was to apply static loads to the knee model [43], [51], [52], [58]–[60]; in other studies cyclic loads were applied, to simulate the continuous stress that the joint undergoes [43], [61]; in other studies joint kinematics and loads based on literature were applied [62]–[64]; lastly, in the most complex models kinematics, muscle and joint contact forces extracted from MS models were imposed [65], [66].

Another important discrimination can be made according to the choice of soft tissue inclusion. Some models are very basic, with just TF joint bones and corresponding cartilage [43], [64]. More sophisticated models also include ligaments, tendons and menisci [50]–[52], [58]–[63], [65], [66]. A part of the models of this last category also account for the PF joint [58], [65]. To obtain a detailed and subject-specific representation of all the tissues involved, the geometries in these models are often based on MR images. However, it is also common to represent soft tissues with predefined objects, such as springs for ligaments [65], [66] and semi-discs for menisci [62], [65] (Fig. 7).

Material properties play an important role in the differentiation between the different models, especially regarding articular cartilage behavior. Basically, there are two main approaches: the first is to assume the cartilage as linear-elastic [43], [50], [58]–[60], [63], [65]; the second is to provide a much more sophisticated law, i.e. define it according to the poroviscoelastic theory [51], [52], [62], [64], [66], [67]. Poroviscoelastic models use a biphasic definition for the cartilage, in which a fluid is free to flow in a solid porous matrix, made of collagen fibrils (usually modeled as a Kelvin solid) and proteoglycans (that follow a hyper-elastic law). These models provide a very detailed description of all the mechanical processes that happen in the cartilage when it undergoes stress. Specifically, they can simulate the depth-wise distribution of collagen fibrils and proteoglycans in the cartilage, and therefore take into consideration the differences in the mechanical response among surface, internal and deep layers. They have a strain-dependent permeability law and can simultaneously account for reaction forces and deformations during swelling, confined compression, indentation and unconfined compression [62], [67]. For the other soft tissues of the joint model (i.e. menisci and ligaments) a non-linear elastic formulation is commonly chosen.

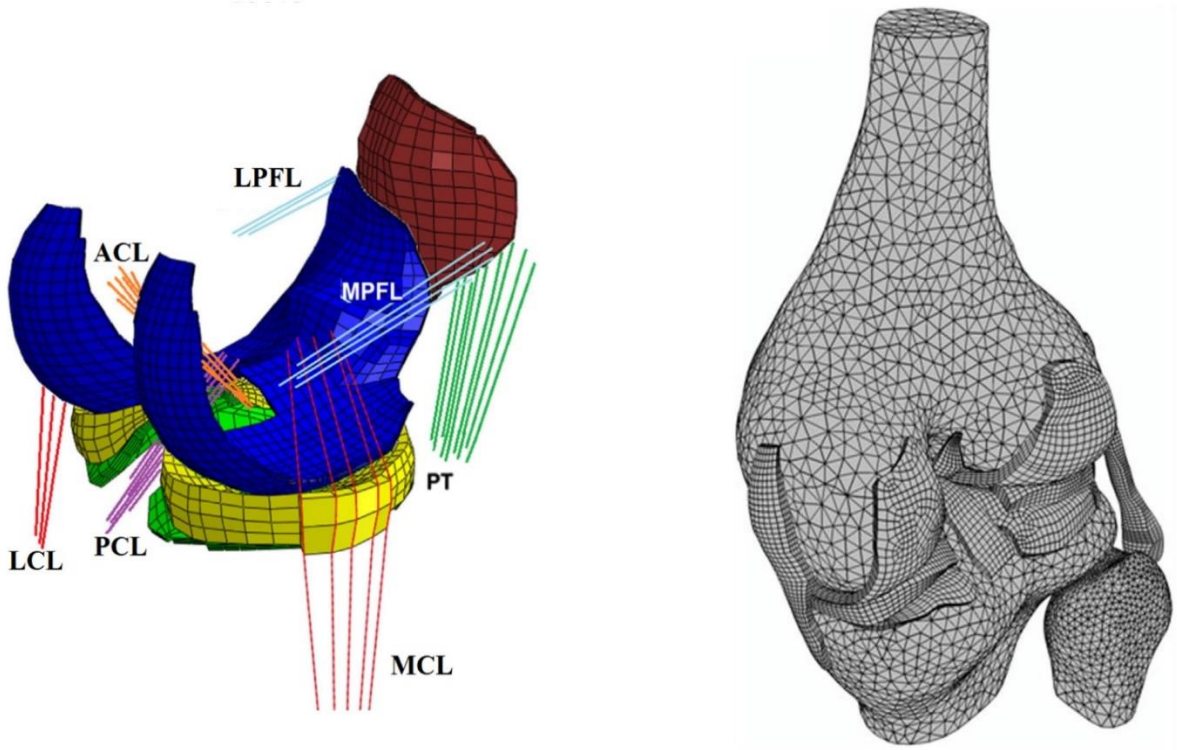

Figure 7 *– Two examples of knee joint representation in FE models. Different modelling choices: (left) ligaments represented as springs* [65]*; (right) ligaments and all soft tissues segmented from MR images* [61]

Moreover, some interesting research studies simulated cartilage defects in their models [43], [51], [52], [63]. In the study of Papaioannou et al. [43] a patient-specific FE model based on the MR images of a cadaveric knee was developed. They created, and then enlarged, some focal defects in knee cartilage of the cadaver, then they scanned the lower limb to create the geometries. The aim was to evaluate the agreement between the experimental tests on the same cadaver leg and the FE model, and then estimate to what extent the focal defects altered the behavior of the joint. A different approach was used in the studies of Shirazi et al. [51], [52] and Venalainen et al. [63], where the defects were simulated through a weakening of the material properties of the cartilage in some determined points (Fig. 8). In both cases, defects were created in a central area of the cartilage surface, according to what really seems to happen in early OA [19], [40], [63], [68]–[70].

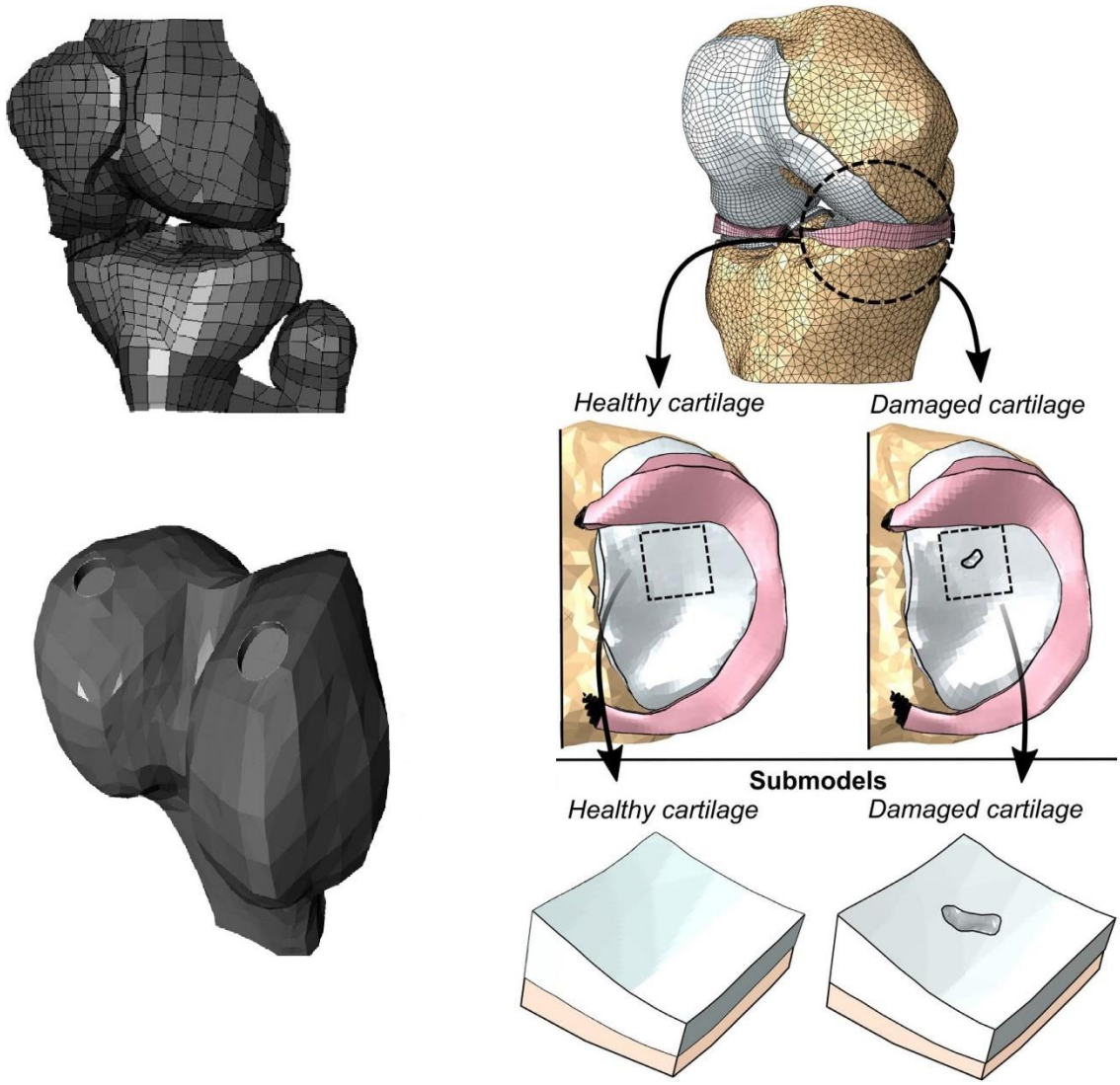

Figure 8 *– Cartilage defect simulation in two FE models of the knee joint. Different modelling choices: (left) MRI-based geometry reconstruction of a cadaver knee joint with defect* [43]*; (right) weakening of a small area on cartilage surface to simulation early OA damage* [63]

Lastly, Erdemir et al. [50], [71] developed an open source and freely available model of the TF joint, called Open Knee. Their purpose was to introduce to the scientific community a model including a detailed anatomical representation of the joint's major tissue structures, their interaction and nonlinear mechanical properties. Indeed, this model includes femur and tibia bones and cartilages, 4 ligaments (MCL, LCL, ACL, PCL) and meniscal attachment. Some studies already used this model to investigate the progression of OA in case of total meniscectomy [59].

A summary of all the models found in literature is shown in Table 1. The models have been categorized according to the differences identified in this section.

Legend: * Studies with simulation of cartilage defects → Ascending complexity		Type of boundary loads →			
		Static	**Cyclic**	**Gait Cycle**	**MS boundaries**
Material properties (cartilage) ↓	**Linear-elastic**	*Watson* [58] *Donahue* [60] *Meng* [59] *Erdemir* [50]	*Papaioannou** [43]	*Venalainen** [63]	*Schmitz* [65]
	Poroviscoelastic	*Shirazi** [51]	*Kazemi* [61]	*Halonen* [62] *Mononen* [64]	*Sharifi* [66]
Tissue inclusion ↓	**Only bones & cartilage**		*Papaioannou** [43]	*Mononen* [64]	
	Tissues with predefined object	*Shirazi** [51]		*Halonen* [62]	*Schmitz* [65] *Sharifi* [66]
	All tissues segmented	*Watson* [58] *Donahue* [60] *Meng* [59] *Erdemir* [50]	*Kazemi* [61]	*Venalainen** [63]	

Table 1 *- Summary of the literature review on knee joint FE models, categorized on their principal modelling differences. Models are labeled with the name of the first author of the study. Arrows highlight the ascending complexity of the model characteristics.*

To conclude this review, it is necessary to underline some aspects of the modelling choices made in these studies. As evidenced, the high complexity of the models in terms of material properties and soft tissue inclusion is often related to a static analysis with simple loading conditions. It is uncommon to find a model with very detailed material properties, such as poroviscoelastic cartilage, together with load conditions taken from MS models, such as muscle forces and gait kinematics. Poroviscoelastic models describe very well the cartilage behavior and can account in detail for what happen in case of injuries or pathologies, explaining also their most relevant chemical aspects. Nevertheless, their complexity is reflected in a high computational cost, especially in tandem with a detailed boundary condition set. These considerations lead to conclude that a compromise between the complexity of the analysis performed and the complexity of the modelling choices is necessary. Another aspect is related to the studies including cartilage defects. On the one hand, most of them are customized on joints from cadaveric subject; on the other hand, models with "computationally

simulated" defect can have very complex material properties. In any case, the idea of the time evolution of the OA defect (e.g. as performed in Shirazi's study) can be interesting in a study on the early detection of the pathology-induced tissue degeneration. In addition, the value of an open source and freely available model like Open Knee can have a good impact on the reliability of the studies on knee biomechanics in terms of FE analysis.

To provide a good comparison with the MS elastic foundation model, FE simulation of the knee joint are required. More to the point, it's necessary to consider a model which takes into account the kinematics, the muscle and the joint contact forces extracted from the musculoskeletal multi-body analysis of a gait task. These data must be used as boundary conditions, and both subject-specific geometries and a suitable material properties set are also required. A comparison of the output of the two models is then needed to verify their agreement in the described conditions.

Chapter 2 – PURPOSE OF THE STUDY

The general purpose of this Master Thesis is to evaluate cartilage contact pressure in the knee joint during walking, both in healthy and degenerated conditions. In order to achieve this goal, a FE modeling analysis is performed.
Two main specific purpose were defined:

Specific purpose I:
Compare knee contact pressure in the cartilage of a healthy subject during walking using a subject-specific FE model developed to the purpose, with knee contact pressure obtained using a previously-developed MS model that included an elastic foundation model at the knee joint.

A multi-body analysis of gait of a healthy subject had previously been performed with the MS elastic foundation model [34]. Knee contact and muscle forces and joint kinematics, obtained from the MS analysis, are used as boundary conditions for the newly developed FE model. Coordinate reference system and bone and cartilage geometries are also adapted from the MS model.
We therefore hypothesize an agreement of the FE and the MS model in terms of magnitude and trends of contact pressure along the motor task.

Specific purpose II:
Analyze knee contact pressure and strain in an early OA degenerated cartilage during the same walking condition, by simulating changes in geometry and material properties of the cartilage in the FE model.

We aim to introduce changes in geometry and material properties of the cartilage in the FE model to simulate early OA and its progression in the joint. Thus, we can evaluate effect of the changes on contact pressure and strain in the cartilage between the models with and without the pathological condition.
We therefore hypothesize contact pressure and strain to be higher in the OA models than in the healthy model.

Moreover, we aim to compare the results of the MS and the FE model with the results of the FE models reviewed in the section *1.3.2*, in terms of contact pressure in the cartilage with and without the defect simulation.

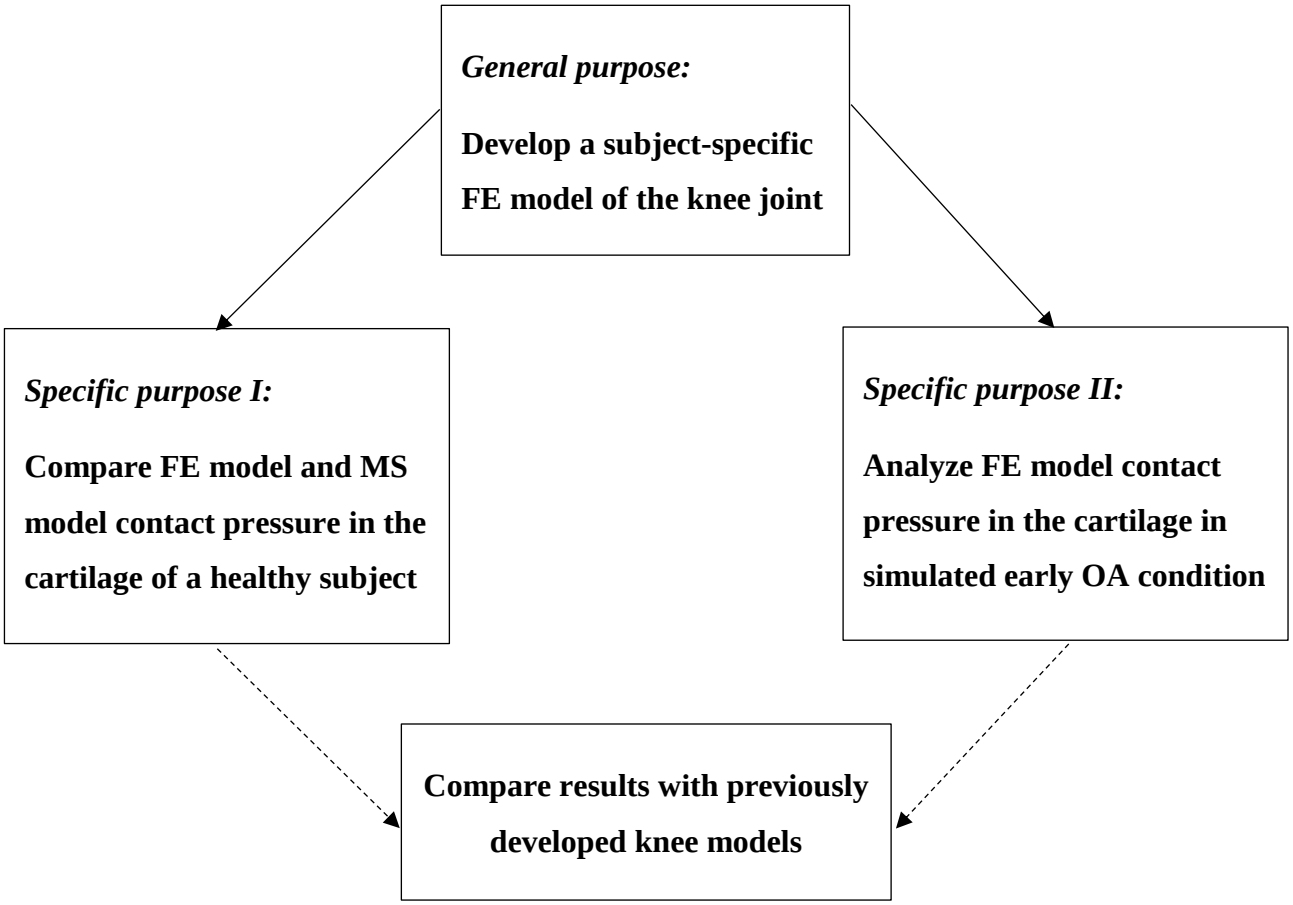

Figure 9 *– General overview of the main purpose of this Master Thesis*

If the hypothesis is confirmed, the newly developed FE model could contribute to indirectly validate the MS elastic foundation model of Thelen et al. [53]. Additionally, a good agreement of the results with other literature studies could both underline the quality of the FE model here described and enforce the potential of the new MS multi-body modelling framework.

This work, in which an advanced multiscale approach is used, could actively account for a deep understanding of the knee joint biomechanics and its articular cartilage, in terms of changes in internal

loading behavior that occur in presence of a wide-spreading disease like OA. Moreover, the FE model can be a valuable tool to estimate the knee cartilage loading patterns for different motor activities and physical conditions. This can be done through an accurate, reliable and non-invasive analysis. Finally, this study can contribute to the implementation of some surgical treatments and rehabilitation techniques to delay the occurrence of OA and the related pain progression.

Chapter 3 – METHODOLOGY

3.1 *Control Subject and initial data set*

The data set used to test the effectiveness of the newly developed FE model included one healthy subject, which has also been included among the controls in Van Rossom et al. [34]. The control subject is a 32-years-old female with no history of chronic knee pain, injury or surgery: during the entire study, all Knee OA Outcome Scores (KOOS) were 100% [72]. A gait analysis has been performed in the Movement and posture Analysis Laboratory of Leuven (KU Leuven, Belgium). Retro-reflective markers were placed according to a Plug-in Gait marker set [73], then marker trajectories and ground-reaction forces were collected using a 10-camera motion capture system (100 Hz, Vicon, Oxford, UK) and two force platforms (1500 Hz, AMTI, Watertown, USA), respectively. The subject had been instructed to walk barefoot at her own self-selected walking speed. A summary of subject characteristics and gait data is shown in Table 2.

Gender	Mass (Kg)	Height (cm)	BMI	Age	Stance time (s)	Gait speed (m/s)	SLS time (s)	DLS time (s)	KOOS QDL	KOOS ADL	KOOS SYMPT	KOOS PAIN
female	*60.1*	*170*	*20.79585*	*32*	*0.62*	*1.37*	*0.38*	*0.24*	*100.00*	*100.00*	*100.00*	*100.00*

***Table 2** – Summary of control subject characteristics and gait data. Physical data and KOOS outcome scores refer to the time of the acquisition. Among gait data, only the ones referring to the Stance phase have been selected and shown. Table is adapted from Van Rossom et al. study, a more detailed explanation of parameters is given elsewhere* [34], [72]

After gait analysis, the MS elastic foundation model [34], [53], [55], scaled to the anthropometry of the control subject, had been used to simulate: kinematics of the entire body; muscle, ligament and contact forces of the lower limbs after COMAK optimization; contact pressures on each mesh facet of the cartilage in the right knee joint, calculated according to elastic foundation formulation. Furthermore, geometries of the joint structures included in the MS model had previously been segmented in the study of Thelen et al. [53]: MR images of a 23-years-old healthy female subject and her dominant knee (right) had then been segmented using MIMICS (Materialise Group, Leuven, Belgium).

All data extracted from gait analysis (i.e. ground-reaction forces) and MS analyses were available for the present study. Geometry files (bone and cartilage contours of femur and tibia as segmented from MRI) were also available.

3.2 *Software used*

In this paragraph is presented a short explanation of the software used in the study. Only the main characteristics of the software are explained. For a detailed description of the FE model development workflow, see Section *3.3*.

3.2.1 *Materialise 3-Matic*

The software 3-Matic (version 12.0 Research, Materialise Group, Leuven, Belgium) was used to extrapolate the volume mesh from the geometry files of joint structures. 3-Matic avails for computer assisted design and engineering in the field of biomedical research. It combines CAD tools and meshing capabilities and is currently used to work on anatomical surface data, generally coming from the segmentation of medical images.
It works with stereolithography (STL) files as input, and allows to modify, separate and combine structures, measure parameters and analyze the quality of 3D images. Many of the software tools are dedicated to the creation and modification of mesh files: there is the possibility to build a surface or a volume mesh leveraging parameters like element type, element size and quality, shape of the mesh (uniform along the structure, finer in some points etc.). Mesh files can then be exported to the software for FE analysis.

3.2.2 *FEBio Software Suite*

The FEBio Software Suite (MRL&MBL University of Utah, Salt Lake City, USA) [74] was used to entirely develop the FE model of the knee joint. It is an open source, freely available set of software tools for FE analysis, specifically intended for biomedical use [74]. The software uses a nonlinear implicit FE framework and is specifically focused on the solution of large deformation problems, mostly faced in solid biomechanics. The suite is composed of 3 packages: PreView, FEBio and PostView.
PreView is the preprocessor package of the software suite. It is designed to define a model with all the aspects of a FE problem, and its primary output is the input file for the FE solver, FEBio. Through

the GUI, it is possible to import geometries, create and customize primitive shapes, generate and edit meshes and specify boundary condition, material properties and analyses options for the solver. A wide range of options for all the described tools are available in the software, specifically regarding the definition of material properties and contact descriptions between surfaces. The model can be exported to FEBio for the FE analysis.

FEBio is a nonlinear implicit FE solver which supports steady-state static, quasi-static and dynamic analyses for deformable and rigid solids. It has no graphical interface, so every aspect of the FE problem must be compiled either in a preprocessor software (e.g. PreView) or directly in the FEBio code (through a text editor), before running the FE analysis. An incremental iterative solution is obtained by discretizing the applied loads and boundaries through an implicit time integration scheme. The results of FEBio can be analyzed in the FE postprocessor package of the suite, PostView. PostView offers tools to inspect and analyze the results through graphical rendering and animation of the model. It also lets the user inspect the data quantitatively, directly determining values at nodes, facets and elements. Variations of rendering layout are possible and are useful for a better understanding of the results. Numerical, graphical and animated results can be exported for a further postprocessing or simply for visualization.

3.2.3 *OpenSim*

OpenSim software system (version 3.3, SimTK, Stanford, USA) [47] was used to calculate the knee kinematics, contact and muscle forces in the MS elastic foundation model for the construction of the boundary conditions. OpenSim is an open source, freely available software platform for modelling, simulating and analyzing the mechanics of the musculoskeletal system in a wide variety of movements [47]. It is commonly used to simulate the multi-body dynamics of individuals and explore the biomechanical effects of pathologies and relative treatments. It allows the creation of subject-specific models and the estimation of joint kinematics and internal loads within the musculoskeletal system during both static and dynamic motor tasks. It is also recognized for the good interaction with FE models. The models of Thelen [53] and Van Rossom [34] have been developed in SIMM, a non-open source software, predecessor of OpenSim. The two software packages can interact with each other. Specifically, it is possible to create a model in SIMM and export it to OpenSim. The export of the model allows, under some moderate adaptations in application and modification to the workflow, to use the MS elastic foundation model in OpenSim for basic simulations of gait cycle [75].

3.2.4 *MATLAB*

MATLAB software (version R2017a, MathWorks, Natick, USA) was used to: generate compatible input data for FEBio, refine the postprocessing of the data extracted from PostView, compare the main features between the MS and the FE model. The MATLAB platform is commonly used for solving engineering problems and to conduct many mathematical operations on data from other software. It contains many pre-built toolboxes which make it very valuable for data refinement and statistical analyses.

3.3 *Development process*

In this section, a detailed description of the development process is provided. Overall, three different versions of the same model were developed. Firstly, a general model for the simulation of the gait task in healthy conditions was developed. The model was named "HC" (Healthy Cartilage). Next, the cartilage geometry was modified to simulate a defect on the cartilage surface, as might be caused by early OA. Thus, a second model was developed in the same way as the first model, but with different tibial cartilage geometry. The model was named "DC" (Damaged Cartilage). Starting from the DC model, a third version was developed to account for the time evolution of early stage OA: material properties of the surface of the defect rim were modified to simulate a softening of the structure affected by OA. The model was named "SC" (Softened Cartilage).
Contact forces, muscle forces, constraints and kinematics were applied to either the segments available from MR images or to objects created to the purpose (e.g. spheres for the muscle origins). The common process for the development of the three models is provided in sub-sections 3.3.1 and 3.3.2. The variations adopted in the DC and SC models are provided in the sub-section 3.3.3. The post processing and data analysis is finally provided in section 3.3.4.

3.3.1 *Mesh creation in 3-Matic*

The volume mesh for the structure components of the model was created in 3-Matic. Geometry files (in STL file format), initially available, were imported in the software and immediately scaled by a factor of 1000, to change the unit from meter (used in OpenSim) to millimeter (used in 3-Matic). This way, pressure data in FEBio could be expressed in MPa instead of Pa (force unit measure in all software: Newton). Consistent with coordinate system recommended by ISB [17] and used in the MS model [34], the segment axes were defined as: AP axis – X (+ anterior, - posterior); vertical axis – Y

(+ top, - bottom); ML axis – Z (+ lateral, - medial) (Fig. 10). Since only the external border of the cartilages had been segmented, the cartilage surfaces at the bone-cartilage junction were not available (Fig. 11a). Therefore, the first step was to create the full cartilage surfaces by including the border of the bone in contact with the cartilage. To this purpose, the "Design" and the "Fix" tools of 3-Matic were used. Next, the "Remesh" tool was used to create a volume mesh of the structures. All structures were meshed using 10-node tetrahedral elements [44], [76]. The surface at the bone-cartilage interface were meshed to have connecting nodes at the cartilage and bone surfaces, using the "non-manifold assembly" command. The maximum element edge length was chosen according to the following criterion: for the cartilage, the maximum length was 1.2mm, to obtain at least three elements in the depth [53], [60], [61], [63], [76]–[78]; for the bones, only the elements in contact with and closest to the cartilage were set at 1.2mm, while the edge length of the other elements (i.e. far from the cartilage) were gradually increasing from 1.2 mm till 6mm [79] (Fig. 11b). This way, cartilage meshes were much finer than bone meshes [55]. Element shape quality was monitored through the "Mesh quality inspector" command. The total amount of element was 202000, divided in: 45000 elements for the femur, 45000 for the tibia, 63000 elements for femoral cartilage and 47000 for tibial cartilage [44], [60], [63], [76], [77]. Volume meshes were exported to PreView as C3D10M elements [24], [77], [80].

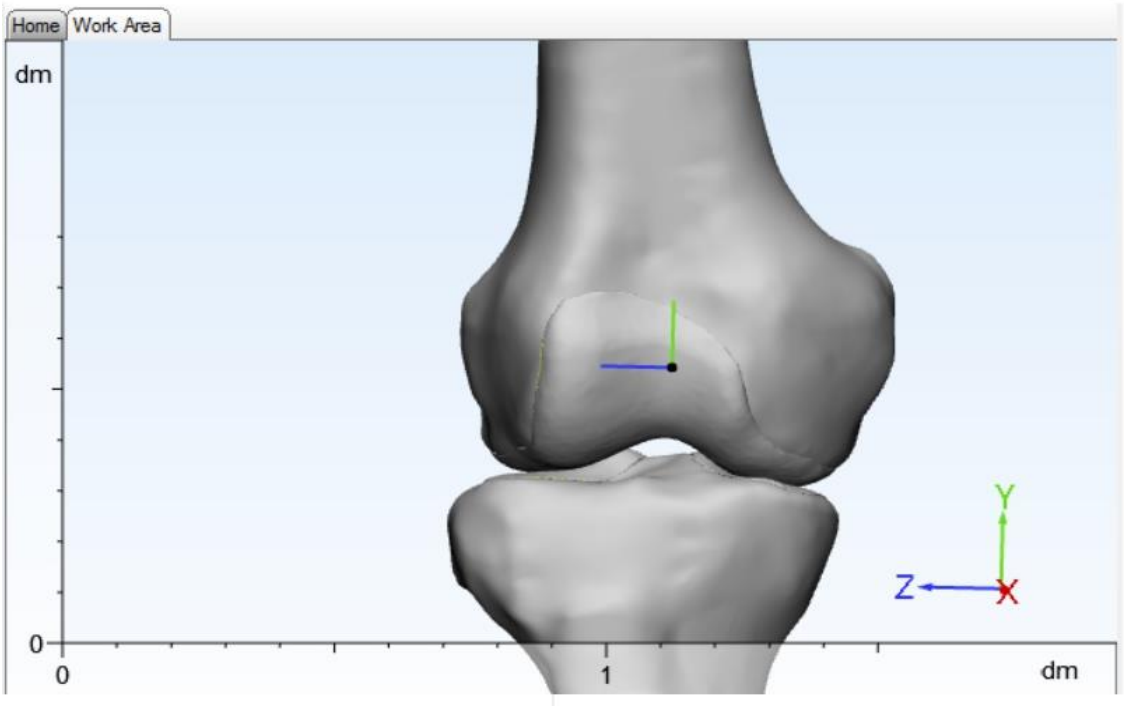

Figure 10 *– Bone and cartilage geometries, with relative coordinate system in the work area of 3-Matic. Coordinate system is coherent with the one used in Van Rossom et al. study* [34] *and with ISB recommendations [17]: AP axis – X, vertical axis – Y, ML axis – Z*

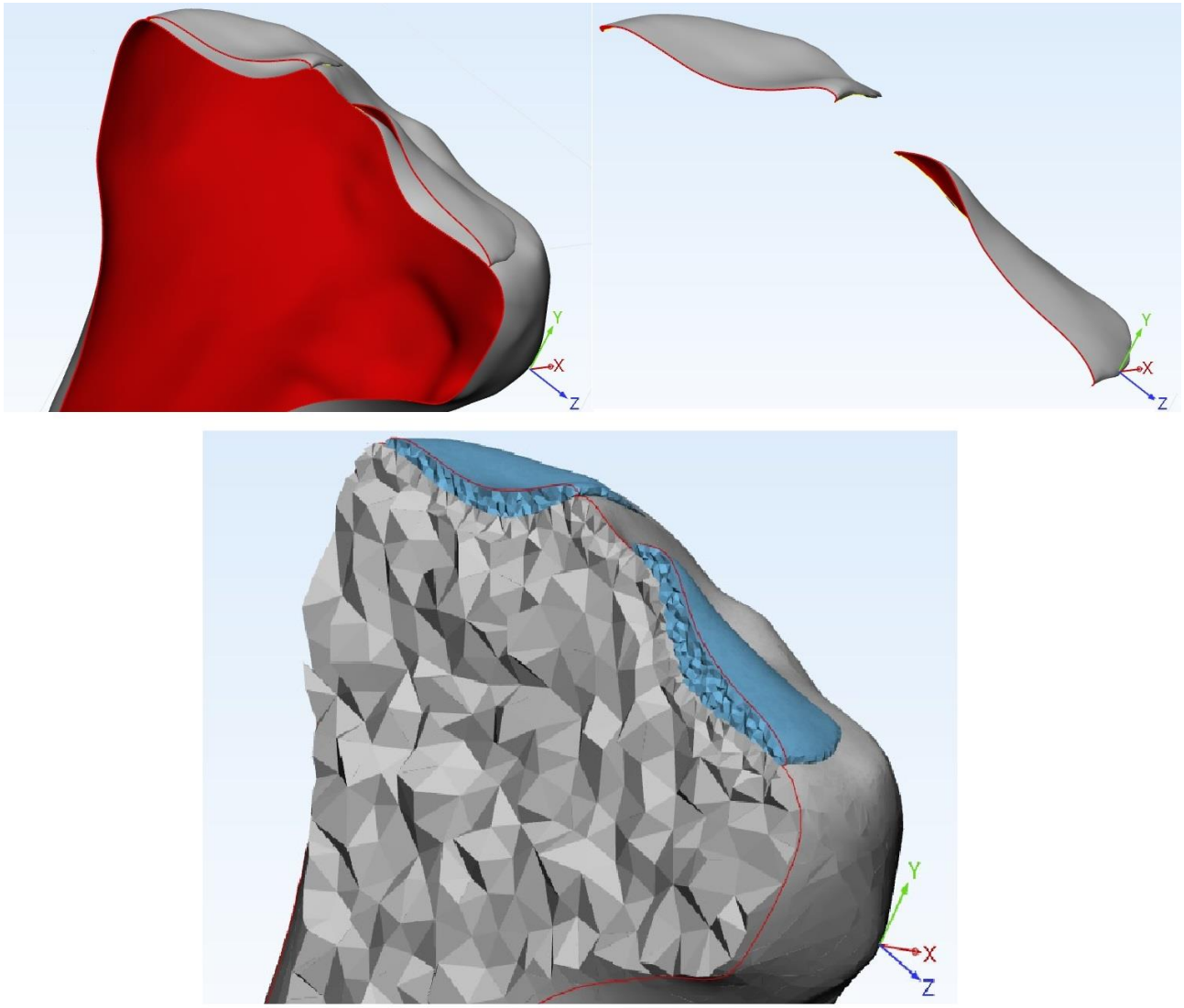

Figure 11 *– Mesh creation from STL geometry file, clip on X axis of tibia and tibial cartilage. 11a: (top left) bone and cartilage segmentation; (top right) view of the external border of cartilage: lack of the internal border at the bone-cartilage junction; 11b: (bottom) final volume mesh of the structures: element density in cartilage is larger than element density in the bone, there is a gradual increase in element size moving away from the bone-cartilage interface*

3.3.2 *Model development in FEBio*

Geometries

The entire FE model was developed in PreView and part of the code was edited in a text editor for further refinements. Over all, the model consists of 5 segments, 7 ligament bundles, 11 muscles and 2 joints.

Volume meshes, created in 3-Matic for the four segment geometries (distal femur, femoral cartilage, proximal tibia, tibia cartilage), were imported in PreView. An additional eight objects were created

to simulate geometries that were not available from the MR images. These objects were intended as extension of the bones and were necessary to correctly impose muscle forces and constraints to the model. Small spheres were created to include forces not directly connected to the geometries available from MRI and were positioned according to the coordinates of the MS model. Six spheres with a 1mm radius were created to simulate the muscle origin points of MEDGAS, LATGAS, BFSH, VASINT, VASLAT and VASMED. All these muscles have the origin on the femur and the insertion on either tibia, patella or calcaneus. These objects were assigned to the femur body. One more sphere with a 1mm radius was used to simulate the LCL insertion point (see Section 3.3.2 - *Constraints*) on the fibula and was assigned to the tibia body. One last sphere was used to simulate the pelvis, containing the origins of other five muscles and tendons: BFLH, SMEM, STEN, RECFEM and ITB. All these muscles have the origin on the pelvis and insertion on either the tibia or the patella. The sphere was 10mm of radius, assigned to a new body called "Pelvis" (Fig. 12, Fig. 13).

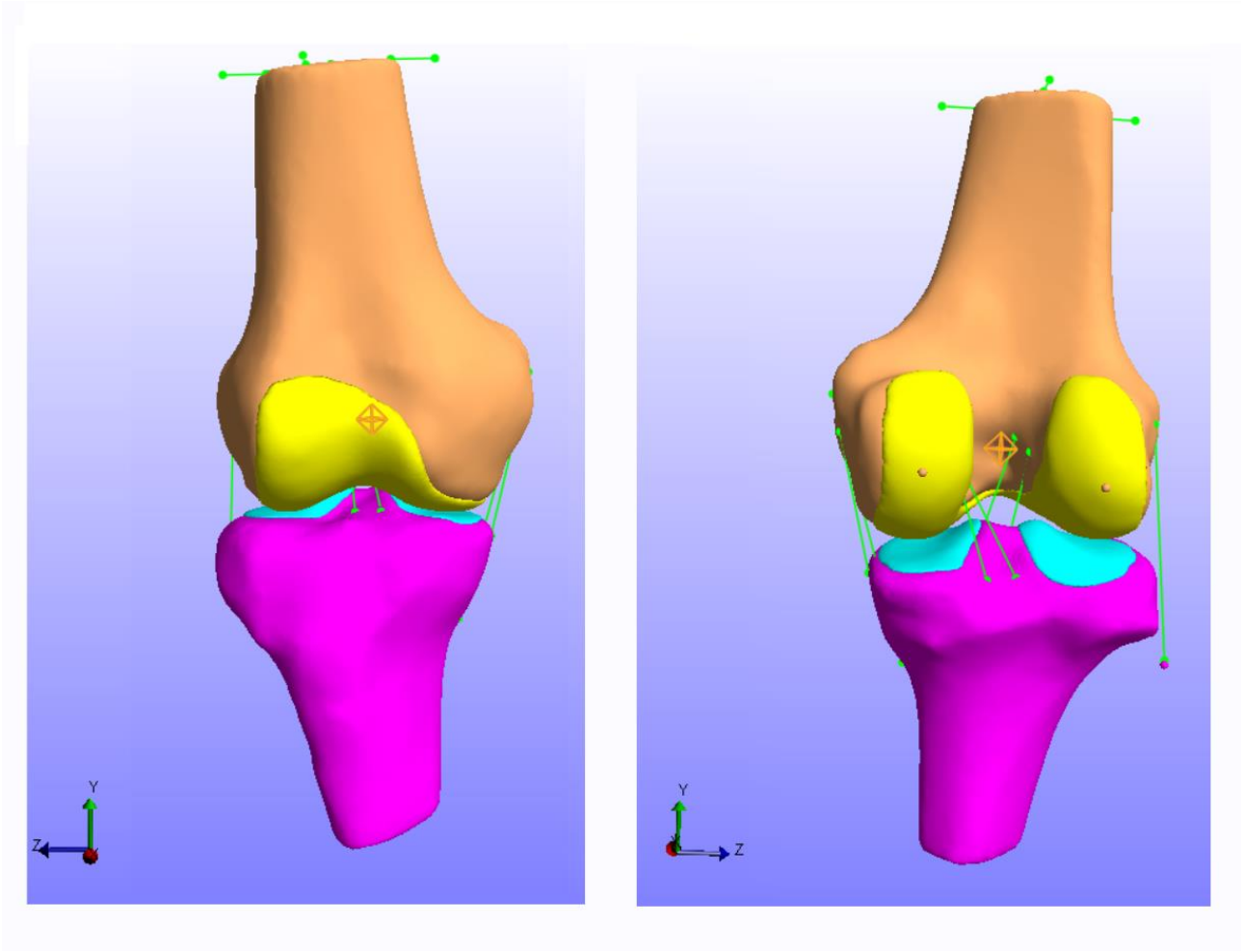

Figure 12 *– FE model in PreView: principal components. (left) anterior view of the geometries imported from 3-Matic, (right) posterior view of the geometries imported from 3-Matic. Green spring objects represent ligament bundles*

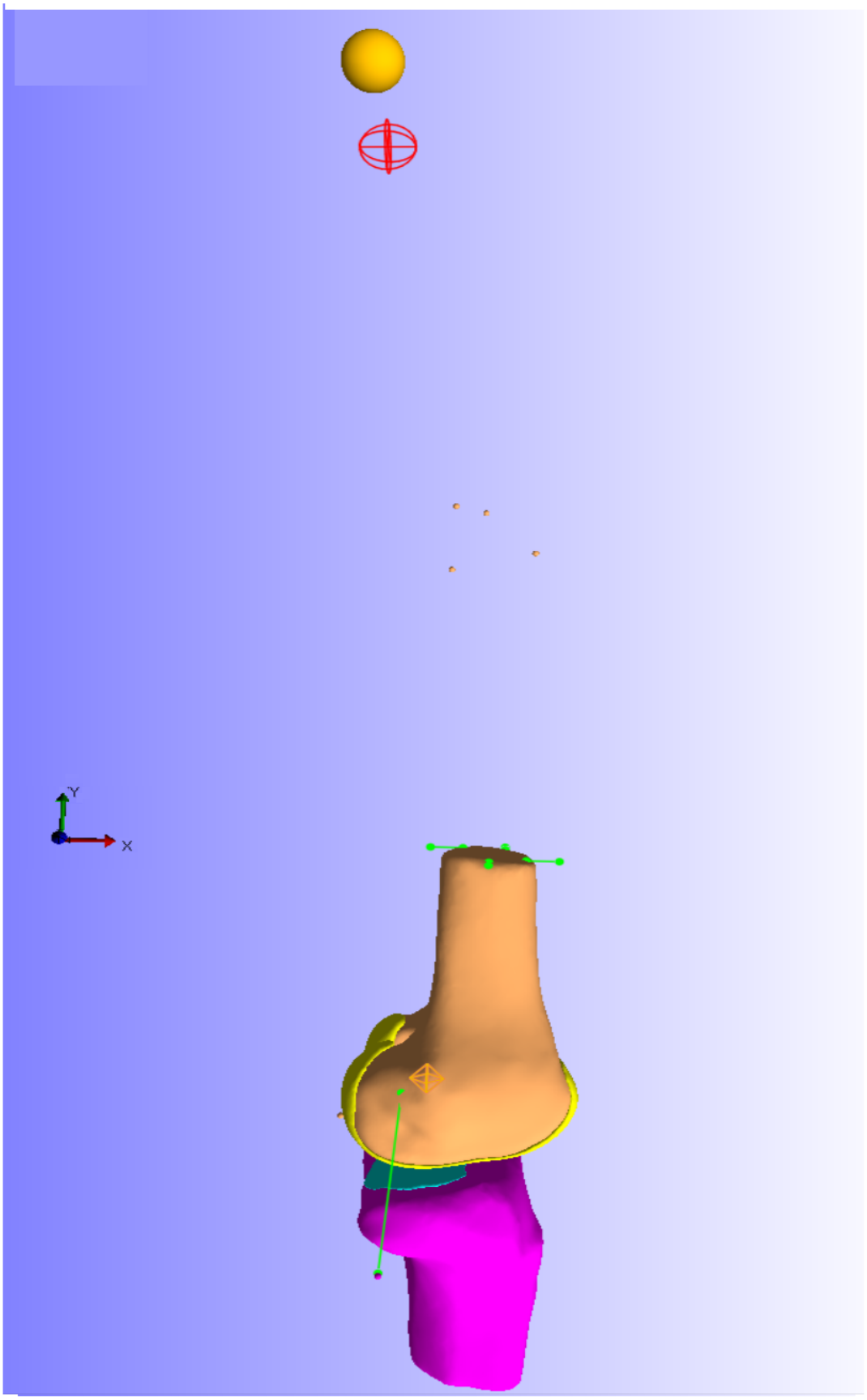

Figure 13 *– FE model in PreView: all components. The small purple sphere represents the attachment of the LCL on the fibula; brown spheres represent the muscle origins on the femur; the yellow sphere represents the pelvis*

Material properties

Material properties were assigned to the five segments using the constitutive models available in PreView (Table 3). Since bone is much stiffer than cartilage, the deformation of bone during motor tasks is negligible [50], [81]. For this reason, the bones were modeled as rigid bodies. This is also time-effective for the simulations, as the number of equations in the system is reduced. Bone density was set at 1.13e-6 tonnes/mm^3, according to previous studies [44], [50], [71], [74], [82]–[87]. The cartilage was modeled as hyper-elastic nearly-incompressible Mooney-Rivlin material. This material is often used to describe the mechanical response of biological soft tissues and in cartilage models it is considered to provide a good compromise between accuracy and computational power [50], [71], [88]–[92]. For this model, the strain energy density function is:

- $W = C_1(\bar{I}_1 - 3) + C_2(\bar{I}_2 - 3) + 1/2K(\ lnJ\ )\hat{}2$

C1 and *C2*: empirically determined material constants; *K*: bulk modulus; *J*: Jacobian; $\bar{I}1$ and $\bar{I}2$: first and second invariants of the deviatoric right Cauchy-Green deformation tensor.

K, C1 and C2 (expressed in MPa) are the parameters required in PreView. In the model, C2 was set to 0 MPa, hereby creating an uncoupled version of a neo-Hookean material. K was set to 335.3 MPa and C1 was set to 1.67 MPa, to create the same mechanical properties of the cartilage as in the MS model in Van Rossom et al. (E=10 MPa, v=0.495) [34]. Cartilage density was set at 1e-9 tonnes/mm^3 [50], [60], [71], [93], [94].

Body	**Material type**	**Material properties**			
		Density (tonnes/mm^3)	**K (MPa)**	**C1 (MPa)**	**C2 (MPa)**
Femur	*Rigid body*	*1.13e-6*			
Femur cartilage	*Mooney-Rivlin*	*1e-9*	*335.3*	*1.67*	*0*
Tibia	*Rigid body*	*1.13e-6*			
Tibia cartilage	*Mooney-Rivlin*	*1e-9*	*335.3*	*1.67*	*0*
Pelvis	*Rigid body*	*1.13e-6*			

Table 3 *– Material properties used in the model for all the bodies. In FEBio, only the density parameter is required for rigid bodies; K, C1 and C2 are required for the Mooney-Rivlin material.*

Contacts

Mechanical interactions between the bodies were defined (Table 4). The attachment of the cartilage to the corresponding bones were modeled as a rigid interface, to rigidly transfer the constraints and loads applied to the bones to the cartilage. As contact between the cartilage layers, a "sliding interface" was defined. This PreView option is used to set up a non-penetration constraint between two surfaces, based on a penalty enforcement method. Specifically, the facet-to-facet algorithm was used: it accounts for a frictionless contact implemented with a Gaussian quadrature to integrate contact equations [74]. A penalty factor parameter (expressed in MPa/mm) and a tolerance factor are required in this formulation. The penalty parameter scales the contact gap between the two surfaces to calculate the contact loads and pressures for each facet and to guarantee the non-penetration. Convergence tolerance sets the maximum percentage of change between two successive iteration of the solver to reach the convergence in a time frame. The penalty factor was set to 1, tolerance was set to 0.05. Moreover, an "auto-penalty" flag, used to automatically modify the factor along the simulation, was enabled. One last contact was defined: a "rigid joint" ("a spherical joint between two rigid bodies", in FEBio [74]) between femur and pelvis. This contact was used to simulate the hip joint. This allowed the muscle forces acting between pelvis and tibia or patella could be transferred to the knee.

Surfaces in contact	**Type of contact**	**Contact parameters**		
		Penalty factor (MPa/mm)	**Convergence Tolerance**	**Flags**
Femur – femur cartilage	*Rigid interface*			
Femur cartilage – Tibia cartilage	*Sliding interface*	*1 (initial guess)*	*0.05*	*auto-penalty*
Tibia – Tibia cartilage	*Rigid interface*			
Femur – Pelvis	*Rigid joint*	*10*	*0.1*	

Table 4 *– Contacts used in the model for all the surfaces. In FEBio, no parameters are required for rigid interfaces. Penalty factor and convergence tolerance are required in sliding interfaces and rigid joints; flags are only available for the sliding interface*

Constraints

Model constraints were included to simulate the stance phase of a gait cycle. The tibia was fixed in all 6 DoFs [59], [95], [96]. The femur was free to translate, while rotations were imposed using the knee kinematics calculated by the MS model. The femur was additionally constraint by four springs to connect the top of the bone to 4 additional nodes, fixed in all 6 DoFs. This was done to avoid large deviations of the femur. To minimally alter the joint mechanics, the stiffness of this springs was set to 1 N/mm, with a linear force-displacement relation. Moreover, pelvis rotations (3 DoFs) were imposed using the MS model kinematics.

Lastly, the collateral and cruciate ligament constraints were simulated by seven additional springs. Springs represented ligament bundles and were named according to their relative position in the joint: 2 springs for the ACL (anteromedial - amACL and posterolateral - plACL); 2 springs for the PCL (anterolateral – alPCL and posteromedial pmPCL); 2 springs for MCL (superior – sMCL and deep - dMCL); 1 spring for LCL. The position was adopted from the ligament definition in the MS model of Thelen [53]. Furthermore, the spring force-displacement relation was adapted from the one used in the MS model, based of Blankevoort et al. [97]. The relation accounts for the nonlinear behavior of ligaments, including both the initial laxity and the progressive tensioning of the fibers. The laxity limit is governed by the linear strain limit (ε_l= 0.03): force is set to 0 for low strains ($0 < \varepsilon < 2*\varepsilon_l$) and increases linearly for higher strains. Stiffness is estimated from literature studies. In our model, the linear strain limit was converted in a displacement value based on spring length, and stiffness was also portioned on the spring length (Table 5). A force-displacement relation for every ligament bundle was imposed in FEBio, as shown in the equations below:

- $L_{lax} = L_0 * (1 + 2 * \varepsilon_l)$
- $dL_{lax} = L_{lax} - L_0$

- $0 < \varepsilon < 2 * \varepsilon_l \quad \rightarrow \quad 0 < dL < dL_{lax}$
- $\varepsilon > 2 * \varepsilon_l \quad \rightarrow \quad dL > dL_{lax}$
- $d = dL - dL_{lax}$

- $\begin{cases} F = 0 & 0 < dL < dL_{lax} \\ F = K * d & dL > dL_{lax} \end{cases}$

L_o: spring rest length; ε_l: linear strain limit; *L_lax*: max spring length in laxity; *dL_lax*: max displacement in laxity; *dL*: total displacement; *d*: displacement in tensioning; *K*: spring stiffness; *F*: ligament force

Ligament bundle	Rest length (mm)	Stiffness (N/mm)	Max displacement in laxity (mm)
amACL	*29.70*	*168*	*1.78*
plACL	*26.89*	*186*	*1.61*
alPCL	*33.25*	*271*	*2.00*
pmPCL	*30.03*	*300*	*1.80*
sMCL	*67.74*	*41*	*4.06*
dMCL	*34.78*	*79*	*2.08*
LCL	*56.90*	*35*	*3.39*

Table 5 *– Ligament bundle properties, expressed as spring parameters. Rest length was calculated from the position of the origin and insertion node; stiffness was taken from literature* [83], [97], [98] *and portioned on spring length; maximal displacement in laxity was calculated with the previous equation (*dL_lax*)*

Boundary conditions

The boundary set was adapted from the initially available data, previously extracted from MS analysis. First, muscle force directions along the stance phase were calculated using an OpenSim plug-in (MuscleForceDirection_v1.0 [99]). Second, a Joint Reaction analysis [100] was performed in OpenSim to recalculate the contact forces at the knee joint, disabling the muscle-tendon actuators of which the muscle force was individually included in the model.

Data exported from OpenSim were further processed in MATLAB: rotations were converted from degrees to radians and data layout was modified to generate compatible input data for FEBio. In total, 42 curves were exported: 33 muscle force curves (x, y and z force for 11 muscles); 3 contact forces (x, y and z force for the knee joint); 6 rotation angles (FL/EXT, IE and ADD/ABD for knee and hip joint) (Table 6). All the curves were imposed to the FE model in FEBio, together with the ligament descriptions (see Section 3.3.2 - *Constraints*) and nine more curves used for the initial positioning of the bodies respect each other. Details on these last curves are provided in the next section.

Step definition and solution

A multistep analysis was performed. Two steps were defined: a first step, the “Displacement step” and a second step, the “Stance step”. The Displacement step was displacement-driven and was used to move the femur towards tibia before applying the MS loads. The Stance step was force-driven and was used to simulate the actual motor task. During both steps, the constraints and springs previously

described (see Section 3.3.2 - *Constraints*) were applied. In the displacement step, nine linear curves were defined: 3 for knee rotations, 3 for knee displacement and 3 for hip rotations. The curves for rotation went from 0 to the value of the first frame of the curves exported from MATLAB. This way, bones were in the correct orientation at the beginning of the Stance step. The curves for displacements were necessary to gradually increase the contact between the cartilage surfaces and obtain contact force values close to their correspondent values in the first frame of the second step. In the second step, the 42 curves of the boundary set (see Section 3.3.2 - *Boundary conditions*) were imposed.
The steps type was "Structural Mechanics". The nonlinear method used for the solution was the BFGS, a *quasi*-Newton method currently implemented in FEBio for its effectiveness in solid mechanics computations [74].

	Displacement step – Initial positioning		Stance step – motor task		
	Translation (in x, y, z)	Rotation (Rx, Ry, Rz)	Muscle forces (in x, y, z)	Contact forces (in x, y, z)	Rotation (Rx, Ry, Rz)
Point of application	• *Knee joint (femur body)*	• *Knee joint (femur body)* • *Hip joint (pelvis body)*	• *MEDGAS* • *LATGAS* • *BFSH* • *VASINT* • *VASLAT* • *VASMED* • *BFLH, SMEM, STEN* • *RECFEM* • *ITB*	• *Knee joint (femur body)*	• *Knee joint (femur body)* • *Hip joint (pelvis body)*

Table 6 *– Boundary set in the model for the case studied. Translations, rotations and contact forces in the joints are applied as "rigid displacement" and "rigid force" to the bodies* [71], [74]*; point of application of the muscles refer to the points on spheres created in PreView, BFLH, SMEM, STEN belong to the same point of the sphere*

3.3.3 *Defect creation – Damaging and Softening*

After the development of the main model (HC), two other models were developed in order to simulate an early OA condition in the knee joint. The second model (DC) accounted for a defect in the cartilage

geometry, while the third model (SC) accounted also for a softening of the cartilage material properties. A superficial defect was created on the medial compartment of the tibial cartilage. The medial compartment is indeed more affected by cartilage defect than lateral [8], [39]–[42]. In detail, the defect was created in a central position on the anterior side of the compartment, since previous studies underlined it to be the most worn location [8], [41]–[43], [63]. The geometry of tibial cartilage was reimported in 3-Matic, where the defect was created. Using the Design tool, a cylinder object with 8mm of diameter was created. The object was moved on the cartilage surface and penetrated the surface for on average a third of the cartilage depth. Next, the cylinder and the cartilage were remeshed together. After that, the cylinder was removed using a sequence of the Boolean union (to create an only surface of cylinder and cartilage) and Boolean subtraction (to separate the two penetrating surfaces) commands, to create a defect in the cartilage (Fig. 14). Last, the cartilage mesh was refined and inspected to obtain the same element size as the "intact" geometry. This newly created geometry contained 42000 elements. Using this process, a defect of 8mm of diameter was induced on the tibial cartilage geometry. The average depth of the defect was 1.1mm (~ 1 element), and maximal depth was 1.4 mm. The defect size was in line with previous literature studies [41]–[43], [51], [101]. The new geometry was then exported to PreView, were the model was rebuilt in the same way already explained in the previous sub-section (3.3.2).

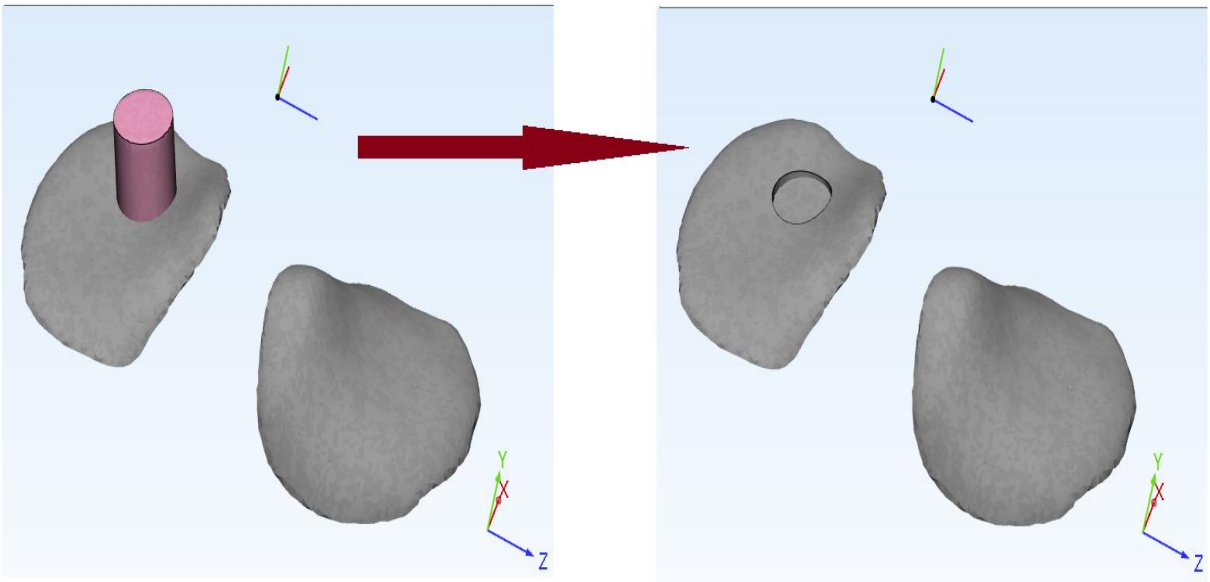

Figure 14 *– Geometry modifications in 3-Matic, creation of the defect on cartilage surfaces. (left) Cylinder element positioned on the surface of the cartilage at the average depth of 1.1mm; (right) Boolean subtraction between the 2 shapes: a circular defect of 8mm in diameter remains on the medial compartment of the tibial cartilage*

The third model, SC, was built in FEBio starting from the DC model. The difference between DC and SC is in a change in cartilage material properties around the defect. A ring of cartilage elements on the rim of the defect was selected: the inner diameter was the same as the defect, the outer diameter was about 2mm larger than the defect (Fig. 15). Material properties of the cartilage in this portion were changed: K was set to 100.7 MPa; C1 was set to 0.5 MPa; C2 and density remained the same. This way, the cartilage properties on the rim were weakened in Young modulus from 10MPa to 3MPa [51], [63] (Poisson ratio was not changed). The weakening simulates the physiological response of cartilage in presence of a defect in early OA: cartilage around defects is softened in order to decrease the pressure on the rim, resulting in a larger contact area [41], [42], [101], [102].

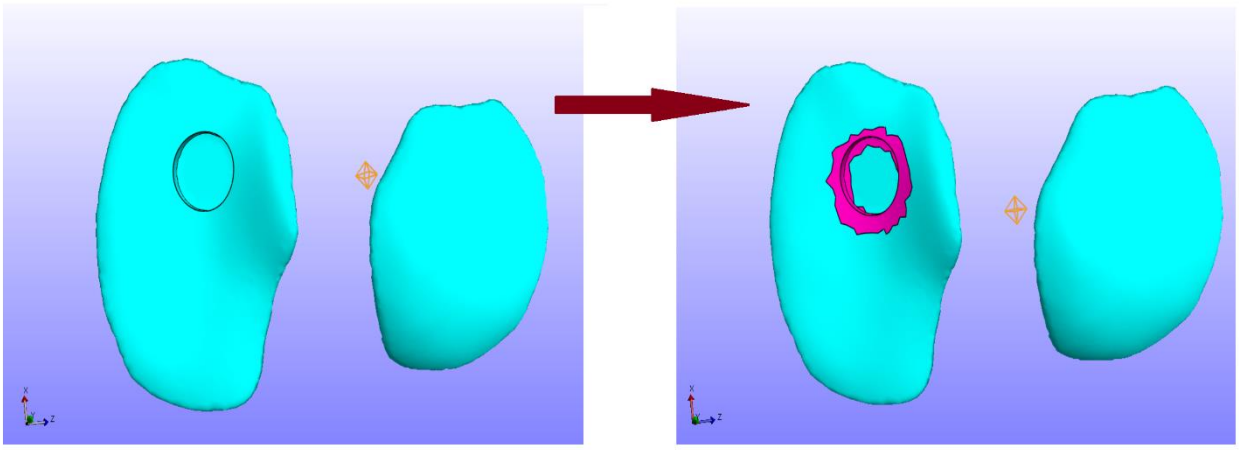

Figure 15 *– Material properties modification, softening at the rim of the defect. K and C1 values of the Mooney-Rivlin material were modified in the SC model, new values were K=100.7 MPa (instead of 335.3 MPa) and C1=0.5 MPa (instead of 1.67 MPa). This way, material properties of the rim were E=3 MPa (instead of 10 MPa) and v=0.495*

Finally, three 3 versions of the knee joint model were developed. These models were then exported to FEBio, to run the FE analysis. The FE analysis was run on a laptop PC (CPU: Intel Core i7-7500U 2.7GHz, RAM: 8GB).

3.3.4 Postprocessing and data analysis

The FE analysis results in two files from FEBio for each of the three models: a log file and a xplt file. The latter can be imported to PostView for the postprocessing.

In PostView, the solution was checked for all the time frames of the Displacement and the Stance step. Firstly, the global motion of the joint was visually inspected. Next, color maps for contact force, contact pressure and contact area were created to consider the magnitudes. The upper limit of the color bar was modified to exclude border artifacts from the visualization. Summary graphs were then inspected, selecting either all the cartilage facets or the spring nodes. Output data were exported to MATLAB for: contact pressure, contact area and nodal position of ligament origins and insertions.

In MATLAB, a further postprocessing of the data was performed both for the FE data, exported from PostView, and for output data of the MS model, available in the initial data set. Since the initial constraint was to fix the tibia in all 6 DoFs and impose all the knee forces and kinematics to the femur, the codes were implemented for tibial cartilage only.

For contact pressure and contact area, both border artifacts and facets never in contact were excluded from the final results. To exclude artifacts, a maximal pressure was set at 60MPa. All the facets, whose values along the steps were higher than the 60MPa, were excluded. In a similar way, a minimal of pressure was set to 0.5MPa. All the facets, whose values along the steps never reach 0.5 MPa, were excluded. Therefore, the data analyses for contact pressure and contact area was only performed for the facets of the cartilage surface involved in the task.

Average values of contact pressure among the facets in the Stance step were calculated and graphically visualized, both for the total and the medial and lateral compartments separately. The results of the FE HC model and of the MS model were compared. Furthermore, the results of the three FE models were compared. Contact areas were estimated in two different ways: first, total contact area (as exported from PostView) and medial/lateral contact area; second, contact area in different portions of the tibial cartilage. To implement the second estimation, the surface area of both medial and lateral cartilage was divided in 4 portions: 1°M, 2°M, 3°M, 4°M (M= medial compartment); 1°L, 2°L, 3°L, 4°L (L= lateral compartment) (Fig. 16). Thus, the contact area was extracted for every single portion. This allowed the identification of the location of the contact along the Stance phase and the comparison among the models.

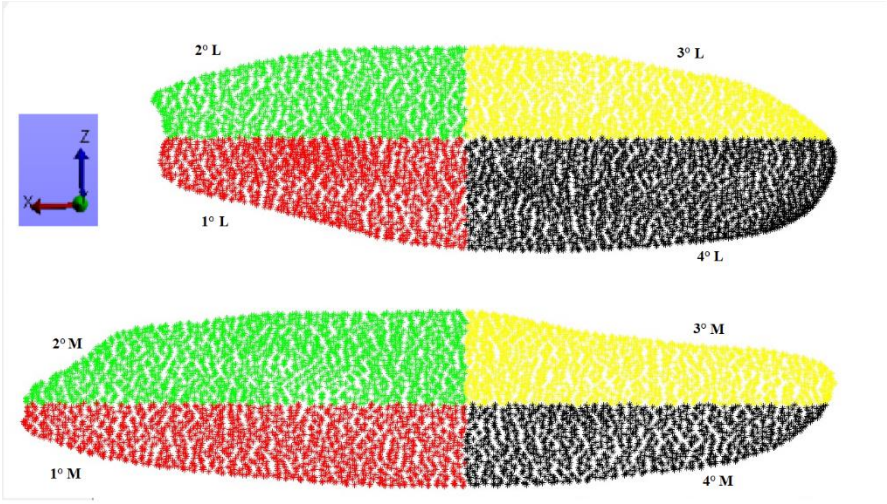

Figure 16 *– Division of tibial cartilage surface in 4 portions per compartment. The division was implemented in MATLAB using the coordinates of the facet centers. The facets in contact could then be assigned to one of the 8 portions for a better localization of the contact during the motor task*

Standard deviation of the contact pressure was calculated and graphically visualized together with the average. Peak values were extracted for all contact pressure and contact area curves and compared between the models. The linear correlation (R^2) between the models was calculated and the Mann-Whitney U Test ($p<0.05$) [103] was performed to evaluate differences between the models for the average contact pressure over the entire stance phase. Lastly, ligament force was estimated from the position of the insertion and origin nodes. The length of the springs was calculated for all the time frames and used to extract the total displacement (dL). The max displacement in laxity was then subtracted from dL, and the final value was multiplied by the stiffness to obtain the force. The force below 0 was not considered, as it was the laxity zone:

- $dL = L - L_0$
- $d = dL - L_{lax}$

- $F = K * d \qquad d > 0$

dL: total displacement; *L*: spring length per time frame; L_o: spring length at first frame (equal to spring rest length); *dL_lax*: max displacement in laxity; *d*: displacement in tensioning; *K*: spring stiffness; *F*: ligament force

This way, it was possible to compare ligament forces extracted from the FE model with ligament forces initially available in the MS model data set.

Chapter 4 – RESULTS

The FE analysis of the stance phase in the newly developed FE model was successfully performed for all the three model versions, the healthy, damaged and softened cartilage models (HC, DC and SC respectively). In this chapter, the contact pressure, the contact area and the strain are shown separately for each version of the FE model. Comparisons between the models are also provided for each model version: the HC model was compared to the MS model; the DC model to the HC model; the SC model to the DC and the HC models. Graphs, tables with numerical results, comparisons between the models and graphic visualization from PostView are provided for each model in the following sub-sections.

Overall, the results obtained with the FE model were comparable with the results of the MS model of Van Rossom et al. [34]. Furthermore, the trends of the contact pressure and contact area in the HC, DC and SC models were similar. Slight differences in magnitude were observed between the models, especially between the intact cartilage and the defect models.

The global trend of the curves showed two main peaks of contact pressure on the tibia cartilage, approximately on the 22% and the 77% of the stance phase, and a minimum at about the 48% of the stance phase. The first peak corresponds to the initial loading response of the right leg in double support, the minimum corresponds to the midstance in single support and the second peak corresponds to terminal stance in single support.

Contact pressure trends in the medial and lateral compartment differed from the MS model, and this difference was also visible in the contact area location.

4.1 *"Healthy Cartilage" – HC model*

The values of contact pressure and contact area for the HC model are summarized in Table 7. Comparison between the results of the HC model and the results of the MS model are also provided (Table 8).

The total time required for solving the HC model in FEBio was 15 hours and 53 minutes.

Trends of contact pressure and contact area of the HC model are provided in Fig. 17 and Fig. 18.

The average contact pressure at the first peak was 4.31 MPa. More specific, the average pressure on the medial compartment was 4.48 MPa and on the lateral compartment 4.18 MPa. At the second peak, the average contact pressure was 5.13 MPa. Pressure on the medial compartment was 5.42 MPa and

on the lateral compartment was 4.84 MPa. Standard deviation was high over the different elements, with a maximum of 9 MPa at the time of the second peak.

The total contact area at the first peak was 339 mm^2, with 127 mm^2 on the medial compartment and 211 mm^2 on the lateral compartment. At the second peak, the total contact area was 288 mm^2. In addition, the contact area on the medial compartment was lower than the contact area on the lateral compartment, with 83 mm^2 vs 205 mm^2 respectively. Furthermore, on the medial compartment there was only contact in anterior portions over the entire stance phase. The percentage of total area in contact in the compartment was lower in the 1° M portion than in the 2° M, respectively 9% and 91%. On the lateral compartment, contact area was more distributed among the portions over the entire stance phase. However, about 70% of the total was on the anterior portions, with a maximum of 36% on the 2° L portion.

The first (tensile) and the third (compressive) principal components of the Lagrangian strain at the peaks were maximum about 19% and −20%, respectively.

Overall, the HC model and the MS model showed a similar trend and the average contact pressure was comparable during the gait (Fig. 19). The correlation between the average contact pressure of the two models was R^2 = 0.938. No significant difference (p=0.0558) between the two models were visible through the Mann-Whitney U Test in terms of average contact pressure. In the HC model, the contact pressure was slightly higher than in the MS model in the first and the second peak, 19% and 29% higher, respectively. In the initial 10% of the stance phase higher values were also observed. Standard deviation was lower in the MS model than in the FE model, the maximum difference at the second peak, 4MPa and 9MPa, respectively (Fig. 20). The medial contact pressure differed more than the lateral from the trend of the MS model (Fig. 21, Fig. 22). A graphic visualization of contact pressure in PostView for the HC model is provided in Fig. 23.

	HC MODEL						HC vs MS models					
	Average Contact Pressure (MPa)			Contact Area (mm^2)			Average Contact Pressure (% difference)			Contact Area (% difference)		
	Total	Medial	Lateral	Total	Medial	Lateral	Total	Medial	Lateral	Total	Medial	Lateral
1st Peak	*4.31*	*4.48*	*4.18*	*339*	*127*	*211*	*+19*	*+34*	*+2*	*+11*	*-22*	*+51*
2nd Peak	*5.13*	*5.42*	*5.84*	*288*	*83*	*205*	*+29*	*+23*	*+36*	*-29*	*-61*	*+7*

Table 7 *– Summary of results for the HC model of the contact pressure and the contact area on the tibial cartilage. (left) Average contact pressure and contact area on peaks; (right) Average contact pressure and contact area comparison between the HC model and the MS model*

HC MODEL	1°M	2°M	3°M	4°M	1°L	2°L	3°L	4°L
Area per portion (% of total area)	*16 (9%)*	*179 (91%)*	*0 (0%)*	*0 (0%)*	*139 (33%)*	*151 (36%)*	*61 (14%)*	*73 (17%)*

Table 8 *– Summary of results for the HC model: area per portion (see Fig. 16) in mm^2 and in % of total area in contact. M= medial compartment, L= lateral compartment*

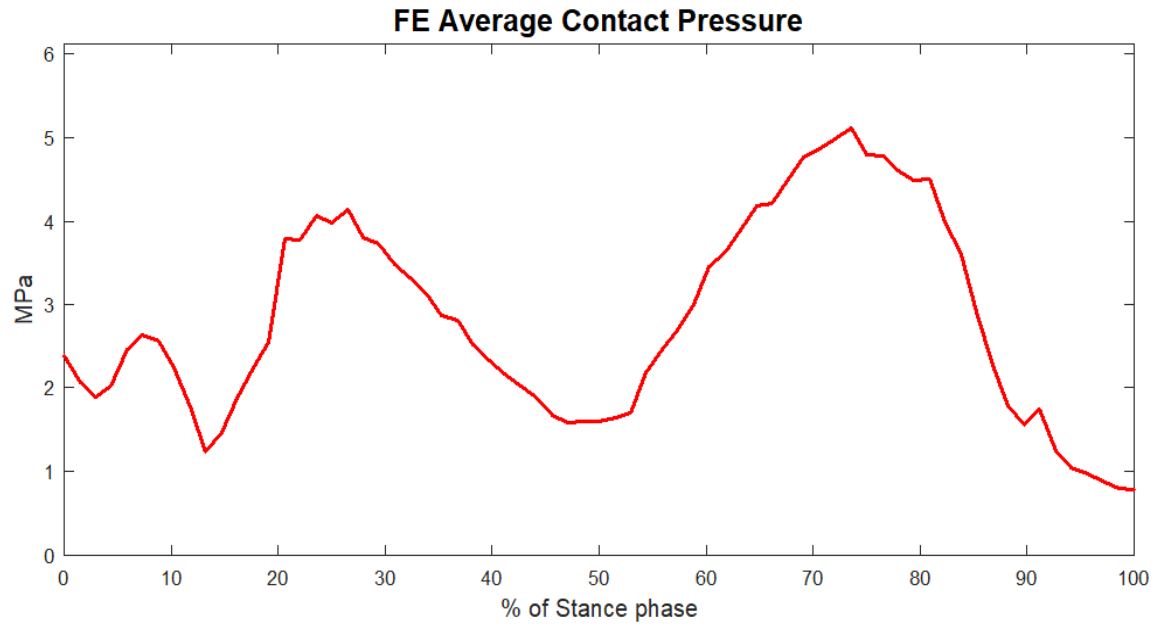

Figure 17 *– HC model: total average contact pressure in tibial cartilage over the entire stance phase*

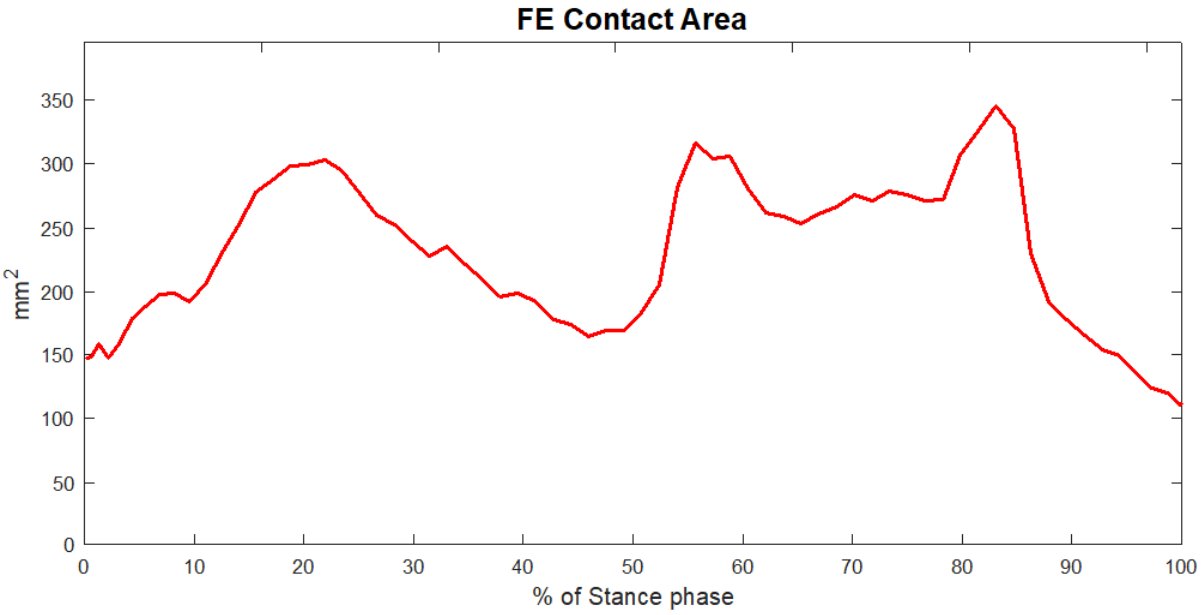

Figure 18 *– HC model: total contact area in tibial cartilage over the entire stance phase*

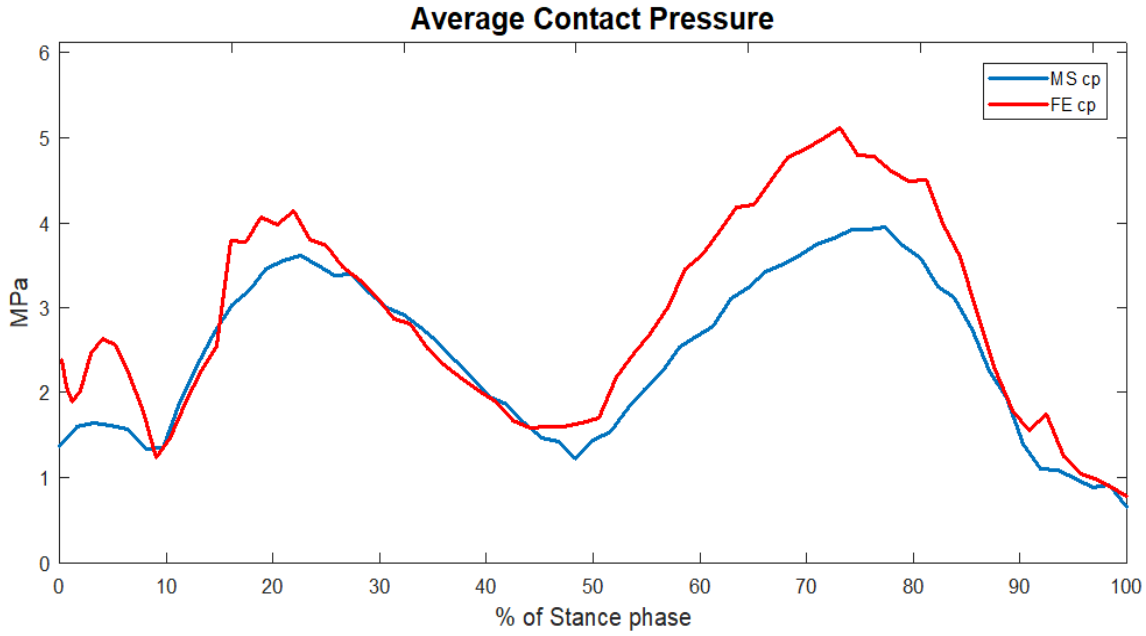

Figure 19 *– Comparison between the HC model (red) and the MS model (blue): total average contact pressure in tibial cartilage over the entire stance phase*

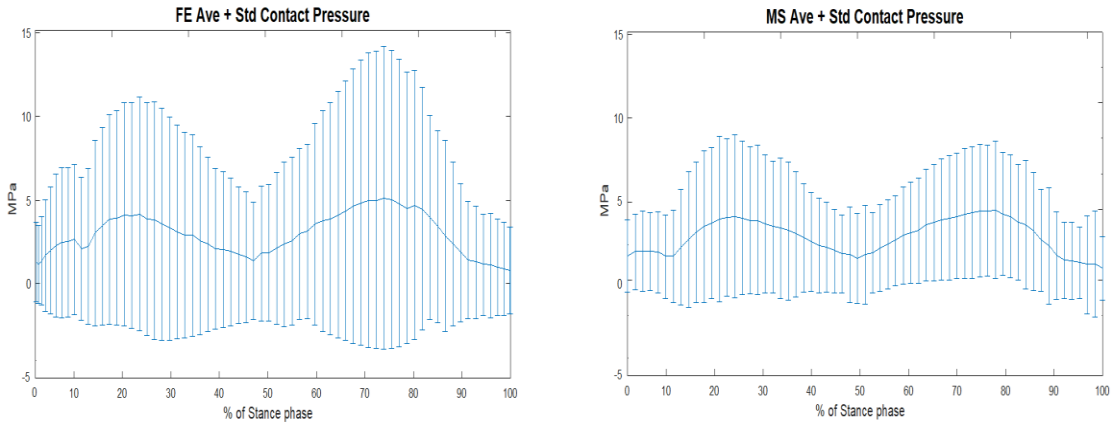

Figure 20 *– Comparison between the HC model (left) and the MS model (right): total average contact pressure + standard deviation in tibial cartilage over the entire stance phase*

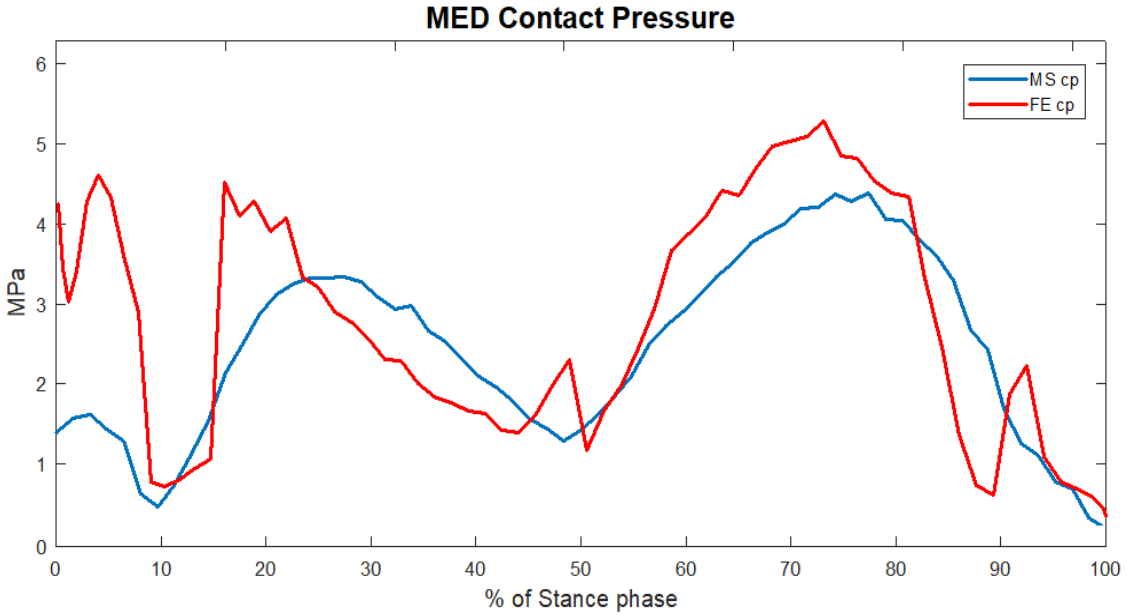

Figure 21 *– Comparison between the HC model (red) and the MS model (blue): average contact pressure on the medial compartment of the tibial cartilage over the entire stance phase*

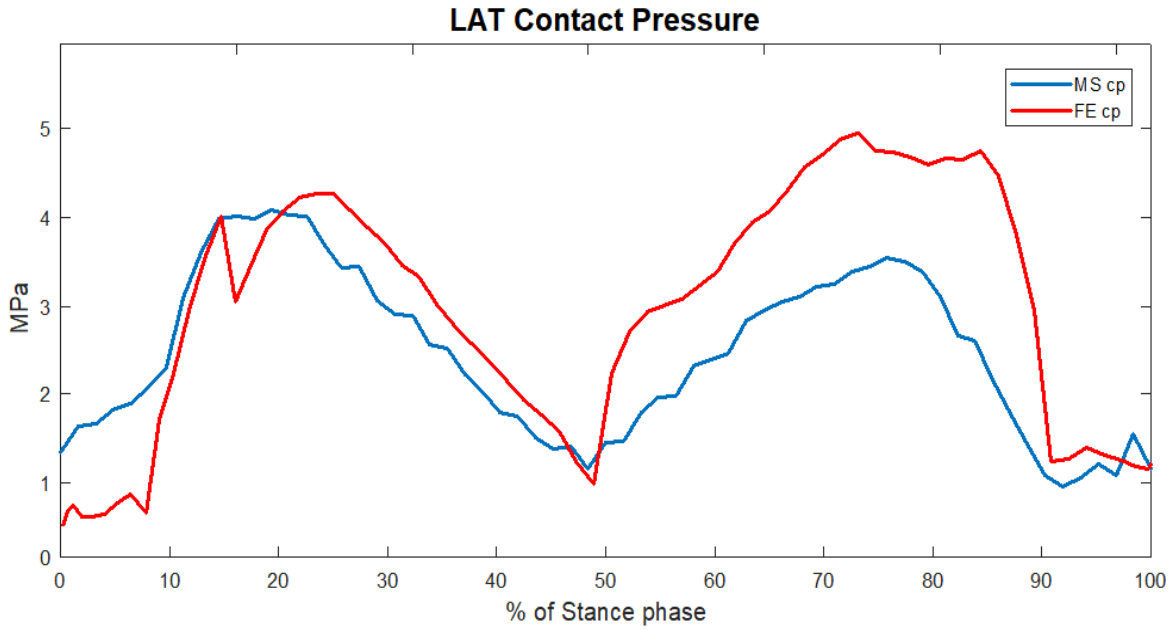

Figure 22 *– Comparison between the HC model (red) and the MS model (blue): average contact pressure on the lateral compartment of the tibial cartilage over the entire stance phase*

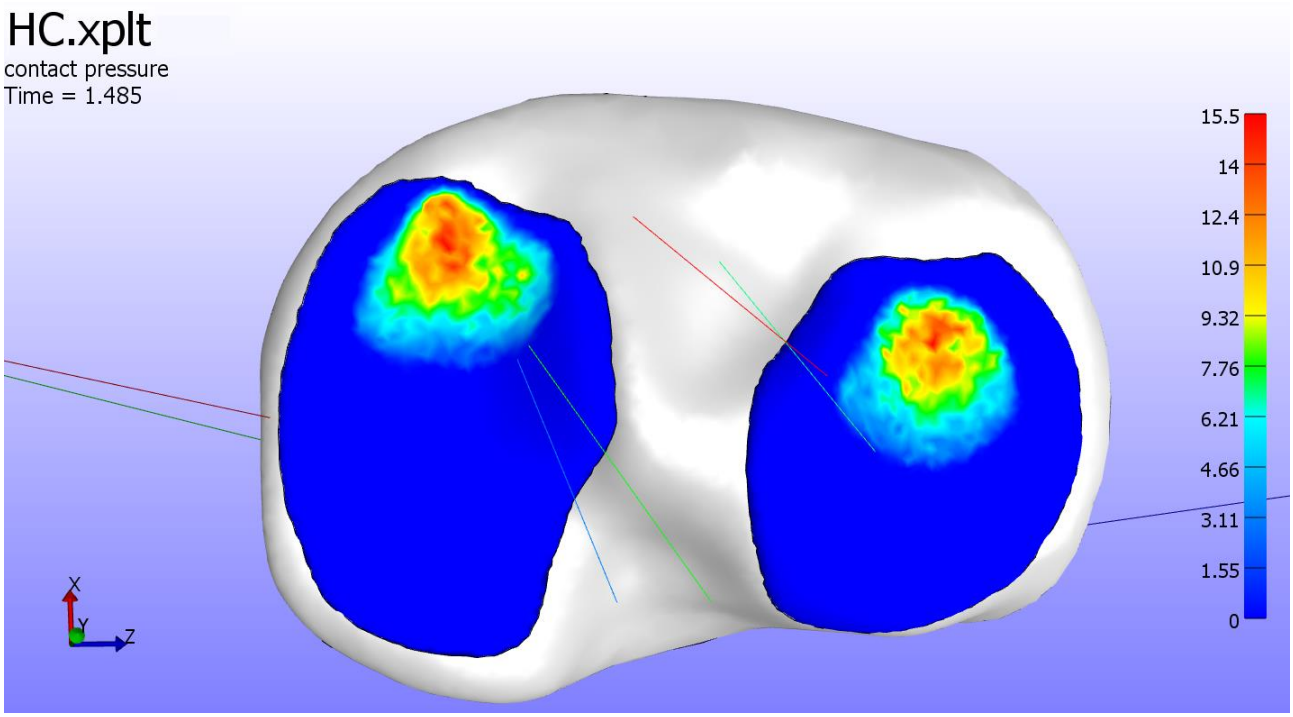

Figure 23 *– HC model: contact pressure on the second peak of stance phase (Figure extracted from PostView). Values in the colormap are expressed in MPa*

4.2 *"Damaged Cartilage" model*

The values of the contact pressure and contact area for the DC model are summarized in Table 9.
A comparison between the results of the DC model and the results of the HC model are also provided (Table 10).
The total time required for solving the DC model in FEBio was 16 hours and 11 minutes.
Trends of contact pressure and contact area of the DC model are provided in Fig. 24 and Fig. 25.
The average contact pressure at the first peak was 5.76 MPa. Specifically, on the medial compartment the pressure was 7.89 MPa and on the lateral compartment 4.52 MPa. At the second peak, the average contact pressure was 5.39 MPa. The pressure on the medial compartment was 5.33 MPa and the pressure on the lateral compartment was 5.49 MPa. As the HC model, standard deviation was high over the entire stance phase (maximum 9.20 MPa, at the second peak).
Total contact area at the first peak was 244 mm^2, with 130 mm^2 on the medial compartment and 114 mm^2 on the lateral compartment. At the second peak, total contact area was 267 mm^2. As in the HC model, the contact area on the medial compartment was lower than on the lateral compartment: 68 mm^2 vs 199 mm^2 respectively. The contact area on the medial compartment was equally divided among the 4 portions: the highest was on 2° M portion, 27%, and lowest was on 4° M portion, 22%. On the lateral compartment, the contact area was about 70% on the anterior portions, as the HC model.
The first (tensile) and the third (compressive) principal components of the Lagrangian strain at the peaks were maximum about 62% and −36%, respectively.
Overall, the DC model showed higher peak contact pressure then the HC model (Fig. 26). Especially at the first peak, the average contact pressure was 33% higher, while at the second peak it was 5% higher. The medial compartment sustained the highest stress: the contact pressure was 75% higher than in the same compartment of the HC model (Fig. 27, Fig. 28). Furthermore, at the first peak, the contact area was lower for the DC model than for the HC model. The correlation between the average contact pressure of the two models was $R^2 = 0.921$. Significant difference ($p=0.0346$) between the two models were visible through the Mann-Whitney U Test in terms of average contact pressure. A graphic visualization of contact pressure in PostView for the DC model is provided in Fig. 29.

	DC MODEL						DC vs HC models					
	Average Contact Pressure (MPa)			Contact Area (mm^2)			Average Contact Pressure (% difference)			Contact Area (% difference)		
	Total	Medial	Lateral	Total	Medial	Lateral	Total	Medial	Lateral	Total	Medial	Lateral
1st Peak	*5.76*	*7.89*	*4.52*	*244*	*130*	*114*	*+33*	*+75*	*+12*	*-28*	*+1*	*-46*
2nd Peak	*5.39*	*5.30*	*5.49*	*267*	*68*	*199*	*+5*	*-2*	*+13*	*-7*	*-17*	*-3*

Table 9 *– Summary of results for the DC model of the contact pressure and the contact area on the tibial cartilage. (left) Average contact pressure and contact area on peaks; (right) Average contact pressure and contact area comparison between the DC model and the HC model*

DC MODEL	1°M	2°M	3°M	4°M	1°L	2°L	3°L	4°L
Area per portion (% of total area)	*44 (26%)*	*47 (28%)*	*41 (24%)*	*37 (22%)*	*140 (33%)*	*140 (33%)*	*60 (16%)*	*74 (18%)*

Table 10 *– Summary of results for the DC model: area per portion (see Fig. 16) in mm^2 and in % of total area in contact. M= medial compartment, L= lateral compartment*

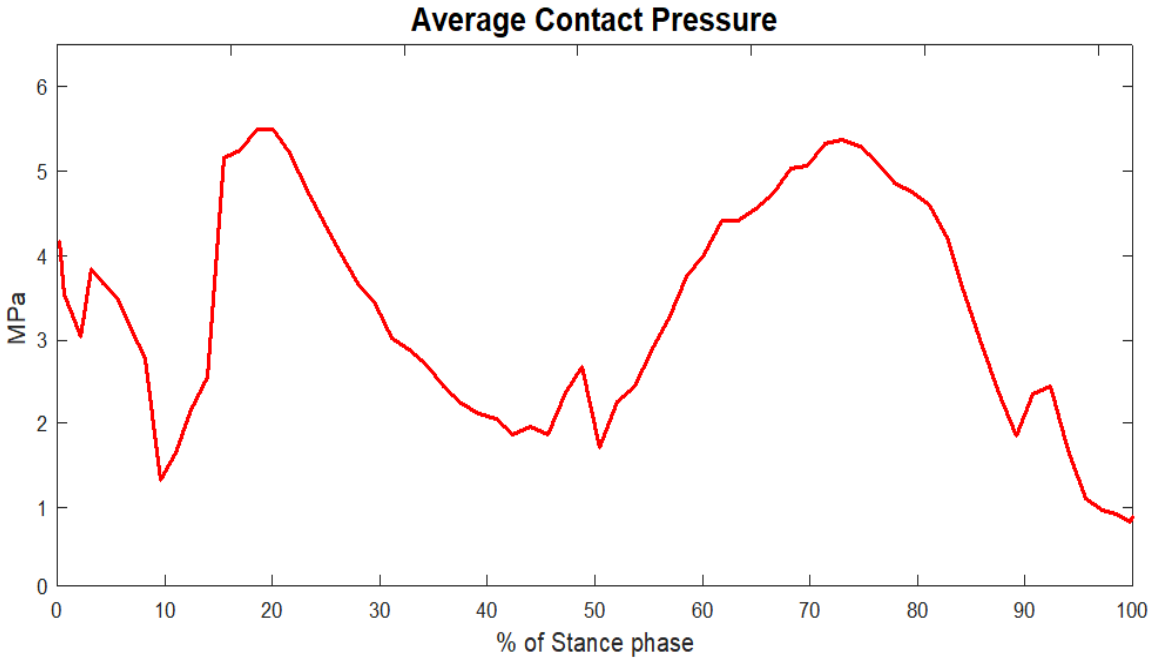

Figure 24 *– DC model: total average contact pressure in tibial cartilage over the entire stance phase*

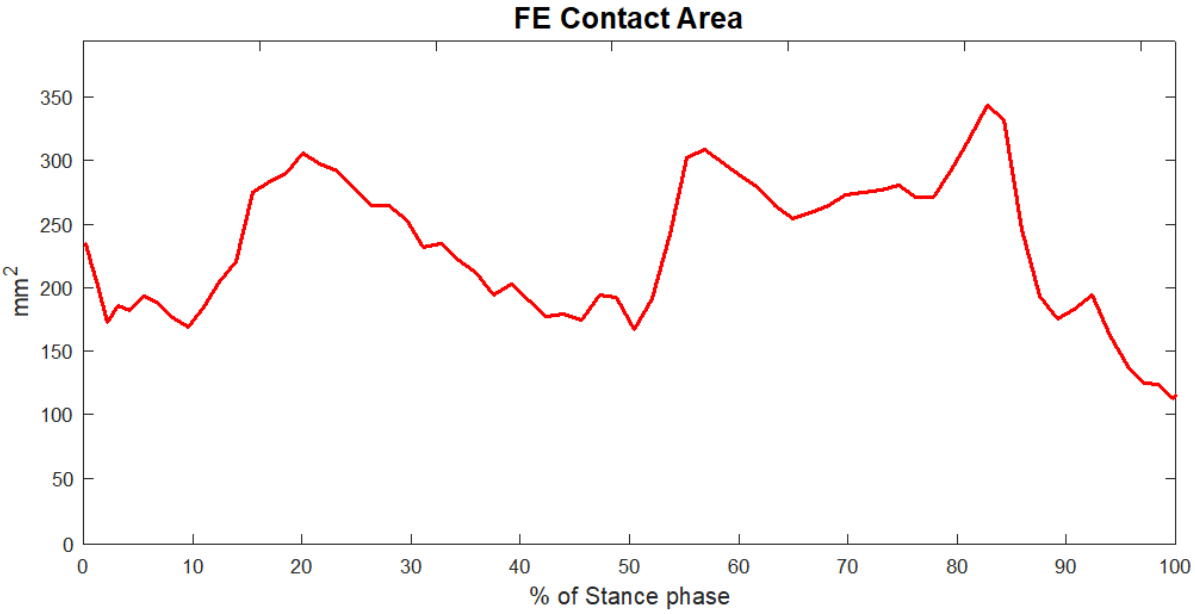

Figure 25 *– DC model: total contact area in tibial cartilage over the entire stance phase*

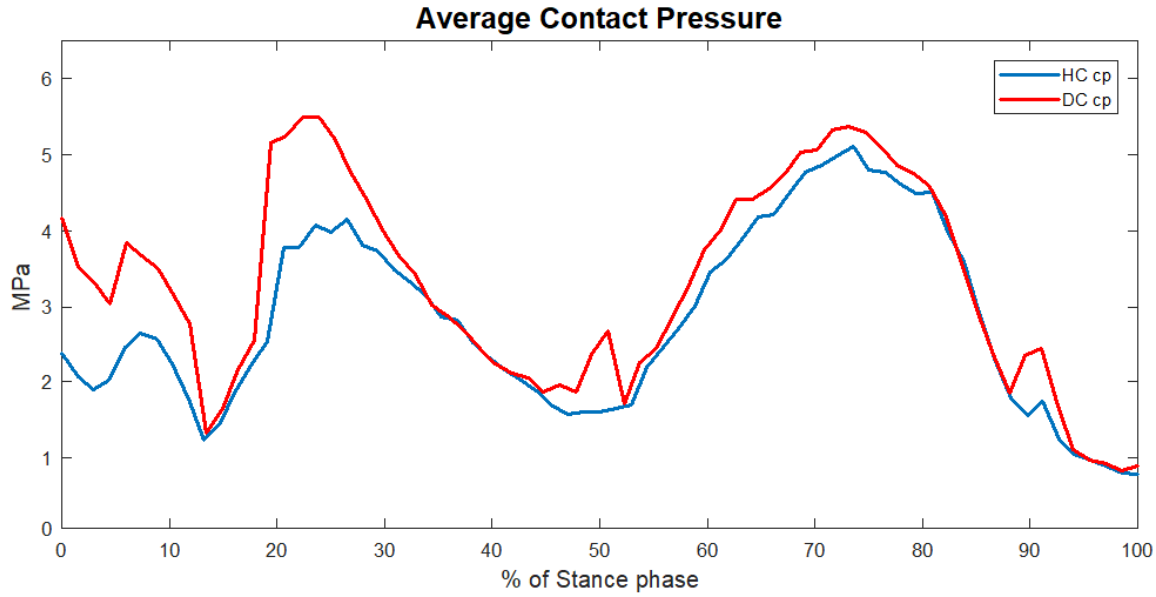

Figure 26 *– Comparison between the DC model (red) and the HC model (blue): total average contact pressure in tibial cartilage over the entire stance phase*

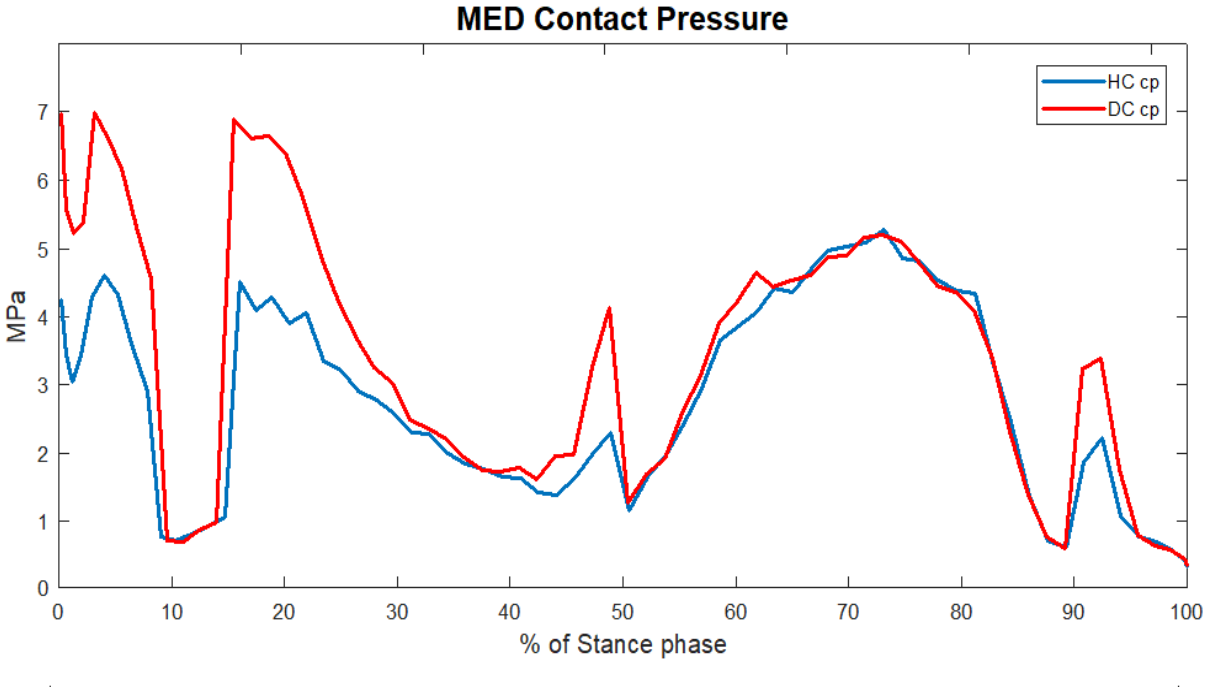

Figure 27 *– Comparison between the DC model (red) and the HC model (blue): average contact pressure on the medial compartment of the tibial cartilage over the entire stance phase*

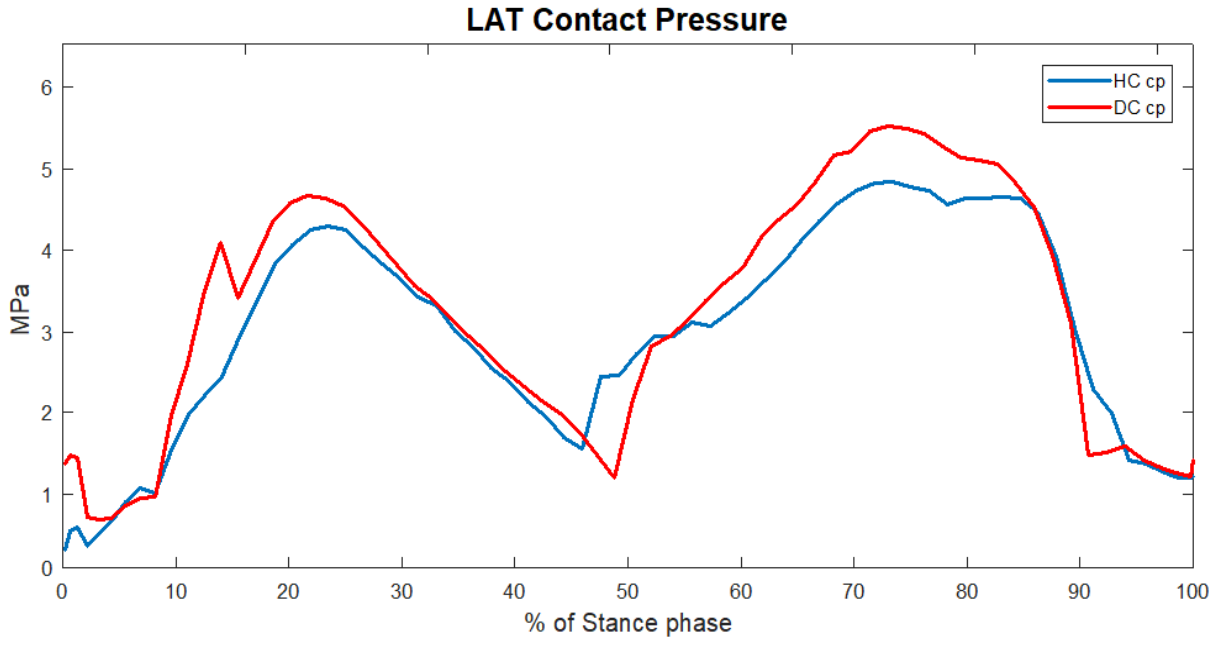

Figure 28 *– Comparison between the DC model (red) and the HC model (blue): average contact pressure on the lateral compartment of the tibial cartilage over the entire stance phase*

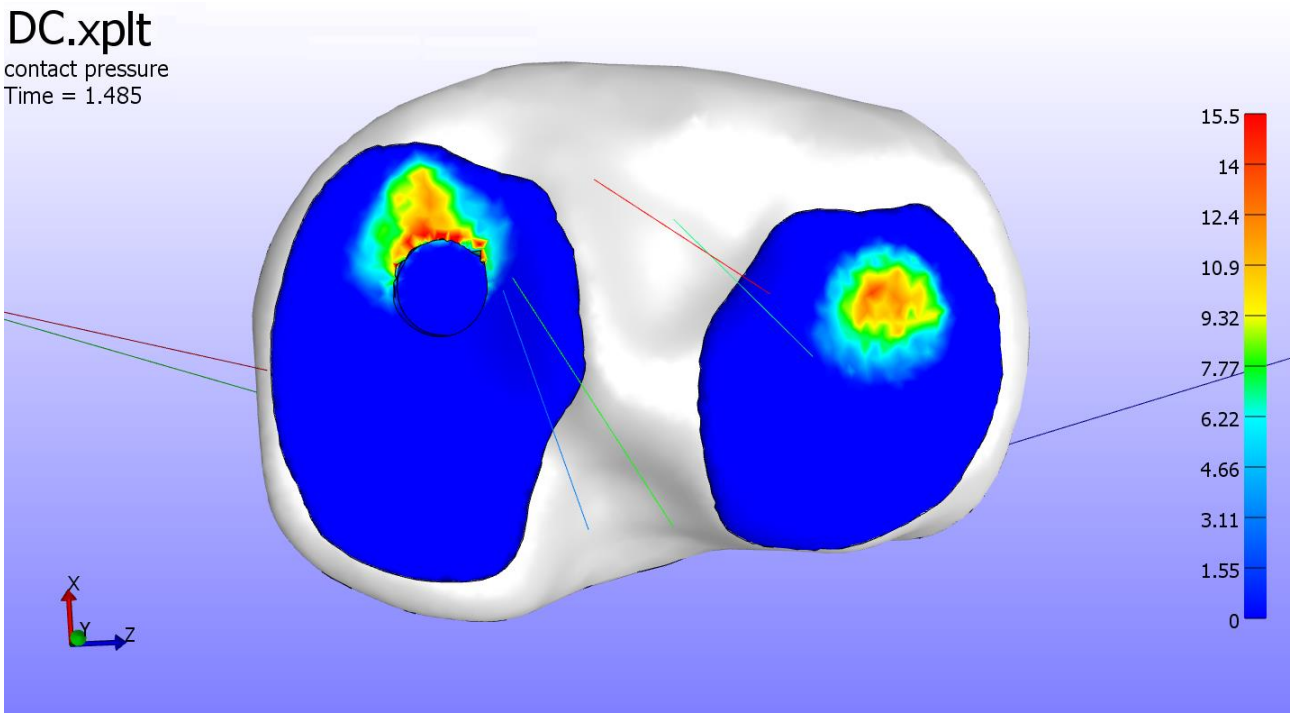

Figure 29 *– DC model: contact pressure on the second peak of stance phase (Figure extracted from PostView). Values in the colormap are expressed in MPa*

4.3 *"Softened Cartilage" model*

The values of the contact pressure and contact area for the SC model are summarized in Table 11. Comparison between the results of the SC model and the results of the DC model and HC model are also provided (Table 12).

The total time required for solving the SC model in FEBio was 14 hours and 36 minutes.

Trends of contact pressure and contact area of the SC model are provided in Fig. 30 and Fig. 31.

The average contact pressure at the first peak was 5.23 MPa. Specifically, on the medial compartment pressure was 6.26 MPa and on the lateral compartment 4.74 MPa. At the second peak, the average contact pressure was 5.18 MPa. The pressure on the medial and the lateral compartment was similar, 5.17 MPa and 5.19 MPa, respectively. As the previous models, standard deviation was high over the entire stance phase.

Total contact area at the first peak was 299 mm^2, of which 170 mm^2 on the medial compartment and 129 mm^2 on the lateral compartment. At the second peak, the total contact area was 297 mm^2, where the contact area on the medial compartment was lower than on the lateral compartment: 84 mm^2 vs 213 mm^2. The contact area on the medial compartment was divided over the 4 portions, although higher on the anterior than on the posterior portions. On the lateral compartment, contact area was more equally divided, only higher on the 4° L portion (35%).

The first (tensile) and the third (compressive) principal components of the Lagrangian strain at the peaks were maximum about 73% and −40%, respectively.

Overall, the SC model showed similar peak contact pressure as the DC model. Specifically, the second peak average pressure was the same in the two models, while the first peak average was lower in the SC than the DC model (9% less) but higher than the HC model (20% higher) (Fig. 32). However, the contact pressure at the first peak on the medial compartment was lower than for the DC model. For all the other portions, the contact pressures were comparable. The trend of the medial and the lateral contact pressures was in agreement with the average trends (Fig. 33, Fig. 34). Finally, the contact area in the SC model was higher than in the DC and the HC models, particularly on the medial compartment. The correlation between the average contact pressure of the SC and DC models was R^2 = 0.937, while between the SC and the HC models was R^2 = 0.893. No significant difference (p=0.404 SC vs DC and p=0.121 SC vs HC) between the models were visible through the Mann-Whitney U Test in terms of average contact pressure. A graphic visualization of the contact pressure in PostView for the DC model is provided in Fig. 35.

	SC MODEL						SC vs DC models						SC vs HC models					
	Average Contact Pressure (MPa)			Contact Area (mm^2)			Average Contact Pressure (% difference)			Contact Area (% difference)			Average Contact Pressure (% difference)			Contact Area (% difference)		
	Total	Medial	Lateral	Total	Medial	Lateral	Total	Medial	Lateral	Total	Medial	Lateral	Total	Medial	Lateral	Total	Medial	Lateral
1st Peak	*5.23*	*6.26*	*4.74*	*299*	*170*	*129*	*-9*	*-21*	*+1*	*+22*	*+30*	*+13*	*+21*	*+39*	*+13*	*-11*	*+32*	*-38*
2nd Peak	*5.18*	*5.17*	*5.19*	*297*	*84*	*213*	*-4*	*-3*	*-5*	*+11*	*+23*	*+6*	*+1*	*-4*	*+7*	*+3*	*+2*	*+3*

Table 11 *– Summary of results for the SC model of the contact pressure and the contact area on the tibial cartilage. (left) Average contact pressure and contact area on peaks; (middle) Average contact pressure and contact area comparison between the SC model and the DC model;(right) Average contact pressure and contact area comparison between the SC model and the HC model*

SC MODEL	1°M	2°M	3°M	4°M	1°L	2°L	3°L	4°L
Area per portion (% of total area)	*33 (31%)*	*36 (28%)*	*26 (20%)*	*26 (21%)*	*82 (22%)*	*79 (21%)*	*82 (22%)*	*127 (35%)*

Table 12 *– Summary of results for the SC model: area per portion (see Fig. 16) in mm^2 and in % of total area in contact. M= medial compartment, L= lateral compartment*

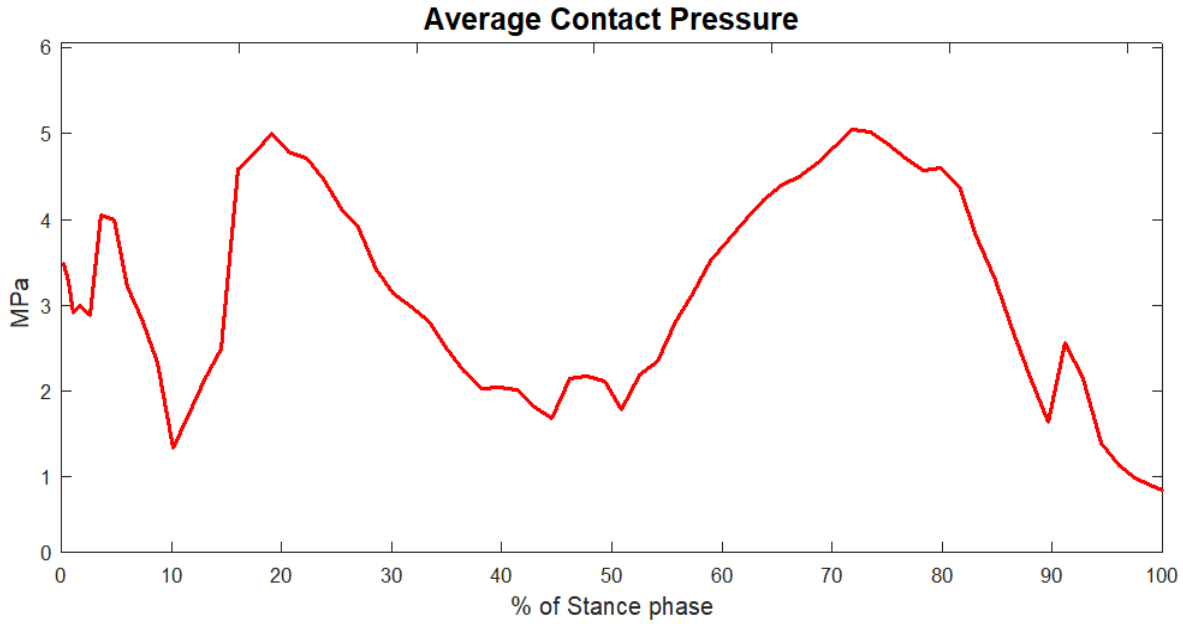

Figure 30 *– SC model: total average contact pressure in tibial cartilage over the entire stance phase*

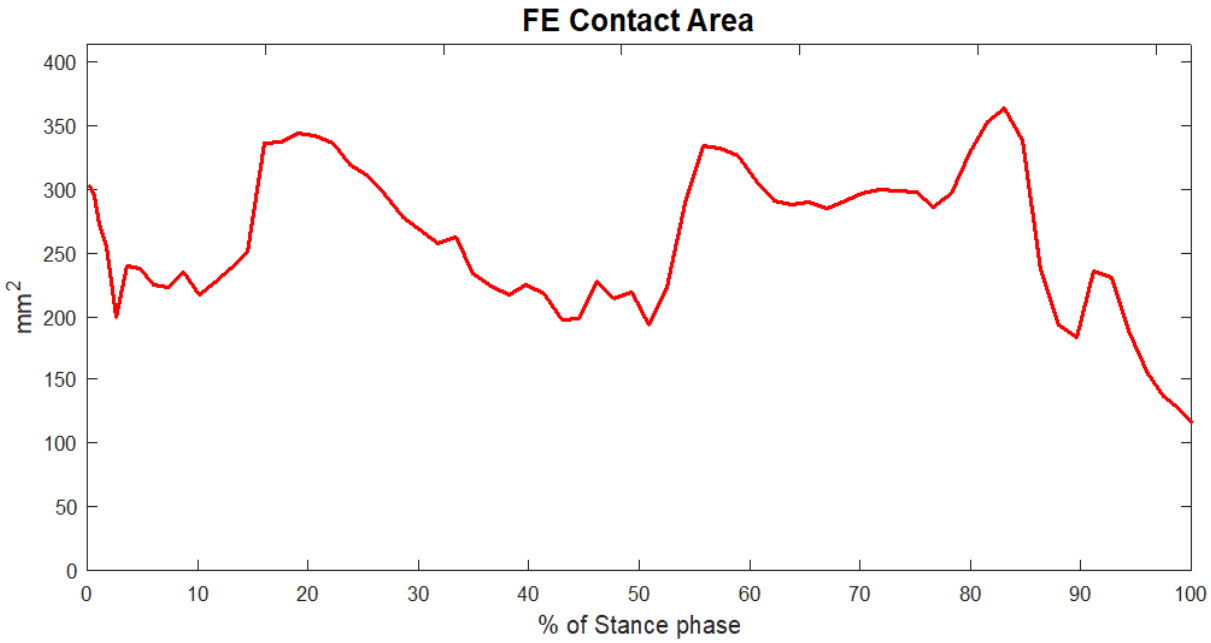

Figure 31 *– SC model: total contact area in tibial cartilage over the entire stance phase*

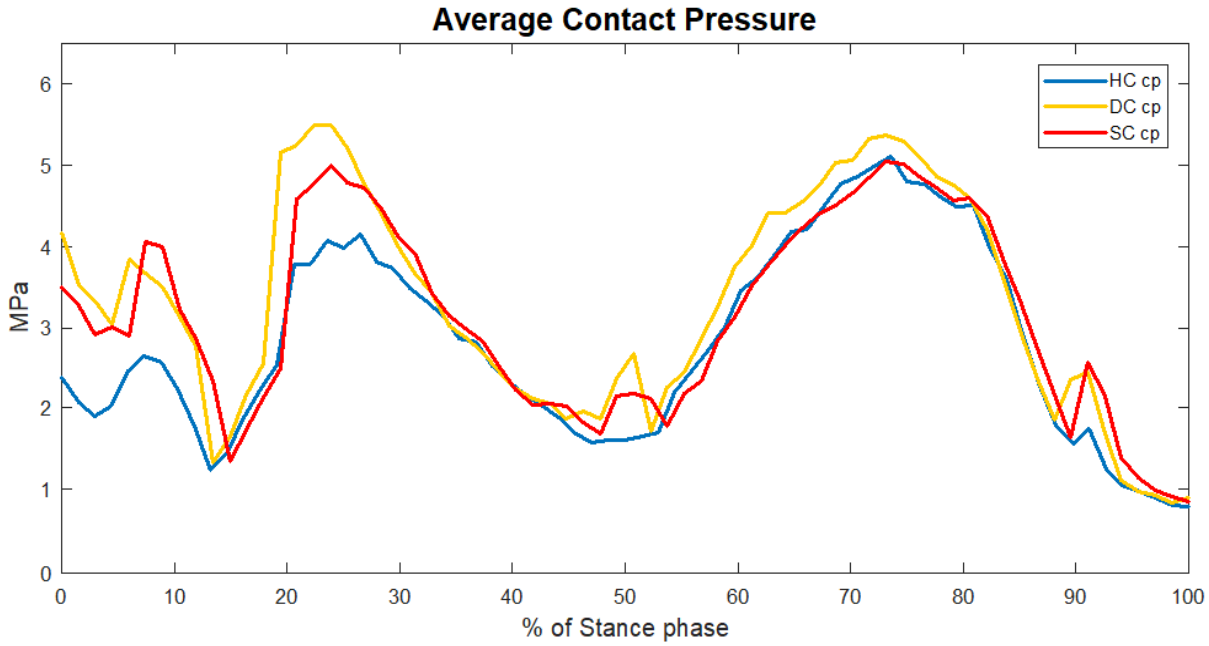

Figure 32 *– Comparison among the SC model (red), the DC model (yellow) and the HC model (blue): total average contact pressure in tibial cartilage over the entire stance phase*

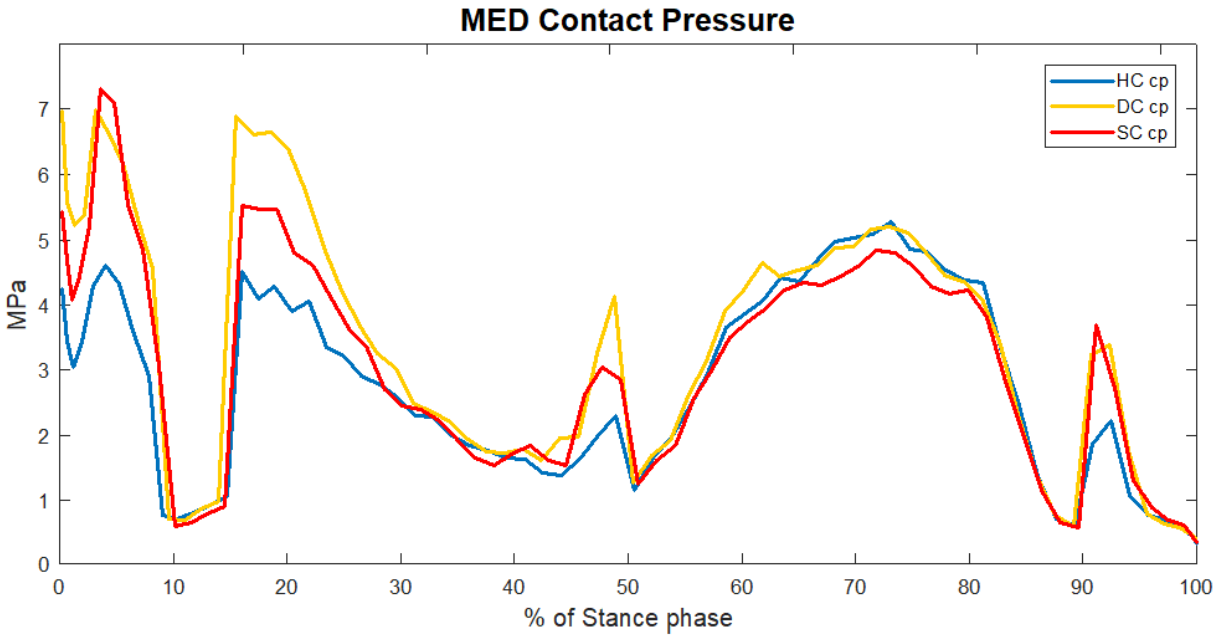

Figure 33 *– Comparison among the SC model (red), the DC model (yellow) and the HC model (blue): average contact pressure on the medial compartment of the tibial cartilage over the entire stance phase*

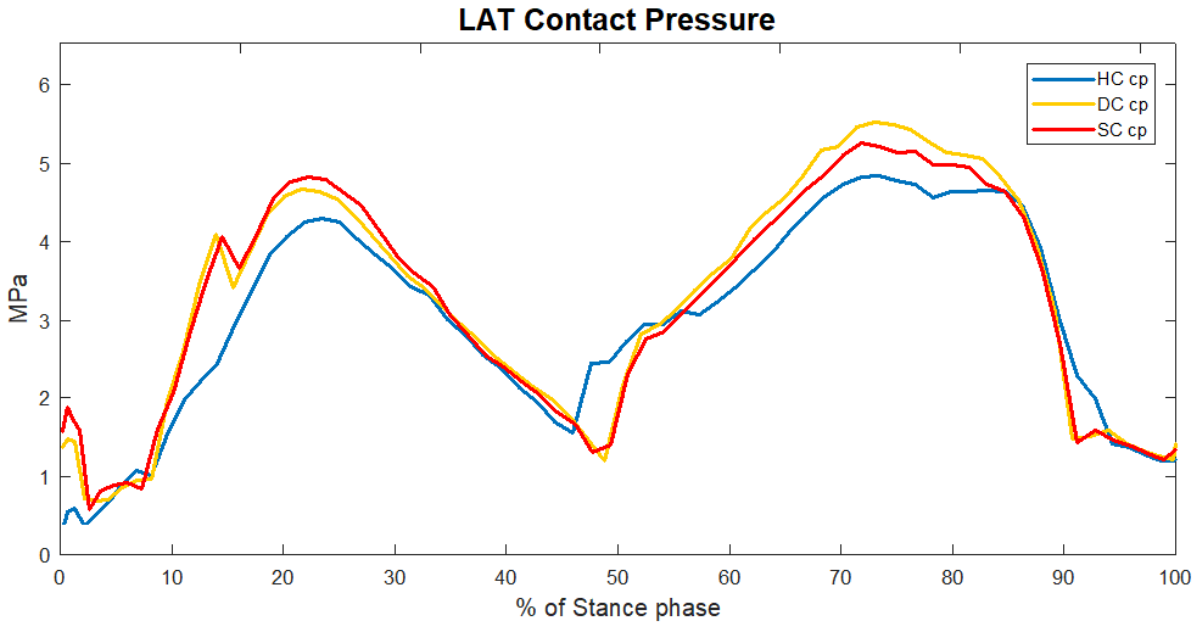

Figure 34 *– Comparison among the SC model (red), the DC model (yellow) and the HC model (blue): average contact pressure on the lateral compartment of the tibial cartilage over the entire stance phase*

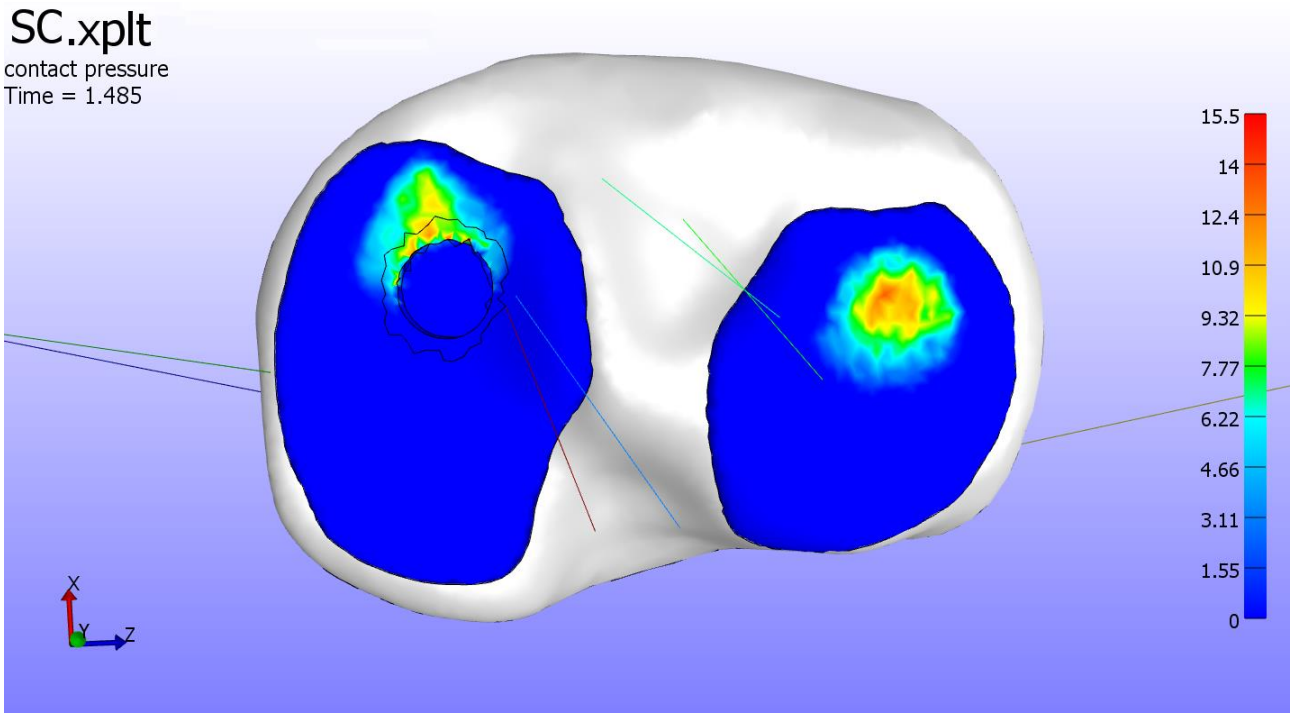

Figure 35 *– SC model: contact pressure on the second peak of stance phase (Figure extracted from PostView). Values in the colormap are expressed in MPa*

Chapter 5 – DISCUSSION

The purpose of this Master Thesis was to evaluate cartilage contact pressure in the knee during walking. We aimed to perform a FE analysis on cartilage both in healthy and degenerated conditions, using a subject-specific FE model of the knee joint that we developed for this purpose. Specifically, we had two objectives. First, to compare knee contact pressure obtained with the newly developed FE model in the cartilage of a healthy subject with knee contact pressure obtained using a previously developed musculoskeletal (MS) model that included an elastic foundation formulation at the knee joint [34], [53], [55]. Second, to analyze knee contact pressure and strain in a degenerated cartilage mimicking early OA during the same walking condition, by using the same FE model with simulated changes in geometry and material properties of the cartilage.

We hypothesized an agreement between the results of the FE model with intact cartilage ("Healthy Cartilage" or HC") and the results of the MS model, in terms of magnitude and trends of contact pressure. We also hypothesized contact pressure and strain in the FE models with the simulated OA defect ("Damaged Cartilage" or "DC" and "Softened Cartilage" or "SC") to be higher than contact pressure and strain in the HC model.

Our simulation confirmed: (I) a good agreement between the cartilage contact pressure in healthy conditions obtained with our FE model and that obtained from the previously-developed MS model, and (II) an increase in contact pressure and strain in degenerated conditions mimicking early OA compared to the intact conditions. Our results were also comparable to the FE models reported in literature (see Section 1.3.2 and Section 5 - *Literature comparison*).

In all three FE models (i.e. HC, DC and SC), the first and the second peak in cartilage contact pressure were, respectively, at 20-25 % and 75-80 % of the stance phase, and the minimum was at 45-50 % (see Section 4). The contact pressure differed between the two peaks in all the three models, as it was highly influenced by kinematics and muscle forces (especially in the intact model) and by geometry (in the models with the defect). In intact cartilage conditions, contact pressure at the second peak was the highest, as the knee was in extension and the gastrocnemii (the strongest muscles in the stance phase for the knee joint [104]) were mostly active there, in y-direction. Conversely, at the first peak, while the knee was in flexion, the vasti were mostly active, but contact force lower than gastrocnemii and was more equally divided in x- and y-direction. In OA mimicking conditions, the change in geometry influenced the contact pressure more than the boundary conditions. This is in line with the MS model and other literature studies [34], [53], [55], [63], [64].

We found a global agreement between the trend curves of the HC and the results of the MS model ($p=0.0558$), except for slight differences in the peak values discussed later. This showed how the two

models, under similar boundary conditions, produced similar results. Significant differences (p=0.0346) were observed between the FE model with the intact cartilage and the FE models mimicking early OA, specifically in terms of contact pressure and strain at the peaks and contact distribution. This demonstrated that the presence of the defect in the geometry strongly affected the global trend of the results of the DC model. In the SC model, the softening of the cartilage surface around the defect rim affected the contact pressure and the strain over the entire stance phase and induced a different pressure distribution in the entire tibial cartilage. This was also in line with our hypothesis on the relation between the cartilage contact pressure and the time evolution of the OA defect.

HC model

The average contact pressure in the HC model was comparable with the average contact pressure in the MS model over the entire stance phase of the gait cycle. The trend was very similar, as confirmed by a strong correlation between the curves (R^2 = 0.938) and by the fact that null hypothesis could not be rejected (p=0.0558) (Fig. 19). Thus, we found a good agreement between the results of the two models, as hypothesized. Nevertheless, at the two peaks, the pressure in the HC model was slightly higher (+19% at first peak and +29% at second peak) than the pressure in the MS model (Table 7). At the first peak, the medial compartment showed higher pressure than in the MS model (+34%), while on the lateral compartment we observed the same pressure (+2%); at the second peak both the medial (+23%) and the lateral (+36%) compartments were more stressed. This higher pressure could be related to two main aspects. On the one hand, cartilage-to-cartilage contact in the FE model could run into some minimal penetration during the stance phase, probably caused by too weak cartilage material properties used in relation to the loads applied. A further critical aspect of the Mooney-Rivlin material in FEBio was underlined by Henak et al. [94]: contact patterns were slightly overpredicted and underpredicted at very large and very small load magnitudes, respectively, compared to experimental data. On the other hand, the contact pressure could be influenced by nodal loads applied for the muscles forces. Load curves for muscle forces were not smooth, instead they often showed severe discontinuities especially in the peaks. These sudden changes in loads could cause high contact pressure.

Overall, contact between the cartilage surfaces in the HC model was more anterior and slightly more lateral than in the MS model over the entire stance phase. This could be related to the action of ligament bundles: considering the initially available data for the MS model (see Section 3.1), ACL and MCL forces were higher than 0N (~ 70N) at the initial time frame of the stance phase. This suggests that there is some pre-tensioning in the ligament bundles. Conversely, pre-tensioning is not

accounted for in the FE model, where all ligament bundles are in the laxity zone (see Section 3.3.2 - *Constraints*) at the initial time frame of the stance step. Indeed, ligament forces calculated after the postprocessing of the FE analysis (see Section 3.3.4) significantly differed in magnitude and trends from the ligament forces in the initially available data set.

DC model

In the DC model, the average cartilage contact pressure at the first peak of was markedly higher than in the HC model: +33% in total and +75% on the medial compartment (Table 8, Fig. 25). Furthermore, although we observed a good correlation between the curves (R^2 = 0.921), we rejected the null hypothesis for cartilage contact pressure (p=0.0346) over the entire stance phase. This is arguably caused by the change in the geometry of the cartilage: the defect on the medial compartment altered the cartilage-to-cartilage contact, reducing the contact surface compared to the intact cartilage. Indeed, pressures on the defect rim were the highest over the entire stance phase. The cartilage pressure on the medial compartment was the highest at the first peak, as in the HC model. At the second peak, the pressure on the lateral compartment was higher than on the medial compartment. Thus, the defect was solicitated less than the first peak. This could explain why the defect affected the contact pressure at the first peak more than at the second peak, and thus why the contact pressure at the second peak are similar in the DC and HC models (Fig. 26).

The contact area in the DC model was overall lower than contact area in the HC model over the entire stance phase. Like the HC model, the lateral compartment had a larger surface in contact than the medial compartment, although along the medial portions the surface was more equally distributed over the different portions than in the HC model: each of the four medial portions had about 25% of the surface in contact, so the contact was more posterior than in the HC model. This suggests that the cartilage, due to the defect, responded differently to the applied loads: parts of the surface, that are normally not stressed, were exposed to higher loading. This adaptation is even more evident in the SC model, where different material properties were applied to simulate the softening of the area around the rim (see below).

These results suggest that a degenerated cartilage geometry influences the contact pressure and the contact distribution in the knee joint, and that the intact cartilage patterns are significantly altered. Specifically, contact pressure in the cartilage around the defect are the highest during walking and different portions of the tissue are in contact. This inference was also demonstrated in other literature studies. Furthermore, in the peaks, the Lagrangian strain in the DC model was higher in modulus than in the HC model (first (tensile) principal component: 19 % vs 62%; third (compressive) principal

component: −20% vs −36%). This aspect can corroborate the idea of a progressive degeneration of the cartilage presenting an early OA defect.

SC model

In the SC model, cartilage contact pressure differed from both the DC model and the HC models (Fig. 30). At the first peak, the average pressure was higher than in the HC model (+21%) but slightly lower than in the DC model (-9%) (Table 9). Despite the difference that we observed, there was a strong correlation between the curves (R^2 = 0.937 SC vs DC and R^2 = 0.893 SC vs HC) and no significant difference (p=0.404 SC vs DC and p=0.121 SC vs HC) in the average contact pressure over the stance phase. The total average pressure trend reflected the trend of the medial compartment of tibial cartilage (Fig. 33), since trends of the DC and the SC model were almost identical on the lateral compartment (Fig. 34). Furthermore, at the second peak, the average pressure of the SC and the DC model were similar (only 3% difference). The behavior of the model at the first peak on the medial compartment could be related to the softening of the cartilage around the rim. Harder materials tend to undertake more load than softer material if they are close to each other. Since the cartilage was softer around the defect, contact loads around the defect were lower than in the DC model, and were distributed over a slightly larger area, with higher stiffness [105], [106]. This larger distribution could be the cause of the slightly lower contact pressure that we found in the SC compared to the DC model.

The results on contact area also corroborate this inference: in the total tibial cartilage surface, contact area at the first peak was 22% larger than in the DC model, with a maximum of 33% on the medial compartment (the compartment with the defect). As in the DC model, medial contact at the second peak was distributed more over the four portions. Moreover, contact area on the lateral compartment was even larger in the SC model compared to the DC model (+13%). This more lateral contact could reflect a further adaptation in cartilage distribution between the two compartments: since the cartilage on the medial compartment was overall softer than the cartilage on the lateral compartment, this last compartment took on more load.

In general, the adaptation that we found is consistent with the time evolution of OA defect (see Section 1.2): the cartilage remodeling lead to softer material around the defect rim in order to decrease and deviate the contact pressure in the tissue, thus minimizing the damage [8], [42], [69], [105].

Softer materials also allow for more deformation. Overall, the strain in the SC model was higher than in the DC model (see Section 4.3). If deformation becomes too large, it can cause further damage to the cartilage: areas of the cartilage that are normally not in contact are less stiff and less prone to

loading, therefore lower contact pressure can eventually affect the tissue in those areas and lead to degeneration [8], [38], [106]. Nevertheless, a more precise definition of cartilage material properties is required to be able to strongly conclude on the biomechanics of the cartilage in both damaged and softened conditions. Including swelling behavior and collagen fibril network degeneration in the material properties can be crucial in this scenario [62], [67].

A long computational time was required for the solution for the three models (more than 13 hours). We also ran a simulation with a coarse mesh using 4-node tetrahedral elements instead of 10-node tetrahedral elements and 1.5 mm as maximum element edge length in the cartilage instead of 1.2mm (see Section 3.3.1). With this model, we could run the FE analysis in less than one hour, but we occasionally had convergence issues due to extreme element deformation. This suggests the necessity of a convergence study, to understand the most effective mesh density for the problem. A similar convergence study for cartilage mesh density was performed by Smith et al. for the MS model [55], which set a lower bound for density at 2.6 triangles/ mm^2. Furthermore, the average contact pressure curves in the DC and in the SC models showed more artifacts than the HC model. This could be related to more difficulties in the FE analysis, specifically related to the high pressure in the defect rim. In order to reduce these artifacts, a mesh refinement in the defect rim could be useful, and a specific convergence study to the purpose could lead to the optimal the refinement.

Literature comparison

As a final goal in this project, we aimed to compare the results of the newly developed FE model with the results of previously developed FE models of the knee joint in literature. We provided a brief description of these models in a literature review in the sub-section 1.3.2, where we also shortly compare the modelling choices in relation to the analysis performed in each study.

As we underlined in the introduction, modelling choices in all reviewed studies were driven by a compromise between model complexity and analysis complexity (Table 1). Since every model was developed for a specific study purpose, the geometries, material properties and boundary conditions were different from our model. Furthermore, results shown in these studies mostly accounted for one or two features of our interest (e.g. only contact pressure, contact pressure and strain, contact area and strain, etc.). For this reason, we could only partially compare our results with each of the models. The results that we obtained using the HC model were in line with the results of Van Rossom et al. [34] for the group of control subjects: the average pressure that we obtained in the total tibial cartilage

surface was in the range of the average pressure obtained for the group of healthy subject in the cited study (4 – 6 MPa). Calculated cartilage contact pressures were also comparable to other FE models [51], [59], [63], [65], [107], [108]. For example, in the study of Meng et al. [59], the average contact pressure was in the range 3-5.8 MPa, and was consistent with our results (Table 7). As for our study, the FE analysis was performed in FEBio and cartilage was modeled as hyper-elastic material. Different from our study, they modeled all the soft tissue from MR images and used static loading to reach the usual peak values of contact force for the knee joint. Therefore, we could only compare our results at the time of the peaks in the stance phase. In other studies, like Hull et al. [60] and Kazemi et al. [61], average contact pressure was lower (1 – 3 MPa). In both these studies, all tissues were segmented from MR images and cartilage material properties were more complex (e.g. Kazemi et al.: poroviscoelastic approach) and loads were either static or cyclic. Moreover, average contact pressure in a model with complex depth-wise dependent material properties (Halonen et al. [62]) was higher than in the present study, about 8-9 MPa. These pressures were calculated by applying boundary conditions from gait analysis data adapted from literature. The contact pressures obtained by Schmitz et al. [65] were in line with our results. As in our model, boundary conditions were extracted from a MS analysis, and cartilage was modeled as hyper-elastic. In the study of Venalainen et al. [63], a FE model of the knee joint was developed for a purpose similar to ours ("evaluate changes in local mechanical responses around cartilage defect"). Their results, and the results of a previous similar study that they used as a model of comparison ([107]), were also consistent with the present study (4 – 7 MPa medial compartment, 4 – 6 MPa lateral compartment).

The contact area was explicitly calculated in only a few studies ([59], [60], [78]). The contact area we obtained was either similar (~ 300 mm^2, [78]) or slightly smaller (~ 400 - 450 mm^2, [59], [60]) than the results of these studies. Nevertheless, in most of the reviewed studies, the contact was more medial than lateral over the entire stance phase. This is partially in disagreement with our model, as especially in the second part of the stance phase, the contact we obtained was more lateral. This might be the results of the lack of ligament pre-tensioning, as discussed before (see Section 5 - *HC model*). Also the boundary conditions could affect the contact location, as suggested by Schmitz et al. [65]. In this study, an analysis of peak pressure location was performed: they varied the alignment of the bones in the knee (on the anteroposterior axis, from varus to valgus) to evaluate changes in contact location. They concluded that contact pressure did not vary with alignment, but that fixing one of the two long bones in all DoFs could cause an offset in contact location of pressure along the gait cycle. In the present study, the tibia was fixed in all the DoFs, which could have slightly influenced the contact location.

Some of the studies that we reviewed in sub-section 1.3.2 included the simulation of a defect on the cartilage geometry [43], [51], [63]. These studies share a common conclusion from the FE analysis: the contact pressure and the strain were higher around the defect than in the remaining cartilage surface. In the present study, this is also concluded for contact pressure and strain. Furthermore, the average cartilage contact pressure in our study was consistent with these studies: the peak in Venalainen et al. [63] was 7 MPa; the peak in Shirazi et al. was 6 MPa [51].

The first (tensile) and third (compressive) strain principal components in our model were also consistent with the reviewed articles both for intact and degenerated cartilage: 15 - 25 % (first principal component) and about –20% (third principal component) for intact cartilage ([50], [51], [59], [62], [63]); more than 30% (first principal component) and less then –40% (third principal component) for degenerated cartilage ([43], [51], [63]).

Overall, we were able to confirm our initial hypothesis: we found an agreement between the results of the newly developed FE model and the results of the MS model of Van Rossom et al. [34] and we found differences in cartilage contact pressure and strain between the model with the intact cartilage and the models with the OA degenerated cartilage.

Furthermore, our results were in line with the results of many of the reviewed studies. The contact pressure was consistent with the studies with similar material properties and boundary conditions. The largest difference between our results and literature (including the MS model of Van Rossom et al. [34]) was related to contact location. However, we could directly compare our results with only a few of the reviewed studies, since modelling choices were heterogeneous as well as boundary conditions.

The results obtained are based on one subject and thus preliminary. A larger number of subjects should be involved in the study, and more simulations must be performed. Moreover, modelling choices must be optimized in the future to take into account all aspects of knee cartilage contact, especially in relation to early OA degeneration. Thus, there is still room for improvement which needs to be addressed. Nevertheless, this Master thesis has set the basis for future work on cartilage biomechanics in the knee using the newly developed FE model.

Chapter 6 – CONCLUSION

In this Master Thesis, we aimed to evaluate cartilage contact pressure in the knee during walking in healthy and degenerated conditions through a Finite Element (FE) modelling analysis. The FE model developed for this purpose was a valuable tool to analyze contact pressure in the intact cartilage and in the two cartilage models simulating an early OA degeneration.

We found that a medial cartilage defect leads to an overall increase in contact pressure and strain compared to healthy conditions, particularly in the medial compartment at the first peak of the knee contact force during the stance phase of the gait cycle, as a major consequence of reduced contact surface. Adding softening material properties around the defect rim leads to a different pressure distribution following a larger contact area with slightly lower contact pressure values, particularly on the medial compartment.

We observed a good agreement between the results obtained with the HC model ("Healthy Cartilage", with the intact cartilage geometry) and the results of the Musculoskeletal (MS) model of van Rossom et al. [34], that included an elastic foundation model at the knee joint [53], [55]. Overall, the contact pressure and the contact area of the two models were similar. Indeed, curve pattern strongly correlated (R^2 = 0.938) and no significant difference were evaluated using the Mann-Whitney U Test (p=0.0558), although there was a slight difference at the two peaks of the stance phase. In our specific purpose I (see Section 2), we hypothesized a general agreement between the two models. Therefore, we could confirm this first hypothesis. This part of our study could help to indirectly validate the MS elastic foundation model and confirm the quality and the reliability of this novel multibody approach in cartilage biomechanics research.

Moreover, we compared the contact pressure and the strain in the HC model and in the DC model ("Damaged Cartilage", with the OA damaged cartilage geometry). We observed a remarkable difference in the contact pressure and in strain at the peaks, as well as in the pressure distribution on the cartilage surface. We indeed rejected the null hypothesis for cartilage contact pressure (p=0.0346). The contact pressure we observed in the DC model was higher than in the HC model. This is what we hypothesized in our specific purpose II (see Section 2). Thus, we could also confirm our second hypothesis. We also extent our comparison to the SC model ("Softened Cartilage", with both the cartilage defect and the softened material properties in the cartilage around the defect rim). We noticed slight differences between the results of the DC and SC models, that could indicate an adaptation of the cartilage to the OA defect in terms of contact pressure and contact area. Nevertheless, we no significant difference were shown through the Mann-Whitney U Test for average cartilage contact pressure (p=0.404). The results observed in the SC model were in line with the

behavior expected for an early OA time evolution, according both to pervious experimental and computational modelling studies. These results could help to set the basis for further comparison between intact and the OA-affected cartilage using the FE analysis. The idea of a time evolution of the defect could be reconsidered and taken forward to achieve a wider comprehension of the joint behavior in degenerated conditions.

Furthermore, the results that we obtained were consistent with the ones of other literature studies on FE modelling of the knee joint. Although different modelling approaches and levels of complexity were used among the studies, we observed a good agreement.

Overall, the newly developed FE model could be an attractive tool in the knee OA biomechanics research for several reasons. Firstly, the model was developed in an open source software, which is specifically intended for large deformation studies and, thus, appropriate for cartilage-to-cartilage contact problems. Secondly, geometries were imported from MR images, which can be obtained in a non-invasive way for a large number of subjects. This aspect is pivotal to perform a detailed subject-specific study and a consistent quantitative analysis of tissue mechanics. Moreover, the type of contact, the material properties and the boundary conditions can be easily adjusted to account for a wide variety of tissue-interaction mechanisms and motor tasks. In addition, the simulation of OA (and of other musculoskeletal pathologies) can help to extend the knowledge on pathology-related biomechanical aspects. A deep understanding of the signs of early OA appearance could be crucial for prevention and surgical treatment.

6.1 *Limitations and future improvements*

In this study, we aimed to compare cartilage contact pressure using a newly developed FE model. As the model was tested for the first time, the results that we obtained should be interpreted taking into account several limitations.

First of all, the study was conducted on a single subject. Therefore, it was not possible to evaluate the performance of the model with any other geometries and boundary conditions. Since only a single motor task was considered, it was also not possible to account for the versatility of the model with respect to other tasks. Thus, no statistical analysis based on multiple subjects performing multiple tasks could be performed. In the future, it would be interesting to use the model to perform FE analyses on more subjects and for more motor tasks per subject. While performing a large number of FE analyses, a modelling choices adjustment would also be attractive. Specifically, it could be possible to vary the model features in two main ways: first, applying boundary conditions extracted from the MS analysis of either healthy or OA subjects; second, simulating either healthy or

degenerated cartilage material properties. Eventually, these adjustments could be made together (e.g. boundaries from OA subjects and degenerated material properties) to properly represent the joint behavior in multiple circumstances, as the change in gait pattern in the late OA stage [3]–[6]. Moreover, a verification and validation study should also be performed for the newly developed model [109].

Secondly, cartilage material properties should be discussed and refined. Contact loads during walking cover a wide range of magnitudes and a Mooney-Rivlin material may be not proper to account for the cartilage-to-cartilage contact over this range. Indeed, a previous study [94] highlighted that a Mooney-Rivlin material has low performance at very large and very small load and strain magnitudes. Furthermore, it does not account for all the mechanical processes that happen when cartilage undergoes stress, and a biphasic formulation for cartilage material properties and contact could be more effective. Poroviscoelastic materials provide a more detailed description and simulation of cartilage properties, since they consider both the collagen fibril network and the synovial fluid within the porous matrix [51], [52], [62], [64], [66], [67]. Moreover, these materials are already implemented in FEBio. The use of sophisticated material properties could also be valuable in the OA defect simulations: early OA and its time evolution could be considered in their different biochemical aspects, such as loss of water content, breaking of collagen fibrils, etc. [8], [22], [24], [42], [110]–[113].

A third limitation, already underlined in the discussion, is related to the ligament behavior. Although the spring objects that we used to model the ligament bundles (see Section 3.3.2 - *Constraints*) accounted for both the initial laxity and the progressive stiffening, we did not consider any pre-tensioning at the beginning of the stance phase step. This could have negatively affected the contact location on the cartilage over the entire stance phase. Furthermore, the MS model (from which we adapted ligament position, length and stiffness) considered between four and six strands per each of the seven ligament bundles that we included. Since we had to find a proper insertion and origin point for each ligament bundle by averaging the position of the strands, we inevitably made slight accuracy errors. These errors also affect the length and consequently the stiffness of the bundles. Moreover, we excluded all the ligaments connected to the patella from our model. A future improvement would be the inclusion of all the knee ligaments. The simplest way to do this would be by extracting ligament geometries from MR images. In addition, we could assign specific material properties to the ligaments and evaluate more mechanical features directly in the PostView (e.g. [50], [71]). Further mechanical simulations could be performed with a detailed definition of the ligaments, such as simulation of the knee behavior in the presence of a ligament injury (typically, the ACL injury [4], [15], [19], [48], [105], [114]). This could give insights on how the knee structures react to the lack of the stability

caused by the injury. Additionally, the relationship between ligament injury, contact abnormalities and OA progression could be analyzed. On a side note, we already attempted to simulate ACL resection using our model: we removed one of the two ACL bundles (the amACL) to evaluate potential changes in knee contact. The FE analysis ran normally and no significant changes in the contact pressure or location occurred, but we observed that ligament force in the remaining ACL bundle (the plACL) was strongly higher than in the original simulation. This indicates that plACL was probably overstretched to compensate for the absence of the other bundle. Hence, further simulation of ACL injury could better replicate our attempt.

As the ligaments, also the muscle forces were a critical aspect of the model. Muscle forces were applied as nodal loads, which can bring boundary artifacts (e.g. very high forces) around the point of application [115] and slightly affect the results. Furthermore, it was difficult to find the exact location of the origins and insertions, since part of the bones were missing in the initially available geometries (see 3.3.2 - *Geometry*). For a precise introduction of points of application and loads applied, the addition of the entire femur and tibia could be helpful. Moreover, the addition of the patella and the pelvis would also increase the level of detail of the model. Even though model complexity would strongly increase, a better representation of the hip joint and the addition of the Patellofemoral (PF) joint could expand the knowledge on the mechanical contributions to knee contact. Actually, a FE study of the hip joint with similar modelling choices and boundary conditions is currently being performed by our group.

As a further limitation, menisci were not included in the FE model. This choice was based on the first specific purpose of the study, the comparison with the MS model of Van Rossom et al. [34]. In the MS model, menisci were also not included, thus, we intentionally neglected them to achieve a more consistent comparison. As a future improvement of the model, the menisci could be introduced. In some previous FE studies, also performed with FEBio, menisci have already been modeled ([61], [62], [80], [82], [108]).

The tibial constraint is another aspect that could still be improved. As underlined in the discussion, our choice to fix the tibia in all 6 DoFs could have created a minimal offset in the cartilage-to-cartilage contact [65]. This could have contributed to the more lateral contact location observed. Hence, a more complex constraint could be applied to the tibia in order to avoid offset and knee malalignment during the simulation. The entire knee kinematics could, for example, be split in the tibia and the femur kinematics, instead of allowing only the femur movement.

Finally, we did not account for any mechanical failure of the tissues. For a more reliable simulation, it could be interesting to consider the maximal stress that the cartilage can withstand before running into irreversible damage. This could be addressed by introducing a “damage limit”, either for the

contact pressure or the strain, preferably based on literature experimental data. This limit would also be a warning sign for constantly high pressure in the cartilage, which could likely lead to a progressive degeneration of the tissue.

Despite all the limitations mentioned, the newly developed FE model could be a valuable tool in knee biomechanics and OA detection research. As highlighted, a deep understanding of the mechanical aspects of the knee joint in intact and degenerated conditions is crucial to improve the chances for early detection of OA. This can help clinicians to treat the disease before it becomes invalidating for the patients. Furthermore, it can help to elaborate prevention and surgical techniques in order to delay the occurrence of the pathology and the related pain progression. Since experimental measures cannot easily account for an early OA detection for several reasons (see Section 1.2), multiscale modeling can be a key tool to detect pathology-related loading abnormalities. So far, multiscale models are mostly used in research. In the future, a stronger inclusion of these models in the clinical practice could be attractive, as they could provide a significant help in the comprehension and treatment of several musculoskeletal pathologies that nowadays affect people all over the world.

REFERENCES

[1] D. Pereira, B. Peleteiro, J. Araújo, J. Branco, R. A. Santos, and E. Ramos, "The effect of osteoarthritis definition on prevalence and incidence estimates: A systematic review," *Osteoarthritis and Cartilage*, vol. 19, no. 11. pp. 1270–1285, 2011.

[2] V. K. Srikanth, J. L. Fryer, G. Zhai, T. M. Winzenberg, D. Hosmer, and G. Jones, "A meta-analysis of sex differences prevalence, incidence and severity of osteoarthritis," *Osteoarthr. Cartil.*, vol. 13, no. 9, pp. 769–781, 2005.

[3] D. Blalock, A. Miller, M. Tilley, and J. Wang, "Joint instability and osteoarthritis," *Clinical Medicine Insights: Arthritis and Musculoskeletal Disorders*, vol. 8. pp. 15–23, 2015.

[4] L. S. Lohmander, P. M. Englund, L. L. Dahl, and E. M. Roos, "The long-term consequence of anterior cruciate ligament and meniscus injuries: Osteoarthritis," *American Journal of Sports Medicine*, vol. 35, no. 10. pp. 1756–1769, 2007.

[5] S. Farrokhi, C. A. Voycheck, B. A. Klatt, J. A. Gustafson, S. Tashman, and G. K. Fitzgerald, "Altered tibiofemoral joint contact mechanics and kinematics in patients with knee osteoarthritis and episodic complaints of joint instability," *Clin. Biomech.*, vol. 29, no. 6, pp. 629–635, 2014.

[6] J. D. Childs, P. J. Sparto, G. K. Fitzgerald, M. Bizzini, and J. J. Irrgang, "Alterations in lower extremity movement and muscle activation patterns in individuals with knee osteoarthritis," *Clin. Biomech.*, vol. 19, no. 1, pp. 44–49, 2004.

[7] A. Mahmoudian *et al.*, "Changes in proprioceptive weighting during quiet standing in women with early and established knee osteoarthritis compared to healthy controls," *Gait Posture*, vol. 44, pp. 184–188, 2016.

[8] J. Z. Wu, W. Herzog, and M. Epstein, "Joint contact mechanics in the early stages of osteoarthritis," *Med. Eng. Phys.*, vol. 22, no. 1, pp. 1–12, 2000.

[9] M. Wesseling *et al.*, "Gait alterations to effectively reduce hip contact forces," *J. Orthop. Res.*, vol. 33, no. 7, pp. 1094–1102, 2015.

[10] M. Wesseling *et al.*, "Muscle optimization techniques impact the magnitude of calculated hip joint contact forces," *J. Orthop. Res.*, vol. 33, no. 3, pp. 430–438, 2015.

[11] G. Giarmatzis, I. Jonkers, M. Wesseling, S. Van Rossom, and S. Verschueren, "Loading of Hip Measured by Hip Contact Forces at Different Speeds of Walking and Running," *J. Bone Miner. Res.*, vol. 30, no. 8, pp. 1431–1440, 2015.

[12] W. Müller, "Anatomy and biomechanics of the knee," in *Sports Injuries: Prevention, Diagnosis, Treatment and Rehabilitation, Second Edition*, 2015, pp. 883–907.

[13] D. R. Wilson, J. D. Feikes, A. B. Zavatsky, and J. J. O'Connor, "The components of passive knee movement are coupled to flexion angle," *J. Biomech.*, vol. 33, no. 4, pp. 465–473, 2000.

[14] S. D. Masouros, A. M. J. Bull, and A. A. Amis, "(i) Biomechanics of the knee joint," *Orthop. Trauma*, vol. 24, no. 2, pp. 84–91, 2010.

[15] D. R. Wilson, J. D. Feikes, and J. J. O'Connor, "Ligaments and articular contact guide passive knee flexion," *J. Biomech.*, vol. 31, no. 12, pp. 1127–1136, 1998.

[16] L. Blankevoort and R. Huiskes, "Validation of a three-dimensional model of the knee," *J. Biomech.*, vol. 29, no. 7, pp. 955–961, 1996.

[17] G. Wu and P. R. Cavanagh, “ISB Recommendations in the Reporting for Standardization of Kinematic Data,” *J. Biomech.*, vol. 28, no. 10, pp. 1257–1261, 1995.

[18] E. S. Grood, S. F. Stowers, and F. R. Noyes, “Limits of movement in the human knee. Effect of sectioning the posterior cruciate ligament and posterolateral structures.,” *J. Bone Joint Surg. Am.*, vol. 70, no. 1, pp. 88–97, 1988.

[19] V. L. Johnson, A. Guermazi, F. W. Roemer, and D. J. Hunter, “Comparison in knee osteoarthritis joint damage patterns among individuals with an intact, complete and partial anterior cruciate ligament rupture,” *Int. J. Rheum. Dis.*, vol. 20, no. 10, pp. 1361–1371, 2017.

[20] J.-S. Li *et al.*, “Prediction of In Vivo Knee Joint Kinematics Using a Combined Dual Fluoroscopy Imaging and Statistical Shape Modeling Technique,” *J. Biomech. Eng.*, vol. 136, no. 12, p. 124503, 2014.

[21] K. B. Shelburne, M. R. Torry, and M. G. Pandy, “Muscle, ligament, and joint-contact forces at the knee during walking,” *Med. Sci. Sports Exerc.*, vol. 37, no. 11, pp. 1948–1956, 2005.

[22] A. J. Sophia Fox, A. Bedi, and S. A. Rodeo, “The basic science of articular cartilage: Structure, composition, and function,” *Sports Health*, vol. 1, no. 6, pp. 461–468, 2009.

[23] L. McCann, E. Ingham, Z. Jin, and J. Fisher, “Influence of the meniscus on friction and degradation of cartilage in the natural knee joint,” *Osteoarthr. Cartil.*, vol. 17, no. 8, pp. 995–1000, 2009.

[24] D. L. Robinson, M. E. Kersh, N. C. Walsh, D. C. Ackland, R. N. de Steiger, and M. G. Pandy, “Mechanical properties of normal and osteoarthritic human articular cartilage,” *J. Mech. Behav. Biomed. Mater.*, vol. 61, pp. 96–109, 2016.

[25] S. R. Kingsbury, H. J. Gross, G. Isherwood, and P. G. Conaghan, “Osteoarthritis in europe: Impact on health status, work productivity and use of pharmacotherapies in five European countries,” *Rheumatol. (United Kingdom)*, vol. 53, no. 5, pp. 937–947, 2014.

[26] R. J. Lories and F. P. Luyten, “The bone-cartilage unit in osteoarthritis,” *Nature Reviews Rheumatology*, vol. 7, no. 1. pp. 43–49, 2011.

[27] D. Prieto-Alhambra, A. Judge, M. K. Javaid, C. Cooper, A. Diez-Perez, and N. K. Arden, “Incidence and risk factors for clinically diagnosed knee, hip and hand osteoarthritis: Influences of age, gender and osteoarthritis affecting other joints,” *Ann. Rheum. Dis.*, vol. 73, no. 9, pp. 1659–1664, 2014.

[28] S. Meireles *et al.*, “Knee contact forces are not altered in early knee osteoarthritis,” *Gait Posture*, vol. 45, pp. 115–120, 2016.

[29] J. Runhaar, B. W. Koes, S. Clockaerts, and S. M. A. Bierma-Zeinstra, “A systematic review on changed biomechanics of lower extremities in obese individuals: A possible role in development of osteoarthritis,” *Obes. Rev.*, vol. 12, no. 12, pp. 1071–1082, 2011.

[30] C. Palazzo, C. Nguyen, M. M. Lefevre-Colau, F. Rannou, and S. Poiraudeau, “Risk factors and burden of osteoarthritis,” *Annals of Physical and Rehabilitation Medicine*, vol. 59, no. 3. pp. 134–138, 2016.

[31] J. W. J. Bijlsma, F. Berenbaum, and F. P. J. G. Lafeber, “Osteoarthritis: An update with relevance for clinical practice,” *Lancet*, vol. 377, no. 9783, pp. 2115–2126, 2011.

[32] C. A. Peach, A. J. Carr, and J. Loughlin, “Recent advances in the genetic investigation of osteoarthritis,” *Trends in Molecular Medicine*, vol. 11, no. 4. pp. 186–191, 2005.

[33] S. Meireles, F. De Groote, S. Van Rossom, S. Verschueren, and I. Jonkers, “Differences in knee adduction moment between healthy subjects and patients with osteoarthritis depend on the knee axis definition,” *Gait Posture*, vol. 53, pp. 104–109, 2017.

[34] S. Van Rossom, C. R. Smith, D. G. Thelen, B. Vanwanseele, D. Van Assche, and I. Jonkers, “Knee Joint Loading in Healthy Adults During Functional Exercises: Implications for Rehabilitation Guidelines,” *J. Orthop. Sport. Phys. Ther.*, pp. 1–42, 2018.

[35] A. Teichtahl, A. Wluka, and F. M. Cicuttini, “Abnormal biomechanics: A precursor or result of knee osteoarthritis?,” *British Journal of Sports Medicine*, vol. 37, no. 4. pp. 289–290, 2003.

[36] D. Pretzel *et al.*, “Relative percentage and zonal distribution of mesenchymal progenitor cells in human osteoarthritic and normal cartilage,” *Arthritis Res. Ther.*, vol. 13, no. 2, 2011.

[37] L. Sharma, “Local factors in osteoarthritis,” *Current Opinion in Rheumatology*, vol. 13, no. 5. pp. 441–446, 2001.

[38] S. Van Rossom *et al.*, “Knee cartilage thickness, T1ρ and T2 relaxation time are related to articular cartilage loading in healthy adults,” *PLoS One*, vol. 12, no. 1, 2017.

[39] O. D. Schipplein and T. P. Andriacchi, “Interaction between active and passive knee stabilizers during level walking,” *J. Orthop. Res.*, vol. 9, no. 1, pp. 113–119, 1991.

[40] F. Cicuttini, C. Ding, A. Wluka, S. Davis, P. R. Ebeling, and G. Jones, “Association of cartilage defects with loss of knee cartilage in healthy, middle-age adults: A prospective study,” *Arthritis Rheum.*, vol. 52, no. 7, pp. 2033–2039, 2005.

[41] J. H. Guettler, C. K. Demetropoulos, K. H. Yang, and K. A. Jurist, “Osteochondral Defects in the Human Knee,” *http://dx.doi.org/10.1177/0363546504263234*, 2016.

[42] E. M. Obeid, M. A. Adams, and J. H. Newman, “Mechanical properties of articular cartilage in knees with unicompartmental osteoarthritis,” *J. Bone Joint Surg. Br.*, vol. 76, no. 2, pp. 315–319, 1994.

[43] G. Papaioannou, C. K. Demetropoulos, and Y. H. King, “Predicting the effects of knee focal articular surface injury with a patient-specific finite element model,” *Knee*, vol. 17, no. 1, pp. 61–68, 2010.

[44] A. E. Anderson, B. J. Ellis, S. A. Maas, C. L. Peters, and J. A. Weiss, “Validation of Finite Element Predictions of Cartilage Contact Pressure in the Human Hip Joint,” *J. Biomech. Eng.*, vol. 130, no. 5, p. 51008, 2008.

[45] M. Viceconti *et al.*, “Multiscale modelling of the skeleton for the prediction of the risk of fracture.,” *Clin. Biomech. (Bristol, Avon)*, vol. 23, no. 7, pp. 845–52, 2008.

[46] D. W. Wagner, K. Divringi, C. Ozcan, M. Grujicic, B. Pandurangan, and A. Grujicic, “Combined musculoskeletal dynamics/structural finite element analysis of femur physiological loads during walking,” *Multidiscip. Model. Mater. Struct.*, vol. 6, no. 4, pp. 417–437, 2010.

[47] S. L. Delp *et al.*, “OpenSim: Open source to create and analyze dynamic simulations of movement,” *IEEE Trans. Biomed. Eng.*, vol. 54, no. 11, pp. 1940–1950, 2007.

[48] A. Kiapour *et al.*, “Finite element model of the knee for investigation of injury mechanisms: development and validation.,” *J. Biomech. Eng.*, vol. 136, no. 1, p. 11002, 2014.

[49] B. W. Stansfield, A. C. Nicol, J. P. Paul, I. G. Kelly, F. Graichen, and G. Bergmann, “Direct

comparison of calculated hip joint contact forces with those measured using instrumented implants. An evaluation of a three-dimensional mathematical model of the lower limb," *J. Biomech.*, vol. 36, no. 7, pp. 929–936, 2003.

[50] A. Erdemir and S. Sibole, "Open Knee: A Three-Dimensional Finite Element Representation of the Knee Joint," *User's Guid.*, 2010.

[51] R. Shirazi and A. Shirazi-Adl, "Computational biomechanics of articular cartilage of human knee joint: Effect of osteochondral defects," *J. Biomech.*, vol. 42, no. 15, pp. 2458–2465, 2009.

[52] M. Adouni, A. Shirazi-Adl, and R. Shirazi, "Computational biodynamics of human knee joint in gait: From muscle forces to cartilage stresses," *J. Biomech.*, vol. 45, no. 12, pp. 2149–2156, 2012.

[53] C. R. S. and D. G. T. Rachel L. Lenhart, Jarred Kaiser, "Prediction And Validation of Load-Dependent Behavior of the Tibiofemoal and Parellofemoral Joints During Movement," vol. 4, no. 1, pp. 139–148, 2015.

[54] E. M. Arnold, S. R. Ward, R. L. Lieber, and S. L. Delp, "A model of the lower limb for analysis of human movement," *Ann. Biomed. Eng.*, vol. 38, no. 2, pp. 269–279, 2010.

[55] C. R. Smith, K. Won Choi, D. Negrut, and D. G. Thelen, "Efficient computation of cartilage contact pressures within dynamic simulations of movement," *Comput. Methods Biomech. Biomed. Eng. Imaging Vis.*, vol. 1163, no. June, pp. 1–8, 2016.

[56] J. P. Halloran, S. K. Easley, A. J. Petrella, and P. J. Rullkoetter, "Comparison of Deformable and Elastic Foundation Finite Element Simulations for Predicting Knee Replacement Mechanics," *J. Biomech. Eng.*, vol. 127, no. 5, p. 813, 2005.

[57] A. Seth, M. Sherman, J. A. Reinbolt, and S. L. Delp, "OpenSim: A musculoskeletal modeling and simulation framework for in silico investigations and exchange," *Procedia IUTAM*, vol. 2, pp. 212–232, 2011.

[58] N. A. DeVries Watson, K. R. Duchman, M. J. Bollier, and N. M. Grosland, "A Finite Element Analysis of Medial Patellofemoral Ligament Reconstruction.," *Iowa Orthop. J.*, vol. 35, pp. 13–9, 2015.

[59] Q. Meng, Z. Jin, R. Wilcox, and J. Fisher, "Computational investigation of the time-dependent contact behaviour of the human tibiofemoral joint under body weight," *Proc. Inst. Mech. Eng. Part H J. Eng. Med.*, vol. 228, no. 11, pp. 1193–1207, 2014.

[60] M. L. Hull, "A Finite Element Model of the Human Knee Joint for the Study of Tibio-Femoral Contact," *J. Biomech. Eng.*, vol. 124, no. 3, p. 273, 2002.

[61] M. Kazemi and L. P. Li, "A viscoelastic poromechanical model of the knee joint in large compression," *Med. Eng. Phys.*, vol. 36, no. 8, pp. 998–1006, 2014.

[62] K. S. Halonen, M. E. Mononen, J. S. Jurvelin, J. Töyräs, and R. K. Korhonen, "Importance of depth-wise distribution of collagen and proteoglycans in articular cartilage-A 3D finite element study of stresses and strains in human knee joint," *J. Biomech.*, vol. 46, no. 6, pp. 1184–1192, 2013.

[63] M. S. Ven??l??inen *et al.*, "Quantitative Evaluation of the Mechanical Risks Caused by Focal Cartilage Defects in the Knee," *Sci. Rep.*, vol. 6, no. October, pp. 1–11, 2016.

[64] M. E. Mononen, P. Tanska, H. Isaksson, and R. K. Korhonen, "A novel method to simulate

the progression of collagen degeneration of cartilage in the knee: Data from the osteoarthritis initiative," *Sci. Rep.*, vol. 6, no. January, pp. 1–14, 2016.

[65] D. G. Thelen, K. Won Choi, and A. M. Schmitz, "Co-Simulation of Neuromuscular Dynamics and Knee Mechanics During Human Walking," *J. Biomech. Eng.*, vol. 136, no. 2, p. 21033, 2014.

[66] M. Sharifi, A. Shirazi-Adl, and H. Marouane, "Computational stability of human knee joint at early stance in Gait: Effects of muscle coactivity and anterior cruciate ligament deficiency," *J. Biomech.*, vol. 63, pp. 110–116, 2017.

[67] W. Wilson, C. C. Van Donkelaar, B. Van Rietbergen, K. Ito, and R. Huiskes, "Stresses in the local collagen network of articular cartilage: A poroviscoelastic fibril-reinforced finite element study," *J. Biomech.*, vol. 37, no. 3, pp. 357–366, 2004.

[68] F. M. Cicuttini, A. E. Wluka, and S. L. Stuckey, "Tibial and femoral cartilage changes in knee osteoarthritis," *Ann. Rheum. Dis.*, vol. 60, no. 10, pp. 977–980, 2001.

[69] S. Hada *et al.*, "The degeneration and destruction of femoral articular cartilage shows a greater degree of deterioration than that of the tibial and patellar articular cartilage in early stage knee osteoarthritis: A cross-sectional study," *Osteoarthr. Cartil.*, vol. 22, no. 10, pp. 1583–1589, 2014.

[70] S. Van Rossom *et al.*, "Knee cartilage thickness, T1ρ and T2 relaxation time are related to articular cartilage loading in healthy adults," *PLoS One*, vol. 12, no. 1, pp. 1–16, 2017.

[71] S. A. Maas, A. Erdemir, J. P. Halloran, and J. A. Weiss, "A general framework for application of prestrain to computational models of biological materials," *J. Mech. Behav. Biomed. Mater.*, vol. 61, pp. 499–510, 2016.

[72] E. M. Roos and L. S. Lohmander, "The Knee injury and Osteoarthritis Outcome Score (KOOS): From joint injury to osteoarthritis," *Health and Quality of Life Outcomes*, vol. 1. 2003.

[73] R. B. Davis, S. Õunpuu, D. Tyburski, and J. R. Gage, "A gait analysis data collection and reduction technique," *Hum. Mov. Sci.*, vol. 10, no. 5, pp. 575–587, 1991.

[74] S. A. Maas, B. J. Ellis, G. A. Ateshian, and J. A. Weiss, "FEBio: Finite Elements for Biomechanics," *J. Biomech. Eng.*, vol. 134, no. 1, p. 11005, 2012.

[75] S. Simm, U. Simm, A. Simm, and O. Opensim, "SIMM 5.0 and OpenSim 2.0," *Science (80-.).*, no. January, pp. 5–7, 2010.

[76] S. A. Maas, B. J. Ellis, D. S. Rawlins, and J. A. Weiss, "Finite element simulation of articular contact mechanics with quadratic tetrahedral elements," *J. Biomech.*, vol. 49, no. 5, pp. 659–667, 2016.

[77] P. Łuczkiewicz, K. Daszkiewicz, J. Chróścielewski, W. Witkowski, and P. J. Winklewski, "The influence of articular cartilage thickness reduction on meniscus biomechanics," *PLoS One*, vol. 11, no. 12, pp. 1–13, 2016.

[78] C. R. Smith, M. F. Vignos, R. L. Lenhart, J. Kaiser, and D. G. Thelen, "The Influence of Component Alignment and Ligament Properties on Tibiofemoral Contact Forces in Total Knee Replacement," *J. Biomech. Eng.*, vol. 138, no. 2, p. 21017, 2016.

[79] E. Schileo *et al.*, "An accurate estimation of bone density improves the accuracy of subject-specific finite element models," *J. Biomech.*, vol. 41, no. 11, pp. 2483–2491, 2008.

[80] P. Łuczkiewicz, K. Daszkiewicz, W. Witkowski, J. Chróścielewski, and W. Zarzycki, "Influence of meniscus shape in the cross sectional plane on the knee contact mechanics," *J. Biomech.*, vol. 48, no. 8, pp. 1356–1363, 2015.

[81] L. Cristofolini, G. Conti, M. Juszczyk, S. Cremonini, S. Van Sint Jan, and M. Viceconti, "Structural behaviour and strain distribution of the long bones of the human lower limbs," *J. Biomech.*, vol. 43, no. 5, pp. 826–835, 2010.

[82] E. Peña, B. Calvo, M. A. Martínez, and M. Doblaré, "A three-dimensional finite element analysis of the combined behavior of ligaments and menisci in the healthy human knee joint," *J. Biomech.*, vol. 39, no. 9, pp. 1686–1701, 2006.

[83] L. Blankevoort, J. H. Kuiper, R. Huiskes, and H. J. Grootenboer, "Articular contact in a three-dimensional model of the knee," *J. Biomech.*, vol. 24, no. 11, pp. 1019–1031, 1991.

[84] S. M. Nazemi *et al.*, "Prediction of local proximal tibial subchondral bone structural stiffness using subject-specific finite element modeling: Effect of selected density-modulus relationship," *Clin. Biomech.*, vol. 30, no. 7, pp. 703–712, 2015.

[85] C. Verroken, H. G. Zmierczak, S. Goemaere, J. M. Kaufman, and B. Lapauw, "Bone Turnover in Young Adult Men: Cross-Sectional Determinants and Associations With Prospectively Assessed Bone Loss," *J. Bone Miner. Res.*, 2017.

[86] Þ. Pétursson *et al.*, "Bone Mineral Density and Fracture Risk Assessment to Optimize Prosthesis Selection in Total Hip Replacement," *Comput. Math. Methods Med.*, vol. 2015, pp. 1–7, 2015.

[87] M. M. Petersen, C. Olsen, J. B. Lauritzen, and B. Lund, "Changes in bone mineral density of the distal femur following uncemented total knee arthroplasty.," *J. Arthroplasty*, vol. 10, no. 1, pp. 7–11, 1995.

[88] J. Nasehi Tehrani and J. Wang, "Mooney-Rivlin biomechanical modeling of lung with Inhomogeneous material," in *Proceedings of the Annual International Conference of the IEEE Engineering in Medicine and Biology Society, EMBS*, 2015, vol. 2015–Novem, pp. 7897–7900.

[89] I. S. Liu, "A note on the Mooney-Rivlin material model," *Contin. Mech. Thermodyn.*, vol. 24, no. 4–6, pp. 583–590, 2012.

[90] N. F. A. Manan, S. N. A. M. Noor, N. N. Azmi, and J. Mahmud, "Numerical investigation of ogden and mooney-rivlin material parameters," *ARPN J. Eng. Appl. Sci.*, vol. 10, no. 15, pp. 6329–6335, 2015.

[91] K. D. Butz, D. D. Chan, E. A. Nauman, and C. P. Neu, "Stress distributions and material properties determined in articular cartilage from MRI-based finite strains," *J. Biomech.*, vol. 44, no. 15, pp. 2667–2672, 2011.

[92] C. P. Brown, T. C. Nguyen, H. R. Moody, R. W. Crawford, and A. Oloyede, "Assessment of common hyperelastic constitutive equations for describing normal and osteoarthritic articular cartilage," *Proc. Inst. Mech. Eng. Part H J. Eng. Med.*, vol. 223, no. 6, pp. 643–652, 2009.

[93] D. M. Pierce, M. J. Unterberger, W. Trobin, T. Ricken, and G. A. Holzapfel, "A microstructurally based continuum model of cartilage viscoelasticity and permeability incorporating measured statistical fiber orientations," *Biomech. Model. Mechanobiol.*, vol. 15, no. 1, pp. 229–244, 2016.

[94] C. R. Henak, A. L. Kapron, A. E. Anderson, B. J. Ellis, S. A. Maas, and J. A. Weiss,

"Specimen-specific predictions of contact stress under physiological loading in the human hip: Validation and sensitivity studies," *Biomech. Model. Mechanobiol.*, vol. 13, no. 2, pp. 387–400, 2014.

[95] O. Klets, M. E. Mononen, P. Tanska, M. T. Nieminen, R. K. Korhonen, and S. Saarakkala, "Comparison of different material models of articular cartilage in 3D computational modeling of the knee: Data from the Osteoarthritis Initiative (OAI)," *J. Biomech.*, vol. 49, no. 16, pp. 3891–3900, 2016.

[96] H. A. Gray, F. Taddei, A. B. Zavatsky, L. Cristofolini, and H. S. Gill, "Experimental Validation of a Finite Element Model of a Human Cadaveric Tibia," *J. Biomech. Eng.*, vol. 130, no. 3, p. 31016, 2008.

[97] L. Blankevoort, R. Huiskes, and A. de Lange, "Recruitment of Knee Joint Ligaments," *J. Biomech. Eng.*, vol. 113, no. 1, p. 94, 1991.

[98] L. Blankevoort and R. Huiskes, "Ligament-Bone Interaction in a Three-Dimensional Model of the Knee," *J. Biomech. Eng.*, vol. 113, no. 3, p. 263, 1991.

[99] L. Modenese, A. T. M. Phillips, and A. M. J. Bull, "An open source lower limb model: Hip joint validation," *J. Biomech.*, vol. 44, no. 12, pp. 2185–2193, 2011.

[100] K. M. Steele, M. S. DeMers, M. H. Schwartz, and S. L. Delp, "Compressive tibiofemoral force during crouch gait," *Gait Posture*, vol. 35, no. 4, pp. 556–560, 2012.

[101] S. Park, R. Krishnan, S. B. Nicoll, and G. A. Ateshian, "Cartilage interstitial fluid load support in unconfined compression," *J. Biomech.*, vol. 36, no. 12, pp. 1785–1796, 2003.

[102] R. Krishnan, S. Park, F. Eckstein, and G. A. Ateshian, "Inhomogeneous cartilage properties enhance superficial interstitial fluid support and frictional properties, but do not provide a homogeneous state of stress.," *J. Biomech. Eng.*, vol. 125, no. 5, pp. 569–77, 2003.

[103] T. Mann-whitney, "Mann Statistics : 2 . 3 The Mann-Whitney U Test Carrying out the Mann-Whitney U test," *Test*, pp. 3–5, 2004.

[104] B. Dingenen, L. Janssens, S. Claes, J. Bellemans, and F. F. Staes, "Lower extremity muscle activation onset times during the transition from double-leg stance to single-leg stance in anterior cruciate ligament reconstructed subjects," *Clin. Biomech.*, vol. 35, pp. 116–123, 2016.

[105] A. M. W. Chaudhari, P. L. Briant, S. L. Bevill, S. Koo, and T. P. Andriacchi, "Knee kinematics, cartilage morphology, and osteoarthritis after ACL injury," *Medicine and Science in Sports and Exercise*, vol. 40, no. 2. pp. 215–222, 2008.

[106] S. Koo, J. H. Rylander, and T. P. Andriacchi, "Knee joint kinematics during walking influences the spatial cartilage thickness distribution in the knee," *J. Biomech.*, vol. 44, no. 7, pp. 1405–1409, 2011.

[107] S. Gilbert *et al.*, "Dynamic contact mechanics on the tibial plateau of the human knee during activities of daily living," *J. Biomech.*, vol. 47, no. 9, pp. 2006–2012, 2014.

[108] A. Kłodowski *et al.*, "Merge of motion analysis, multibody dynamics and finite element method for the subject-specific analysis of cartilage loading patterns during gait: differences between rotation and moment-driven models of human knee joint," *Multibody Syst. Dyn.*, vol. 37, no. 3, pp. 271–290, 2016.

[109] J. L. Hicks, T. K. Uchida, A. Seth, A. Rajagopal, and S. L. Delp, "Is My Model Good

Enough? Best Practices for Verification and Validation of Musculoskeletal Models and Simulations of Movement," *J. Biomech. Eng.*, vol. 137, no. 2, p. 20905, 2015.

[110] C. Florea *et al.*, "Alterations in subchondral bone plate, trabecular bone and articular cartilage properties of rabbit femoral condyles at 4 weeks after anterior cruciate ligament transection," *Osteoarthr. Cartil.*, vol. 23, no. 3, pp. 414–422, 2015.

[111] Y. Chen *et al.*, "Abnormal subchondral bone remodeling and its association with articular cartilage degradation in knees of type 2 diabetes patients," *Bone Res.*, vol. 5, no. December 2016, p. 17034, 2017.

[112] J. Day *et al.*, "Adaptation of subchondral bone in osteoarthritis.," *Biorheology*, vol. 41, no. 3–4, pp. 359–68, 2004.

[113] I. J. P. Henderson and D. P. La Valette, "Subchondral bone overgrowth in the presence of full-thickness cartilage defects in the knee," *Knee*, vol. 12, no. 6, pp. 435–440, 2005.

[114] S. J. Shultz, R. J. Schmitz, A. Benjaminse, A. M. Chaudhari, M. Collins, and D. A. Padua, "ACL Research Retreat VI: An update on ACL injury risk and prevention," *J. Athl. Train.*, vol. 47, no. 5, pp. 591–603, 2012.

[115] G. Valente *et al.*, "Relationship between bone adaptation and in-vivo mechanical stimulus in biological reconstructions after bone tumor: A biomechanical modeling analysis," *Clin. Biomech.*, vol. 42, pp. 99–107, 2017.